University of Padua

Department of Information engineering

Engineering of automation

Master's thesis

Simulation-based study of novel control strategies for inverters in low-inertia system: grid-forming and grid-following

Advisor: Luca Schenato
CoAdvisor: Adolfo Anta, Ali Tayyebi-Khameneh

Author: Alessandro Crivellaro

February 24, 2020

Author: Alessandro Crivellaro

Abstract

The narrowness of the carbon fuels and the problems of pollution related to their combustion have lead to an increasing interest for new sources of energy. In particular, in the last years, thanks to the new technologies available and to the politics of some countries, the use of the so called *green energies* has raised significantly. Nevertheless, the substitution of the traditional power plants, based on the combustion of fossil fuels, with inverters, which are power electronics devices able to convert wind and solar power into electrical energy, has brought new challenges in terms of grid stability and reliability. Indeed, the transition towards a 100% converter-based grid has as consequence the constant reduction of the mechanical inertia in the network, due to the reduction of the number of synchronous machines. With the goal of guarantee the frequency stability also in the case of *low-inertia* systems, new techniques of control have been proposed. In this work, specifically, two different kind of devices will be taken into consideration, *grid-following* and *grid-forming* devices; the first ones are based on the presence of the *PLL* (phase-locked loop) to detect the frequency of the grid, while the others have not this element in their control loop. The goal of the thesis is to analyze the behavior of the network, in terms of frequency and power, with an increasing level of converters in the grid. At the beginning, the models of grid-following and grid-forming converters are presented, analyzing in particular four techniques of control for the grid-forming ones: *droop, matching, virtual synchronous machines (VSM)* and *dispatchable virtual oscillator control (dVOC)*. In the second part, these types of converters are tested and their performances are analyzed, considering especially two parameters, the frequency at *Nadir* and the rate of change of frequency ($RoCoF$). The simulations are performed at first on the *IEEE 9-Bus system*, which is used as benchmark to validate the different models, and then on the *Hydro-Quebec network*. With this last model, in particular, it is possible to analyze the behavior of the converters in a real system; it will be shown that not only with an appropriate control the stability of the grid is kept, but better performances will be obtained in the response to the contingencies which can happen in the network.

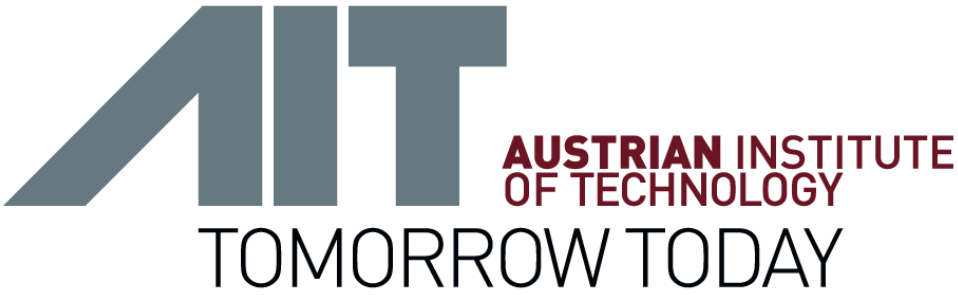

AIT Austrian Institute of Technology is Austria's largest Research and Technology Organisation (RTO) and an international key player in many of the research areas it covers. This makes AIT a leading development partner for the industry and a top employer within the international scientific community. [1]

Acknowledgements

I wish to show my gratitude to my supervisor, Mr. *Luca Schenato*, to have offered me the opportunity to do this work abroad and for his availability and support both during the stage period and in the writing phase. I would also like to thank Mr. *Tommaso Caldognetto* for the help in the revision of the thesis and for the precious advice he has given to me. I wish to express my deepest gratitude to the *Austrian Institute of Technology (AIT)* to have welcomed and to have supported me during the six months in Vienna; it has been a real pleasure to work for that organization and I found many good friends, beyond expert colleagues. In particular a special thank to Mr. *Adolfo Anta*, to have encouraged me to do my best and to not put me off in front of the difficulties and to Mr. *Ali Tayyebi*, to have been my reference point, always ready to answer to my questions and to help me in case of problems. Moreover, I would like to mention also *Denis*, the other student from Padua, for the moral support: the coffe break, the dinner at 7p.m. and the afternoon at the Donau will be for long time in my memory.

Un ringraziamento speciale va a *mamma* e a *papa'*, per avermi supportato (e sopportato) in ogni momento e per aver contribuito con ogni sforzo per la realizzazione dei miei progetti e per il raggiungimento dei miei obiettivi. E' merito vostro se oggi siamo qui a festeggiare! Grazie anche a *Gio'*, con cui "discuto" sempre e da sempre, in modo piu' o meno "animato"; hai un bel caratterino, ma con determinazione ed impegno riuscirai a raggiungere altri importanti traguardi! Un grazie speciale a *Melissa*, perche' da quando le nostre strade si sono incontrate quasi per caso, sei entrata poco alla volta nel mio mondo; la pazienza ed il sostegno che mi hai dimostrato in questi mesi sono il segno della tua voglia di esserci sempre. Non potevo desiderare una migliore compagna di viaggio!
Non posso non parlare della nonna *Lilliana*, che e' da sempre il mio esempio per la sua determinazione ed il suo spirito. Perche' anche nelle giornate piu' difficili basta passare da lei e perche' da quasi 25 anni cerco invano un pasticcio migliore del suo... Senza risultati! Grazie anche allo *zio Roby* e alla *zia Orni*, per avermi viziato da quando sono nato e per non avermi mai fatto mancare nulla.
Meritano un grande grazie anche tutti gli altri zii, i cugini e i figli dei cugini; e' bello sapere di poter contare sempre su una grande famiglia!
Un ringraziamento speciale devo farlo al *Celin* e al *Berni*, i due grandi compagni

degli anni universitari e non solo; siete stati un sostegno prezioso nei momenti di crisi e avete sempre saputo tirarmi su di morale. Sono stati anni indimenticabili e vi saro' sempre legato, ovunque ci porti il futuro. In bocca al lupo!
Ringrazio poi tutti gli scouts incontrati lungo la strada, quelli di oggi e quelli di ieri. Mi avete insegnato e trasmesso uno stile di vita di cui vado orgoglioso.
Un grazie speciale ad *Anna, Maria* e *Piper*, conosciuti in branco e diventati compagni di mille avventure (e altrettante feste). So che su di voi posso sempre contare!
Grazie anche ad *Angelo* e *Walter*, i miei vecchi compagni delle superiori, con cui ci vediamo poco a causa dei molti impegni ma che so essere grandi persone; vi auguro di raggiungere i vostri sogni!
Agli amici di una vita, *Carlo* e *Vitto*, dico grazie per esserci sempre stati; abbiamo intrapreso strade diverse e ci vediamo di rado, ma e' bello saper di poter contare sul vostro aiuto!
Non ultimi in ordine di importanza, desidero ringraziare gli arbitri e soprattutto le "*Degne persone*". Avete contribuito a farmi crescere e migliorare e siete degli amici molto piu' che dei semplici colleghi!
Grazie a tutti coloro che fanno parte della mia vita, alle persone che ho conosciuto in Erasmus in Belgio e a Vienna e che hanno contribuito a rendere queste esperienze indimenticabili, a chi ha fatto un pezzo di strada con me, a chi c'e' stato e a chi c'e' ancora. Tutti voi avete contribuito a farmi diventare quello che sono, ve ne sono grato!
Un ultimo grazie, infine, lo voglio riservare a me stesso; per i sacrifici fatti per raggiungere questo traguardo, per la capacita' di affrontare anche i momenti piu' difficili, per aver dimostrato che con determinazione e forza di volonta' si puo' andare lontano.

Contents

Chapter 1

Introduction

1.1 Global transitions towards a 100% renewable grid

According to the necessity of a more sustainable way to produce energy due to environmental and climate problem, a transition from the conventional fossil-fuel based power plants to the renewable sources is happening in the last decades. The goal is to achieve a 100% renewable grid, through the combination of all the possible methods of producing energy basing on the so-called *green sources*. Actually, some countries have already reached this result, thanks to both their attention to the environmental question and to particular advantages of their land; Iceland, for example, supplies 100% of its electricity trading on geothermic and hydro-power, and this last source is also used in a large way from other countries such as Norway, where it provides the 97% of the electricity needs or Canada (62%) [2]. More problems arise at country that have not a sufficient quantity of hydro-power/geothermic energy to satisfy their demand; in this case, the solution can be found adopting the *variable renewable energy* (VRE), such as wind and solar photo-voltaic (PV), to contribute in the energy production. These sources, also thanks to the reduction of the costs for the technologies that are necessary to make use of them, have been largely installed in different countries all over the world. For example, in Australia the level of penetration of combined wind and solar capacity covers more than 20% of the National Electricity Market [3], German, Ireland and Denmark have reached the same level of annual VRE use [2], in the Ercot (Electric Reliability Council of Texas) grid the wind generation supplies for the 15% of the total electric energy [3].
Morevorer, according to the *"Forecast International's energy portal"* [4], it was only since 2000 that a massive use of wind and solar energy has been done. Looking at the graph 1.1 below, at the beginning of the new millennium the installed wind capacity was equal to 17GW, while for the solar energy it was 1.3GW. As it is possible to see, both the sources have made an extraordinary expansion in these 20 years, but their development has been different. In particular, wind installations have increased in the first year of 2000, and in 2009

there were yet 159GW. In the same year, there were only 23GW from solar power. But in the last ten years the situation has changed and the expansion of solar energy is becoming more significant year by year. In 2020, the forecast indicates that the cumulative installations of solar power will overtake the one of wind turbine. Even, in 2023 it is expected that solar energy will reach a value of 1293GW, while wind capacity will be around 903GW. This sudden growth is due especially to the interest of new countries in the installation of solar plants; China, in 2018 has installed more than 44GW, which is not far from the half of the total quantity installed all over the world in the same year, while India has contributed with around 8GW, resulting the third country in the world after USA (10.5GW).

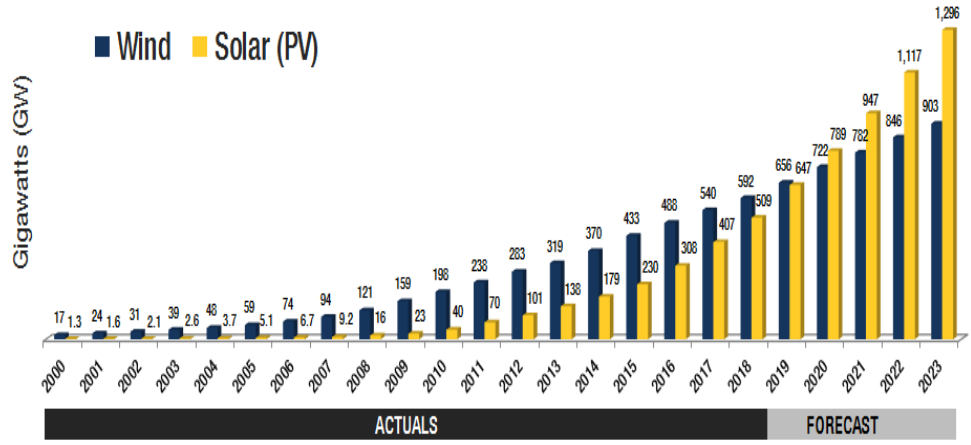

Figure 1.1: Actual global capacity of solar (PV) and wind power in GW and future scenario [4]

If the problem of providing energy in the power plants with a large use of VRE, which can generate variable and uncertain power output according to the weather conditions, has been partially solved expanding the transmission system in order to be able to transfer large amounts of power from regions where VRE production is overtaking the limit to areas where load is currently needed or storing wind and solar power when the production exceed the demand and providing this energy when the requirement is higher than the production, lots of other issues regarding the increasing use of renewable sources have not been solved nowadays.
Indeed, adding more VRE into power systems, means also a deep change in the network grid, due to the fact that these sources are typically connected via power electronics to the system and they interact differently with respect to the traditional SM that are based on steam and hydro-turbines. Specifically, renewable sources generally use inverter to connect to the grid, while the conventional fossil-fuel power plant adopts synchronous generators; a system in which the

instantaneous level of penetration of VRE overtakes the 50% is called "inverter-dominated" and have different characteristics and properties comparing to the traditional ones. In Fig. 1.2, it is well depicted the difference between the present grid, based on synchronous generators, and the future one, which is based on inverter devices.

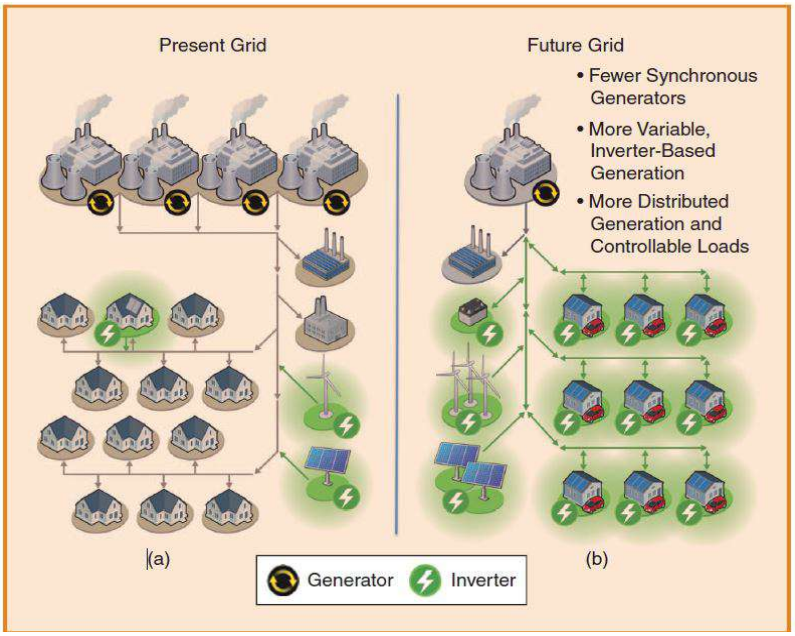

Figure 1.2: Comparison between a SM-based grid and an inverter-based grid [2]

These technologies, as it is shown in Fig. 1.3 are based on the conversion from *dc-side* to grid-compatible *ac-side*, through multiple ac-dc and dc-ac conversion stages.

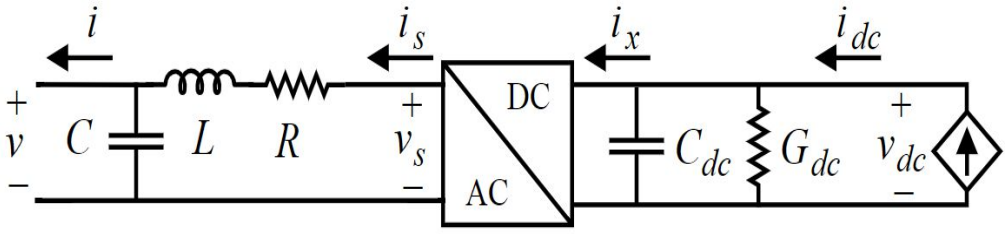

Figure 1.3: Model of a converter unit

Differently, the synchronous machines have a stationary part (*stator*) and a rotating one (*rotor*) that produces a rotating magnetic field inducing a voltage in the stator windings, as it is depicted in Fig. 1.4.
The full model of the synchronous machine is described in A; the mechanical

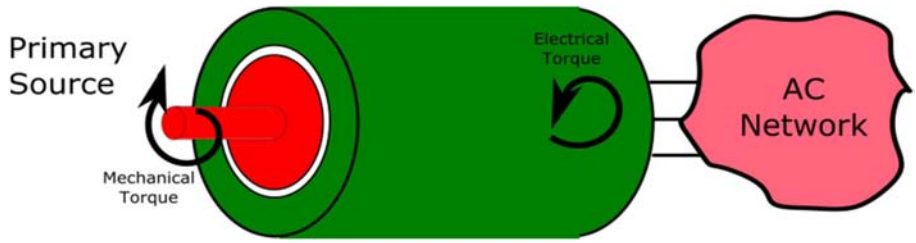

Figure 1.4: Model of a synchronous generator connected to the grid [5]

equation which governs the system is

$$J\frac{d\Omega}{dt} = T_m - T_{em} \tag{1.1}$$

where T_m and T_{em} are respectively the mechanical and electromechanical torques, while Ω stands for the mechanical rotational speed of the rotor and J is the momentum of inertia of the rotational masses . In 1.1, it is highlighted the proportional relationship existing between the electrical frequency of the rotor electromagnetic force (which derives from the number of the pole pairs of the rotor) and its mechanical rotational speed. Moreover, a fundamental intrinsic property of the synchronous generator is the coupling between the frequency of the grid and the imbalance between electrical and mechanical torques. This generators also produce a synchronizing torque between interconnected synchronous machines and, along with inertia, it has a strong influence on the initial rotor speed behavior when a contingency event in the grid happens. Once the synchronization to the rest of the grid has been obtained, the real power is controlled through the shaft torque, while the reactive power is governed by the field current. With these devices, frequency and voltage are the two of the variables which need to be regulated and will constitute one of the main objective of the control; to ensure the stability of the entire system, a combination of fast-closed-loop controllers (primary frequency response) and slow-centralized ones (automatic generator control, used to restore the system frequency to its nominal value) is implemented.
The synchronous generators have also an important characteristic, which directly comes from a physic point of view; indeed, the rotating components and the turbine system create mechanical inertia and are capable of storing kinetic energy in the rotating part. Thanks to this property which allows the generators to absorb or supply energy into the rotating masses, the traditional system can balance fluctuations in net load and generation; practically, when a net excess verifies in the grid, it creates an excess of energy in the rotating mass which has as consequence an increment in the system frequency (a deficiency causes a decrease of the frequency itself). Therefore, analyzing the direction of the frequency deviation leads to detect net energy excess or deficiency inside the network. Additionally, the total inertia of the system makes it stable against

faults and variations which verify across the network.
On the opposite, VRE devices utilize a completely different technologies to connect to the grid, based on power electronics inverters. Referring again to Fig. 1.3, the conversion is governed through switching semiconductor at a fast timescale. In this case, the mechanical part is not existing anymore and with it, it also misses the capacity of storing energy. It is important to specify that, in some cases, this mechanical part is emulated with specific techniques (for example, adding "virtual inertia"), which allow to have the same properties but the mechanic components have been removed. However, not always the inertia is emulated in these devices (it depends on the control technique) and consequently the quantity of energy stored is usually lower if compared to the amount stored by the synchronous machines. It is important to remind that these devices are necessary when the VRE are involved; indeed, with wind turbines, in a first step there is a conversion of all the power delivered by the wind in dc and successively the inverters make it compatible to the grid ac power through a second step of conversion; photovoltaics (PV) also requires inverters, due to the fact that they generate dc electricity and it has to be supplied in ac to the grid.

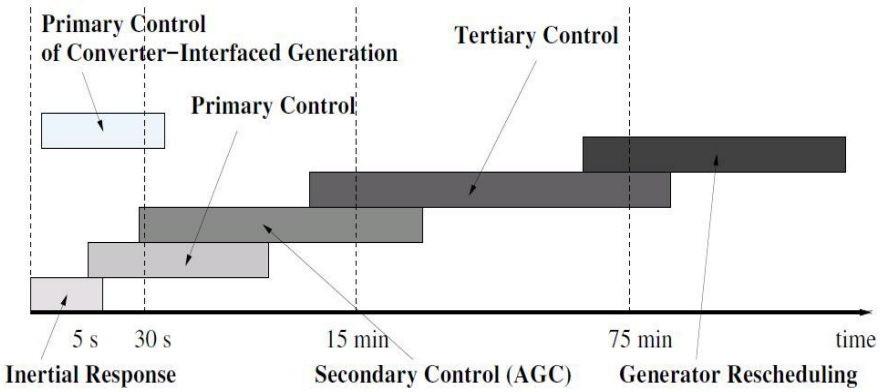

Figure 1.5: Time scales of frequency control for SM and converters [3]

Due to their different way of connection to the grid, there are some important differences between inverters and synchronous machines also from a control prospective. Analyzing Fig. 1.5, where the different time scales of control action are reported schematically, it is easily understandable that inertia impacts at the beginning, when disturbances (load variations or contingencies) verify. In a second moment, further controlling actions are operated from the controller of the generators; specifically, the primary and secondary control take place after some seconds (primary frequency control) or minutes (secondary frequency control), while sometimes also a tertiary control is implemented and can act also on time scales of hours. It is possible to conclude that the influence of the rotating part in terms of control is related to the beginning of the compensation.
On the other hand, power electronic devices are faster in terms of primary and

secondary control, but the main problem is related to the absence of the rotational part which does not guarantee a response in the first instants after the contingency (the time scales in this case is about the first seconds or hundred milliseconds).
Finally, it is also important to remind the concept of *reserve*, which has become extremely important with the increasing use of the VRE sources. As it has been explained before, due to the fact that the availability of renewable energy depends on the weather conditions and varies in an unpredictable way, an additional quantity (*reserve*) is necessary to guarantee the system's frequency stability when an event occurs. The same services illustrated before (primary, secondary and tertiary control), which in a system constituted of synchronous machines are provided directly from the generators, can be implemented also in an inverter-based system through the right amount of reserve. A summarizing scheme which well depicts the importance of this concept is reported in Fig. 1.6; on one side, the system has to be able to face up to normal situations, such as the correction of the current on the DC side, on the other it needs to respond to instantaneous events, stopping as fast as possible the rate of change of frequency ($RoCoF$) through an efficient primary response and taking the frequency to its nominal value using the secondary response. The tertiary response is only used when the reserve of the primary and secondary has yet been used and a further event happens.

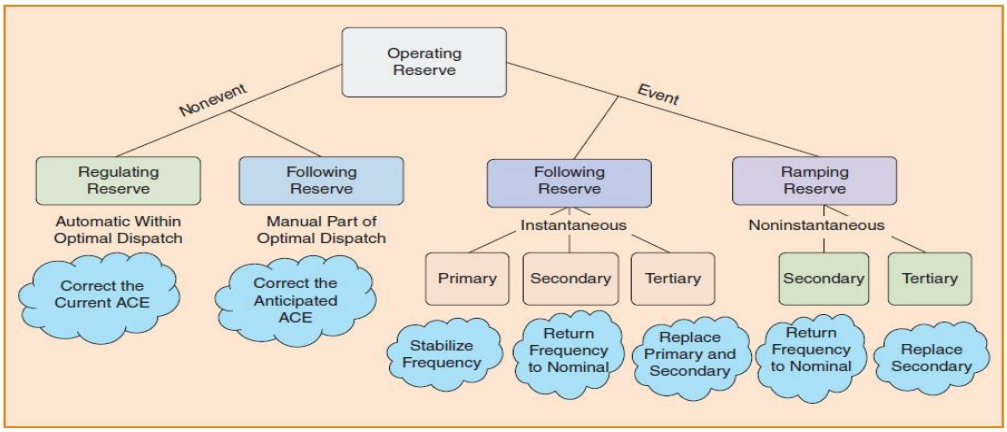

Figure 1.6: Classification of the operating reserve [2]

1.2 The nowadays situation and the future prospective

As it has been explained in the previous sections, the need of a transition towards new ways of energy generation, which is strongly based on the renewable sources, in order to reduce the environment contamination and to answer to the climate global warming problem, has had as consequences the arise of new problems,mainly due to the impossibility to substitute completely the existing grid; in order to solve this issue, there is the necessity of adapting the new converter devices, through which it is possible to exploit the green energy, in place of the technologies that are installed in the nowadays grid. This transition from a network dominated by SG to one where they have been supposed to not exist anymore or in a minimal part, has lead all the countries in the world to develop projects with the aim to increase the possible level of penetration of the renewables in their grid.
The EU community, for example, is developing different programs to increase the percentage of energy which comes mostly from wind and solar sources; in this direction works the *High Penetration of Power Electornic Interfaced Power Sources (HPoPEIPS)* program [6], with the aim of finding solutions to the problems of stability that have been analyzed before, but also to answer to smaller ones such as the power quality and other issues related to the different response time between traditional generators and new converters.
Another project, called *Migrate* (*Massive InteGRAtion of power Electornics device*) [5], tries directly to develop the problems of a transmission grid 100% inverter based, dividing the problem in small sub-tasks. Specifically, on one side there is the attempt to analyze the present situation and substitute the largest number of generator as possible in order to understand which are the current limitations of the grid; on the other side, a studio is carried out about a system constituted only by converters, in order to develop new control strategies and to understand the advantages of this scenario. Moreover, the interest is also on the protection devices that need to be installed in the future grid, due to the different behaviors that the new technologies have if compared to the traditional synchronous machine. The European Union has also created a *Research and Innovation program Horizon 2020* [7], where it is possible to find the requested levels of renewable energy from the different countries before 2020. However, there are yet some region in the EU which have to face the problem of inadequate inertia (such as Ireland and Northern Ireland and Great Britain) as it is reported in [6]. Besides, although the percentage of energy coming from renewable is lower, also the rest of Europe is starting concerning about the modifies on the electric grid that the introduction of renewable has caused.
Due to the problems related to inertia, in the Irish grid (which constitutes an isolated system, connected with Grait Britain trough the "East-West Interconnector" and to Scotland through the "Moyle HVDC") an upper limit on the

level of penetration of converter technologies has been set equal to 50% at the beginning. In August 2011, in order to increase this limit, EirGrid and Soni's Delivering a Secure Sustainable Electricity System (DS3) program [8] has been developed. The main goal of the project is to increase the penetration of non-synchronous generator till the 75% of the entire grid. In November 2017, the limit has been set to 65% [9] but the program is still going on; moreover, it also concerns about financial incentive to develop new devices which improve the converter performance and redefines the standard for wind farms and traditional plant.

The transition towards a 100% inverter-based grid has brought as a consequence a deep research in the modelling and controlling of power electronics devices, with the goal to keep the stability in a low-inertia system; in the next chapter, this aspect will be analyzed in detail and it will show that the new technologies can also provide fast response in the case of faults or load changes. In the present scenario, there are two different approaches that are taken into consideration in order to substitute the SM with converters: grid-following and grid-forming inverters. In literature, a clear distinction on the various topology of converters is missing; in the rest of this work, it is assumed as element of distinction between the two strategies the presence (or the absence) of the PLL.
Indeed, grid-following units basically looks at the characteristic of the existing grid through a phase locked loop (PLL), which allows to evaluate the frequency and the phase angle of the network, which is set by SG or other grid forming devices; this type of device is not able to impose its frequency to the grid, but it can adapt to the one which is set by other converters or synchronous machines. Generally, a reference value in terms of active and reactive power is assigned to this converter, and this amount of power is used to adjust the frequency and the voltage of the system keeping them as close as possible to the reference values.
Grid-forming converters, instead, are able to operate also in a grid where there are no other SG or converters which impose the frequency, because they can directly transform energy from the source and provide power to the rest of the grid. According to their structure, they offer the possibility of operating in black start condition (it represents the condition in which the system turns on), they allow frequency and voltage control. Taking as starting point the work of [10], four different grid-forming techniques are studied and analyzed in the second chapter: droop control, virtual synchronous machine (VSM), matching control and dispatchable virtual oscillator control (dVOC).
In this project an increasing level of penetration of converters-based technologies into a realistic grid is explored, and different techniques of control which are available nowadays are tested and their performances are compared. In details, in the second chapter an overview on the new sources of energy is given with a particular attention to the transition to a low-inertia system. In the final part of the chapter the stability problems which affect these types of network are presented and analyzed. The third chapter aims to describe the model of

grid-following and grid-forming inverters, highlighting the main differences between these two approaches; moreover, also the different grid-forming techniques will be presented, in order to have a good knowledge of the models also from a mathematical point of view. At the beginning of the fourth chapter, the network modelling will be briefly discussed and basic components such as load, lines and transformer which will be used later will be analyzed. In the second part, it will be explained how to obtain an aggregate model of multi-converter system and how the parameters have been scaled. This represents an important point to well understand how the converters that are tested inside the different models are built.
In the fifth chapter the converters previously analyzed are tested in the *IEEE 9 Bus-system benchmark* [11], where at the beginning there are three SG. It will be showed how it is possible to increase the percentage of converters in the grid, keeping the stability in terms of frequency and reaching the reference power. The following chapter represents an extension of this one, and the attempt to test the different inverters developed before in a real case of study, specifically the *Hydro-Quebec* grid, adopting as reference model the one that is described in [12]. The attempt is to study the behavior of the system for increasing level of power electronics based device in order to overcome the limit of penetration that have been explained in the previous section. It will be shown that a grid formed with only converters work in a proper way, but problems arise when there is a low percentage of SG and an high one of converters; this is a situation that deserves a particular attention, since in the transition towards a 100% renewable energy it is a scenario that needs to be analyzed. In the last chapter, the most significant results are presented; this work will show that it is possible to reach an high-level of penetration of converters in the grid and, due to the faster dynamics of these devices, the performance of the system will also improve.
Comparing to similar existing works, this one tries to improve what has been done in two different ways; first of all, the grid-following and grid-forming techniques which are taken into consideration are tested not only in a simple model such as the one that is used in the fifth chapter, with the goal to validate them and to better understand their behaviour, but they are also put inside a real network, i.e. the Hydro-Quebec grid. This last step is not trivial, since lot of studies have been done at theoretical level in order to validate the different converter techniques with infinite-bus or simple model, but the large scale simulations have not been yet far explored. Moreover, comparing to similar studies, the penetration approach inside the network has been obtained differently; as a matter of fact, each SM of the original model has not been substituted completely with a converter, but thanks to the model of a so called *Hybrid-block* (that will be shown later on), the penetration has been obtained gradually.
The main goal of the project is, in synthesis, the demonstration, through simulations in a real and complex network, that it is possible to obtain a complete converter-based grid, with the right techniques of control. Moreover, there is

also an interest in the analysis on the effects that different contingencies can cause to the network, in order to explore the advantages and the limits of the converters.
In this activity it has been used *MATLAB/SIMULINK* as software to develop the models and to test the different scenarios. SIMULINK is a graphical environment where it is possible to draw the models of dynamic systems and simulate their behaviour. In particular, due to the nature of the project, the library *SimscapePowerSystems* (formerly SimPowerSystems) has been widely explored; it contains models of electrical power components, such as three-phase machines and electric drives. Moreover, it helps the user with some tools, such as the automate solution of the load-flow equations, that allow a faster investigation on the phenomena appearing in the network.

Chapter 2

New sources of energy

Since the 19th century when the industrial revolution started, the demand for energy has increased incessantly and in an exponential way, involving in time new form of sources. As it is depicted in the graph 2.1 [13], the consumption of fossil fuel is still increasing nowadays, but if at the beginning of the industrial revolution the only raw material was the coal, crude oil and natural gas constitute nowadays the most significant source for the production of energy. In the present situation, coal contributes for the 33% of the total global fossil fuel consumption, while the crude oil is the most employed source (39%); finally, natural gas accounts for 28% of the total consumption.

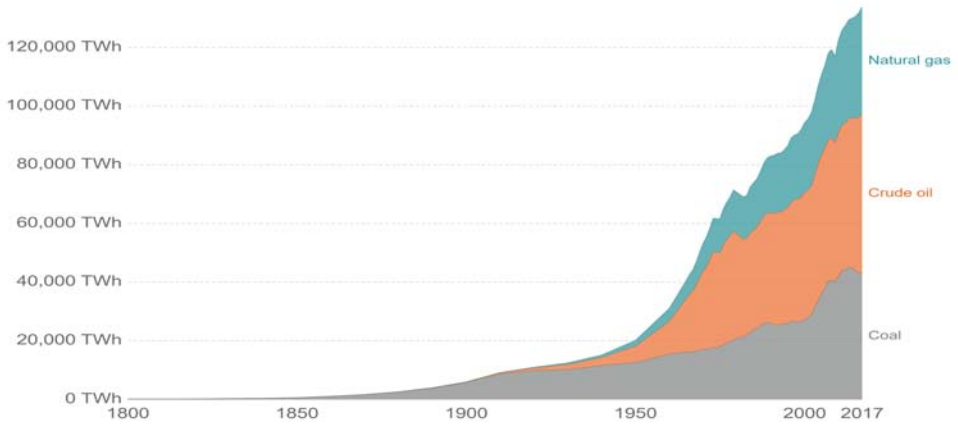

Figure 2.1: Fossil Fuel Consumption since 1800 [13]

However, the fossil fuels provide still the 80% of the world's energy and are largely the most-used source of energy. Nevertheless, different problems have forced a transition to the renewable sources, whose using is increasing in the last decades. The first problem is about the efficiency of the power fossil fuel generating plant, because if the three processes which are necessary to obtain energy are considered (thermal, mechanical and electrical), around 60% of the

energy is lost; moreover, if old generating plants are taking into consideration, this percentage could increase till 70% [13].
A second problem is represented by the pollution that derives from the combustion of the fossil fuels; indeed, fuels are not pure and, despite they undergo to different processes of refinements before being burned, they still contain other components that can release unpleasant gases and solid particles in the air. Specifically, the combustion of the coil produces sulphur dioxide and oxides of nitrogen, which are both elements that contribute to phenomena as acid rain; moreover, the crude oil usually contains trace of other particles, for example mercury and cadmium. In order to solve this problem, many countries have set some laws that regulates the combustion process, that force to treat the fuels in an appropriate way before their use. However, this implies an increment in the cost of the electricity, since these processes and their control are particularly expensive.
Nevertheless, is the global warming the reason for which, in the last years, the interest in the renewable energies and in new solution for the production of electricity has raised. Indeed, the combustion of any fossil fuel produces the so called *"greenhouse gases"*, which are in particular carbon dioxide (CO_2) but also sulphur dioxide (SO_2) and methane (CH_4). All these elements are responsible for the global warming and the research of solutions for different ways of generating energy and capturing the CO_2 which is produced constitutes one of the main challenges that nations will face in the next decades.
As it has yet been pointed out in the introduction, different programs have been creating all over the world with the goal of reduce the use of fossil fuels. The European Union, for example has developed its objectives through its $20-20-20$ targets, that were established in 2009. According to them, the goal is to reduce the greenhouse gas emissions by 20% with respect to 1990, to increase the energy efficiency of 20% and to produce the 20% of the total energy through renewable sources by 2020 [14].
In the two histograms below, Fig. 2.2, are depicted respectively the installed electricity capacity and the electricity generation considering the 28 countries that are members of the European Union. Analyzing the graphs, it is possible to note that in 2016 the quantity of electricity generated using renewable sources was around 30%, also if the more consistent part was made by hydro-power. In the last decades, new technologies have been introduced and the focus is now on the energy that comes from PV and WT. According to the predictions, it is estimated that these two sources will contribute for the 51% of the total electricity capability by 2050, doubling the nowadays percentage that is around 25%; however, being the capacity factors quite low, this will imply that only 36% of the total electricity will be generated through PV and WT.

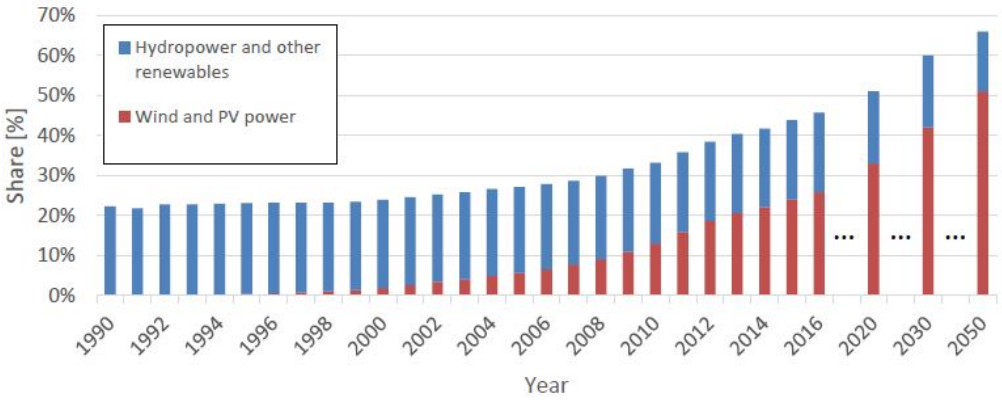

(a) Installed Electricity Capacity

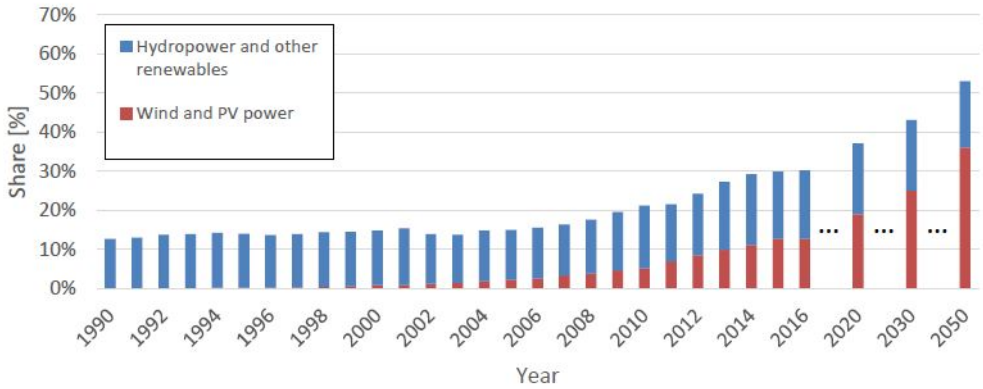

(b) Electricity Generation

Figure 2.2: Installed Electricity Capacitance and Electricity Generation [14]

This transition also brings a transformation in the way in which generation units are connected to the grid. Indeed, the network have been created more than a century ago and were projected for specific generators, the SM. Usually, a traditional grid is based on a small number of large-size generators that are directly connected to the grid. This fact, and the capability of the SM of storing kinetic energy inside the rotor-part, has contributed to the creation of a network stable in case of frequency fluctuations. On the other side, PV and WT are converter-based technologies and usually they are located in different parts of the network; indeed, the size of these devices is not comparable with the one of the power plant and the total amount of inertia decreases as long as more inverters are implied. Before analyzing the concept of inertia and the stability problems that arise in the case of low-inertia system, a brief explanation on the PV and WT use is given in the following sections.

2.0.1 Wind Energy

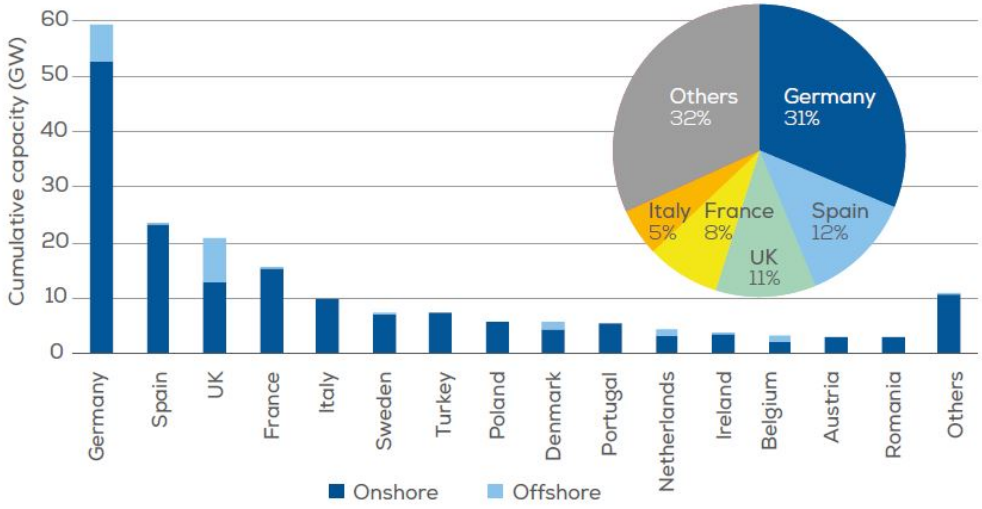

Figure 2.3: Cumulative onshore and offshore installations by country [15]

According to the data published in [15], in 2018 in Europe the capacity of installed wind power was equal to 180GW in total, 170GW onshore and 17GW offshore. This accounts for 18.8% of the EU's total power capacity but the distribution of the WT is not homogeneous in the continent. Indeed, as it is possible to observe in fig. 2.3, the 68% of the wind power generation is distributed in five countries: Germany, that accounts for 31% of the total, Spain, United Kingdom, France and Italy. The trend in the installation of wind turbines has always increased in the last ten years; in 2008, the amount was equal to 66GW, (1GW offshore and 65GW onshore), in 2018 the total quantity has been equal to 180GW. It is also worth to mention that 14% of the electricity demand has been provided from wind turbines in 2018, with an increment of 2% with respect to the previous year.
A WT converts wind power into electrical energy, which is then provided to the grid. Usually, the turbines are not directly connected to the high-voltage level, but there is a transformer from medium to high voltage before they connect to the grid. The structure of the turbine is based on three main components:

- the **rotor**, which includes the blades that convert the wind energy in low speed rotational energy;

- the **generator**, which is responsible of the conversion of the mechanical power absorbed through the blades into electric energy. This conversion is usually obtained through an inverter and in this part there is also the control part;

- the **gearbox**, which is not always present, but that has the goal of converting the low rotational speed of the blades into high rotational speed, which is more adapt for the conversion into electric energy.

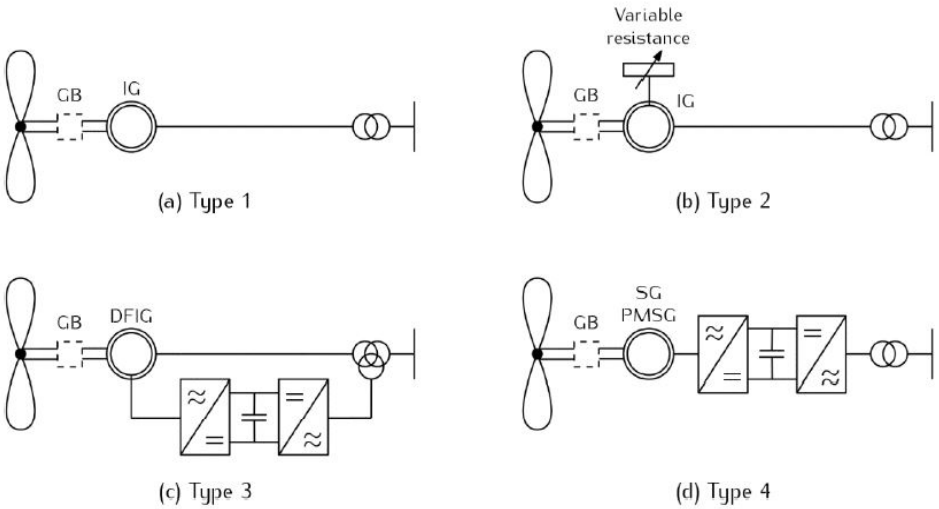

Figure 2.4: Different Types of Wind Turbines [14]

Actually there is not a single way in the conversion of the mechanical power into electrical energy. Through the years, different typologies of WT have been developed and they are schematized in Fig. 2.4. The firs two types, which are also the oldest ones, are characterized by a direct induction generator (IG) coupling and for this reason they are able to give an inertial response to the system. Thanks to this property, they can provide the system with a similar inertia constant with respect to the traditional SM. The most relevant change regards the way according to which this contribution is given, that is slower and lower. Moreover, there are also some drawbacks in the use of this WT: for example, there is the necessity to compensate the reactive power and this turbine has not a full capacity on adapting its speed according to the variations of the wind intensity and this leads to have a low efficiency. Due to these reasons, the attempt is to substitute these WT with more recent ones.
Referring to the data of the *European Wind Energy Association* [16] yet in 2010 the turbine equipped with doubly-fed induction generator (DFIG) or with a converter interface (type 3 and 4 in Fig. 2.4) count for the 80% of the market in Europe. Specifically, with turbines of type 3, the stator windings of the DFIG allows a partial coupling with the grid but, being the converter controller installed quite fast, the inertia response that is provided in this case is really small. Indeed, the regulator aims to balance the electrical torque, also in presence of disturbances. In this case, the rotor current is controlled in order to keep the electrical torque to its nominal value. The last topology is the one that

guarantees an higher efficiency, due to the presence of a full scale converter that regulates also the speed according to the wind intensity. For these WT, the controller on the generator side and the one on the grid side is completely decoupled. Due to this reason, there is no contribution in terms of inertia when these devices are employed.

2.0.2 PV Energy

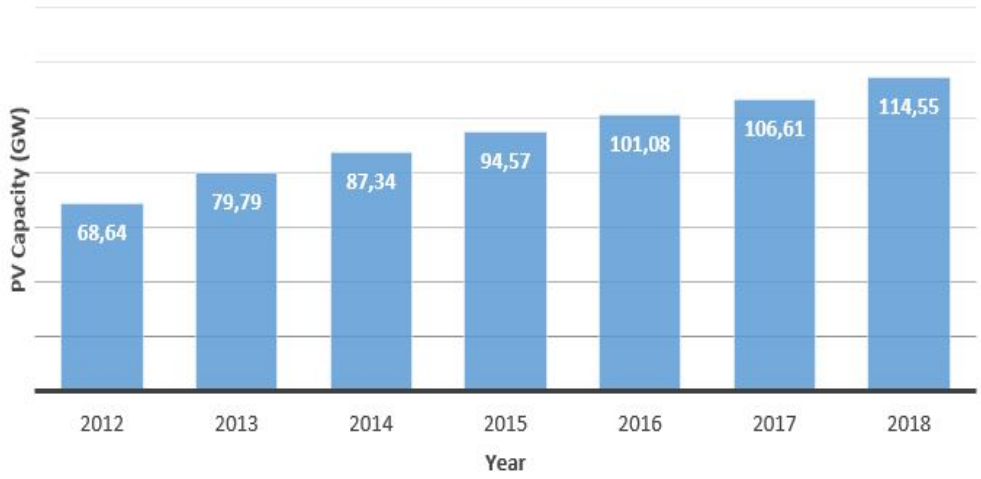

Figure 2.5: Total PV installed in Europe over the years [17]

Referring to the data published by the [17], approximately 102.4GW of solar PV have been installed in 2018, increasing the total capacity to 509.3GW. China has contributed to this growth for 744GW, while the 28 countries of the EU have installed around 8GW, which represents a significant increase if compared to the 5.5GW installed during 2017. In Fig. 2.5, it is depicted the GW of solar PV that have been installed in the EU in the last years. As it is possible to see, there has been a decline in the last few years, especially if the comparison is with the 2011, when more than 23GW has been installed in the continent. The main reason of this slowdown is represented by a change in the PV market; indeed, there has been a new policy that strictly regulates the building of big power plants; this has lead to a reduction of this type of installation, while the interest has moved to commercial and residential roof-mounted system. Nevertheless, the installations of solar PV all over the world is constantly raising and it is estimated that the total capacity installed will overtake that related to wind yet in 2019.
Fig. 2.6 shows the 5 European countries that have installed more solar PV; as for the wind power, Germany is the leader also in this sector, having installed more than 3GW also in the last year. Other countries are in expansion, like Italy, France and UK, while Spain has not followed the same trend.

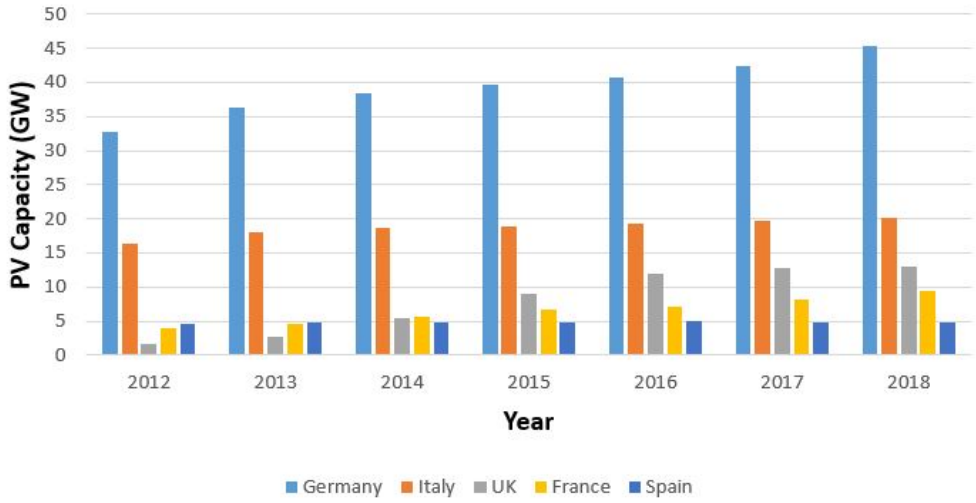

Figure 2.6: Top 5 European countries in PV installation over the years [17]

The working principle of solar PV is based on solar modules, which are composed of simple unit called solar cells. Specifically, these cells are built as p-n junction, with an internal electric field. The photons, hitting the structure, excite the electrons and create electron-hole pairs. Due to the electric field, these couples tend to separate increasing the voltage in the junction. About the connection to the grid, a scheme is represented in fig. 2.7; compared to the WT diagram, generator, gearbox and blades are replaced with the PV arrays. This system provides yet DC power and it implies that only a DC-AC converter is needed. Nevertheless, usually also a DC-DC conversion stage is adopted in order to maximize the power that is extracted. Obviously, since the system is fully decoupled and there are no rotational parts, no inertia is provided by this device.

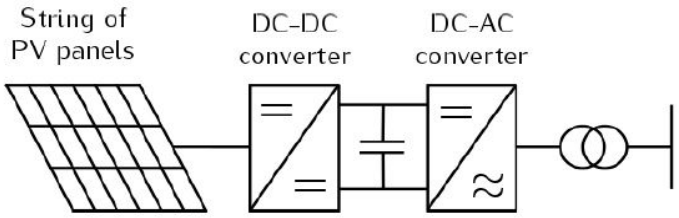

Figure 2.7: PV connection to the grid [14]

2.1 Low-inertia system

In the first chapter, the concepts of inertia and low-inertia system have been quickly introduced but with the increasing use of renewable sources they are

becoming of fundamental importance. Here, the definition of inertia is reminded and it will also be explained how to compute the inertia of a system. Before going on, it is important to specify what is the meaning of *low-inertia* and how this expression has to be seen in the rest of the work. In this context, it is taken into consideration the mechanical inertia of the system, i.e. the quantity that is provided by mechanical parts (for example, the turbines). With the increasing use of the converters, the SMs are going to be substituted and with them the mechanical parts. With this idea, a low-inertia system is a system with a low quantity of mechanical inertia. As it will be clarified later, however, in some cases there is the attempt to emulate the inertia (for example, introducing "virtual inertia"); this allows to have similar properties, but being the nature of this inertia different, this kind of system will also considered low-inertia one (in the sense of system with low mechanical inertia).
Coming back to the concept of inertia, it is one of the basis of the traditional mechanics and it is adopted to describe the motion of objects. It is possible to define the inertia as the resistance that a physical object make against a change of its velocity, considering both a change of the direction or of the speed. Let us consider an electrical system, with AC quantities, where the power is provided through traditional power plant (SM); in this situation, the rotational speed of the generators is linked directly with the frequency of the system. Therefore, in a grid with only SM and turbines, there is a huge quantity of inertia that is not only useful to face the sudden changes in rotational speed, but also it contributes in an important way to the stability of the frequency and voltage of the network.
Being nowadays the existing network mostly based on the SM, it is useful to recall the swing equation in per unit of a SM; reminding that the quantities T_m and T_{em} stand for, respectively, the mechanical and electro-mechanical power, indicating with f the standard frequency and with H the inertia it results [18]

$$2H\frac{df}{dt} = T_m - T_{em} \tag{2.1}$$

The parameter H is the inertia constant of the SM and it indicates the ratio between the stored energy at a rated speed and the rated apparent power of a given machine. From the relation just written 2.1, it comes that the inertia represents the resistance of a synchronous generator to the change of its frequency, which is imposed by a power imbalance. Referring to [14]

$$H = \frac{K}{S_n} = \frac{\frac{J(2\pi f^\star)^2}{2}}{S_n} = \frac{\frac{J{\omega^\star}^2}{2}}{S_n} \tag{2.2}$$

in which K stands for the kinetic energy, S_n is the rated power of the machine, J the momentum of inertia and $\omega^\star$ the rated rotational speed, the relation between the inertia and the kinetic energy of a rotational mass is described. Sometimes, the inertia of a single unit is also defined as $2H$, which is the time needed to the

machine to drive it to its rated speed $\omega^\star$ from null initial condition, applying a constant torque.
It is now possible to extend the concepts that have been analyzed for a single SM to a more complex AC power system, in order to study a way that allows the estimation of the total inertia of the network.
First of all, in a system where there are multiple generators of different size, all of them work at the same frequency (that is around the standard frequency) when they are in a steady-state condition. However, when a power imbalance takes place, that can be due to many reasons such as, for example, the tripping of a SM or a new load in the network, the generators will have a different oscillatory behaviour, determined by the relationship 2.1, around their centre of inertia. In any case, there are some expedient that help to keep the SM synchronized also when a power imbalance verifies; in particular, the damping property of the generators, together with the regulator of each machine which usually includes also a *power system stabilizer* (PSS), help the SM to keep the same speed, after a brief transient situation.
Thanks to this property of the system, there is the possibility to build an aggregate model of the network, considering all the SM which are in the grid as an unique big one, whose behavior is controlled by only one swing equation [14], that is:

$$2H_{tot} = \frac{df_{COI}}{dt} = P_{gen} - P_{load} \tag{2.3}$$

P_{gen} and P_{load} are, respectively, the power generated by the all SM and the power requested by the load, whose imbalance causes a change in the frequency of the system. In this case, it is taken into account the frequency of the center of inertia (COI), while the total inertia, H_{tot}, is obtained as a weighted sum of the inertia of all the generators [14]:

$$H_{tot} = \frac{\sum_i^n H_i S_{n,i}}{S_{n,tot}} = \frac{K_{tot}}{S_{n,tot}} \tag{2.4}$$

In 2.4, $S_{n,tot}$ stands for the total nominal power, i.e. the sum of the nominal power of each generator. Usually, the generators are projected to work at their nominal power, but in the reality they operate at a lower value. Finally, it is necessary to introduce the expression of the frequency at the COI [14], $f_{COI} = \omega_{COI}$, that is equal to

$$f_{COI} = \frac{\sum_i^n H_i S_{n,i} f_i}{H_i S_{n,i}} \tag{2.5}$$

Indicating with n the number of SM in a system, in a steady-state condition the P_{gen} by all the generators is equal to the one consumed by the load. Looking at 2.3, the total inertia of the system can be seen as the resistance, which is stored in the form of kinetic energy, that all the SM in a network oppose to the change of the speed of the COI, due to power imbalance. It is easy to understand that the inertia is not a constant parameter, but it changes according to the network

and to the typologies of generators that are connected to it.
The main problem of 2.3 is that in a real network, where the number of connected generators is really high, the frequency at each node results to be quite different from the one at COI, i.e. it will oscillate around COI when a fault is verified. An other problem is that to use a similar relation in a complex system it should be necessary to know exactly the power generated and the one consumed by the load, a thing almost impossible in a huge network. Finally, in the equation the damping effect of the SM is not taken into account, giving only an approximate model of the system.
Before going on with the problem related to the system stability in a low-inertia system, it is worth to analyze the contribution in terms of inertia of each generator, that can be really different according to the type. It is possible to make a distinction between the various components of the grid

- Conventional generators: the traditional power plants use SM to convert oil, gas, nuclear and hydro-power into electrical power and represent the devices that give the main contribute to the inertia of the system. The parameter H is usually between 2 and 9s for these types of generators. Depending on the typologies, the inertia is differently distributed between the rotor of the generator and the prime mover. Actually, there is no a strong correlation between the different SM (which are used for the conversion of different form of sources) and the constant of inertia. Most of all, this parameter is related to the design of the turbine and generator. It is instead possible to mention that the SM installed nowadays are usually lighter than the ones developed during the $'$70s.

- Wind and photo-voltaic power: as it has been yet explained previously, these two sources of energy require converter and, except for old types of wind turbines, the contribution in terms of mechanical inertia is quite low.

- Storage devices: also in this case, the quantity of inertia that is provided to the system depends on the technology which is used. Specifically, considering hydro storage and compressed air energy storage, they deliver an important quantity of inertia due to the presence of a synchronous generator for the connection to the grid. On the other side, considering chemical batteries, they are based on a power electronic converter to interface with the grid, and this means that they are not able to provide inertia to the network.

- Motor on load side: also on the load side, it can happen that motors are installed; in the case of pumps or fans, for example, they work exactly as a SM and so they are able to contribute to the inertia of the network. Actually, in every grid (residential and industrial) motor constitute a fundamental components and they consume around $60 - 70\%$ of the power

which is provided to the network. As it is expected, however, only the motors which are used in the industries contribute significantly to the total inertia, while small machines are characterized by a low value of inertia constant. It is also worth to mention the case of the motors that are equipped with variable speed drive (VSD), that do not provide contribute in terms of inertia due to their electrical decoupling. These types of machines are increasing their importance in the last years, contributing to decrease the total inertia of the grid.

In the table below 2.1, the inertia coefficient of the main elements of the network are reported, in order to summarize what has been explained previously. The inertia coefficient is usually expressed referring to the nominal power; as a consequence, also the size of the machine is fundamental to establish the contribution of a single component.

Energy source type	**Generator**	**Power electronics**	**Inertia**
Conventional power plants (hydro, nuclear, gas, oil)	SG	/	H=2-9s
Concentrated solar power	SG	/	H=2-9s
Wind Power	IG (Type 1-2)	/	H=5s
Wind Power	DFIG (Type 3)	AC/AC to rotor windings	0
Wind Power	SG, PMSG (Type 4)	AC/AC with intermediate DC bus	0
PV Power	/	DC/AC with intermediate DC bus	0
Microturbines	SG, IG	Optional: AC/AC with intermediate DC bus	Without AC/AC H=1-4s
Battery storage	/	DC/AC with intermediate DC bus	0
Synchronous condenser	SG	/	H=1s

Table 2.1: Technology of interface and inertia coefficient [14]

At the end of the day, in a real system there is a huge number of small generators and load units that are equipped with a motor; the estimation of the total inertia of the system is, therefore, quite difficult, also if in the last years different tools have been developed to estimate the inertia. Being not possible to know

in an exact way the inertia of a network, and also considering that it varies a lot according to the moment of the day and the period of the year, the main fact is that the traditional power plants contribute in a significant way to the amount of the inertia of a given grid. Due to this reason, the introduction of new sources of energy based on power electronics devices are leading to a transition towards low-inertia grid, which are characterized by new stability problems that need to be clarified. The main issues related to these types of network are going to be treated in the next section.

2.2 The Low-Inertia System stability

In the previous section, the problem of stability in a low-inertia system has been briefly mentioned and in the last part the concept of reserve has been illustrated. Actually, the power system stability is a problem on which lots of studies have been done since quite long time; in 1967, the *"IEEE Poower System Dynamic Performance Committee"* was founded and now it is formed by two subcommittees: the *Power System Stability* and the *Power System Stability Controls*[**?**]. A definition of power system stability has been formulated in [3] and states that *"Power system stability is the ability of an electric power system for a given initial operating condition, to regain a state of operating equilibrium after being subjected to a physical disturbance, with most system variables bounded so that practically the entire system remains intact"*.
In a large scale system as the ones represented by the electrical grid which are going to be studied in the following chapters, it is clear that the interest is for the overall system stability, while in some cases a local instability can be accepted, as in the case of a motor stall or of a small region which can become unstable. As in a mechanical system, also in the network at the equilibrium the forces result balanced; lots of disturbances can occur and they are different from multiple points of view; specifically, it is possible to distinguish between small and big ones, but also they can be classified as short circuit, load variances or loss of a generator. From a control point of view, the focus is on how the system reacts to disturbances which can really verify in the system; indeed, it is not possible to create a system able to be stable for all the disturbances, especially the big ones, but it is important that it can regain a new equilibrium in particular real situations. At each equilibrium condition, the system has a region of attraction, which determines the magnitude of the disturbances that the system can supply;the larger is this region, of course, the larger are the faults which it can face to.
In the case of a failure, different behaviors could occur in the grid; first of all, if the fault happens in a critical device, it might be possible that a protective element leads to the switch off of the component, in order to preserve it; this event causes variations and fluctuations in all the other devices of the grid, which need to be controlled and that can also lead to instability. If the instability condition

persists, a worst situation can also occur: an increasing number of generators and other devices can switch off in order to avoid further damages but this has as counter-effect an increment of the instability of the system. This is, for example, the situation which verifies in Australia, on 28th of September, 2016; due to a violent storm, lot of protection devices were activated in order to protect the generators, switching them off; after multiple automatic attempts of restarting them, being the quantity of energy required too high, the system went black. In order to solve the problem, a human restart of the units has been necessary; first of all, it has been created a connection with a region close to the one where the event verifies in order to supply the network with a stable frequency, and then gradually the generators have been restored. Only in the first days of January 2017 the problem was partially solved, but the last works to repair the damaged structures finished only 12 months later [19].
However, it can also happen that the system is stable after a fault, and so it reaches a new equilibrium point. In this case, an automatic control can also be used to take the system back to the normal conditions.

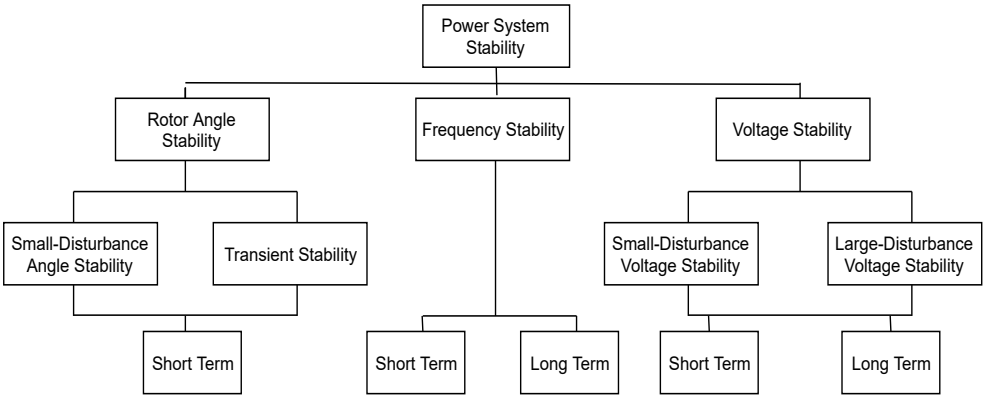

Figure 2.8: Classification of the power system stability [20]

Being a power system extremely complex, due to its high non-linearity, also if the problem of stability can be seen as a single issue, it is useful to classify the stability of the system in different categories. As explained in [2] and in [20], and also illustrated in Fig. 2.8, there are three main classes of stability:

1. Rotor angle stability: it represents the property of the synchronous machines which are located in an interconnected grid to keep the synchronism when disturbances occur; in particular, this type of stability is directly linked to 1.1, because it depends on the capability to restore the equilibrium between the mechanical and electromechanical torques after a fault; in the case of instability, there is an increasing of angular swings in one or more generators, which leads to the loss of synchronism with respect to the other ones of the grid. Specifically, in a condition of equilibrium, all the generators are synchronized and rotate at the same speed. If a distur-

bance appears, the condition of equilibrium is broken and the rotor starts accelerating or decelerating respectively if the load increases or decreases. Consequently, the synchronism of the involved rotor with respect to the other ones is lost, but when this happens, the load is partially transfer from the slow machines to the faster one, in order to slow it down. Nevertheless, the relationship between power and angular displacement is not linear at all; if the speed of the rotor overcomes a certain limit, the load transfer starts decreasing, leading to an increment of the angular displacement; in this case, there is a situation of instability and the synchronism is lost. A further subdivision in the rotor angle stability can be done; there are

- Small disturbance rotor stability, which is referred to the capability of the system to maintain the synchronism in presence of small disturbances (i.e. a disturbance can be considered small if it is possible to linearize the system in order to analyze it). These events are considered short time disturbances, because the studies need to be done $10 - 20$ seconds after the fault occurs.
- Large disturbance rotor stability concerns with the ability of the system to keep the synchronization when a strong fault happens in the network, such as a short circuit on a transmission line. Being the size of the disturbance quite big in this situation, the relationship between the angular displacement and the power is non-linear. Also these disturbances are classified as short term ones, because the interest is in the $3 - 5$ seconds after they verify in case of reduced size system, or $10 - 20$ seconds if the analysis is based on a large one.

2. Frequency stability: it represents the ability of the system to keep steady frequency when the system works in normal operation conditions and to regain the nominal value in case of large contingencies which happen in the system and cause a large imbalance between the load and generation. If the unbalance between load and generation is too high, the instability in the system causes frequency swings.
   When strong imbalances occur in the system, strong variations of frequency, power flows and voltage may verify; due to this severe changes, the control and protection of the system do not follow the studies on the transient stability. Depending on the size of the fault and on the components which are involved, the controlling actions can be actuated in a short-term scale (considering for example the protection of a generator unit which switches it off) but also in a long-term scale (referring to the action of turbine overspeed control).
   It is also important to remind that in the electric grid there is the necessity to keep the frequency really close to the nominal value (60Hz in America and 50Hz in Europe); with the increasing use of converter technologies in place of the traditional SG, the total inertia of the grid decreases and

consequently also the primary response that it could provide. This reason explains the importance of projecting controllers which guarantee an adequate primary, secondary and also tertiary response, in order to avoid damages to the components of the system or blackout.

3. Voltage stability: it refers to the capability of the system to keep steady voltages at all buses after contingencies have verified; in order to reach this goal, it is necessary to have an equilibrium between the voltage which is supplied and the one that is required from the load. If the voltages are not kept constant, a fall or rise of voltage in some areas occur, creating instability in the system. If the fault at one bus is too large, it can happen that multiple generators activate their protection system and disconnect from the network, preventing further damages, leading to cascading outages. In the worst situation, a *voltage collapse* can also take place, when lot of generators are switched off and an huge quantity of voltage is required only to the generators that are still working. In this case a blackout verifies, because the system is not able to supply sufficient power. Nevertheless, the voltage instability is usually linked to the loads; in particular, when there is a contingency, the system tries to balance the power through rotor slip adjustment but this increases the stress on high voltage network. As counter-effect, the increasing in the demand of reactive power implies more voltage reduction and, if the disturbances overtake the capability of the network, a phenomena of instability occurs. It is also possible to talk about two different groups of voltage stability, as it has been done in the case of angle rotor stability:

   - Small disturbance voltage stability concerns with the ability of the system in keeping a steady voltage when small contingencies are applied to the system (i.e. a constant increment of the load). According to the characteristics of the load, the continuous and the discrete control, the system will be stable or not. In presence of these types of disturbances, the system can also be linearized and this operation allows to better understand which are the main factors which determine instability around a given configuration; however, it is necessary to remind that this procedure does not take into account nonlinear aspects, such as saturation or discrete steps.
   - Large disturbance voltage stability is referred to the capability of the system to maintain the voltage constant also when a large disturbance occurs in the system, such as a large fault or loss of generation. In order to determine if the system can keep voltage stability when a strong contingency verifies, it is necessary to analyze the load and the system behaviors, and also the discrete and continuous control and protection. Moreover, in this case the behaviour of the system is completely in the non-linear region, so sometimes it could be necessary

to study it for some minutes.

Finally, it is also useful to remind that also in the case of voltage stability there are different scales of time in which it is necessary to operate; on one side, with components characterized by fast acting load (the induction motors, for example), the control needs to be done in terms of second, through the solution of differential equations; on the opposite side, with components characterized by a slower acting load, such as generator current limiters, the analysis can also require several minutes with the aim of well understanding the behavior of the system.

Chapter 3

Grid-following and Grid-forming converters

3.1 Grid-following converters

The grid-following converters are the first that are taken into consideration; they are also known as *grid-feeding* or *grid-imposed* converter, due to the reason that they look at the characteristic of the grid in terms of frequency and phase angle through a PLL and adapt themselves to the grid properties. Specifically, in order to put this kind of converters inside the network, the AC has to be kept stable from the other devices connected to the grid (the SM or grid-forming converters). This fact represents the cause for which in most cases it is not possible to have a network with only grid-following inverters and SM or grid-forming converters are required. The focus in this chapter is not the structure of the converter itself, but how the control system is built.

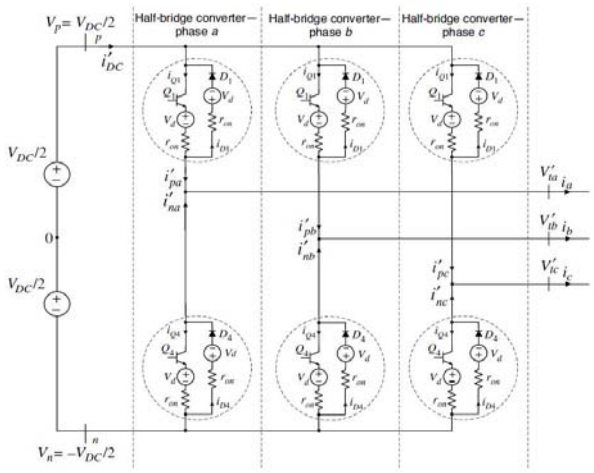

Figure 3.1: Model of a non-ideal two-level VSC [21]

In order to have the three-phase voltage source converter (VSC) that is adopted in the model, an half-bridge inverter is used, whose principle of working is presented in details in [21]. If the goal is to design a three-phase VSC, three half-bridge converters are put together, in the way that is depicted in Fig. 3.1. On the DC-side, a simple voltage-source can be connected, that can be for example a PV or a wind-turbine. The AC terminals can vary between $-V_{DC}$ and $+V_{DC}$, according to the configuration of the switches, and they can be connected to an utility grid through a resistive-inductive branch. There is a node, called *point of common coupling* (PCC), where the VSC and AC systems are linked; here the exchange of power between the two systems take place. In Fig. 3.2 the connection between the two parts is depicted; in this case, it has been chosen an *infinite bus* (IB) as grid on the AC side, which is able to impose the frequency to the system. The interest is to build a real/reactive power controller with the aim of keeping the power of the connected grid at a reference value.

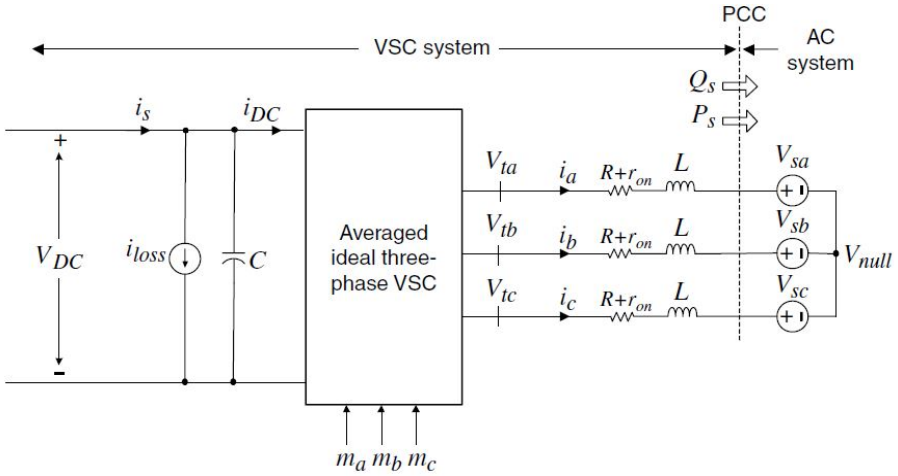

Figure 3.2: Model with the connection between a VSC sytem and an AC grid [21]

Before developing more in details the structure of the controller, it is worth to mention why it has been adopted the $dq - frame$. The same results can be obtained using the standard $abc - frame$, but a first transition towards an $\alpha\beta - frame$ is useful to reduce the number of signals that need to be controlled from three to two. The second step is represented by the transformation in $dq - frame$, which has the further advantage of working with DC quantities instead of sinusoidal signals (as regards the variables of interest that have to be controlled); the drawback of this strategy of control is that it needs a synchronization, that is performed through the PLL. A brief explanation of how this two transformation are performed is given in the Appendix B.
There are two different approaches that can be implemented for the control of the active and reactive power in the VSC system: *voltage-mode control* and

current-mode control. Here, only this second method is going to be explored, since it is the one that has been adopted for the simulations. Nevertheless, for a more exhaustive explanation the reader can referred to [21]. In the structure of this type of controller, which is represented in Fig. 3.3, the line current of the VSC is controlled through a current-regulator which is built on the AC-side. Moreover, in order to guarantee a control of the active and reactive power, the phase angle and amplitude of the VSC line current are compared with the one measured at PCC. One of the main advantages of the current-mode control is the possibility to protect the VSC from current overload thanks to the current regulator. Moreover, it results more precise in control performance and more robust to parameters variation of the VSC with respect to the voltage-mode.

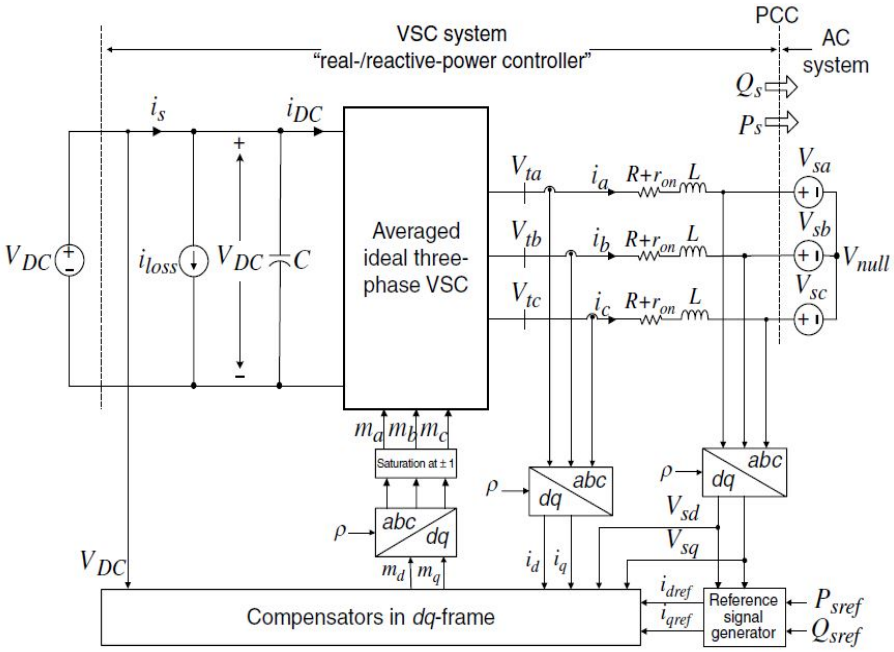

Figure 3.3: Model of a current-controlled controller in $dq - frame$ [21]

Referring to the block scheme, the reference signals are the active and the reactive power, indicated respectively as P_{ref} and Q_{ref}, while the measured signals are taken at the PCC, where the i_{abc} current and v_{abc} voltage are computed. Through a conversion in the *dq-frame*, these signals are compared to the reference ones and the i_d and i_q current components are generated. The protection of the VSC is ensured by the saturation block, which limit the currents that enter in the device.

3.1.1 Dynamic model of the real and reactive power controller

In this part it is reported the dynamic model of the controller of the active and reactive power for the scheme depicted in Fig. 3.3. It is possible to express the AC voltage in the VSC in 3.1

$$\begin{aligned} V_a(t) &= V_p cos(\omega_o t + \theta_0) \\ V_b(t) &= V_p cos(\omega_o t + \theta_0 - \frac{2\pi}{3}) \\ V_c(t) &= V_p cos(\omega_o t + \theta_0 - \frac{4\pi}{3}) \end{aligned} \tag{3.1}$$

where V_p represents the peak value (line to neutral voltage), ω_0 stands for the AC frequency and finally θ_0 is the initial phase angle. Rewriting the previous equations using the space-phasor, it results

$$\vec{V} = V_p e^{j(\omega_0 t + \theta_0)} \tag{3.2}$$

The dynamic of the AC-side of the VSC can be obtained through the next equation

$$L\frac{d\vec{i}}{dt} = -(R + r_{on})\vec{i} + \vec{V}_t - \vec{V} \tag{3.3}$$

where with $\vec{V}_t$ is indicated the voltage before the filter RL. Substituting in 3.3 the expression found before for $\vec{V}$, it is possible to write

$$L\frac{d\vec{i}}{dt} = -(R + r_{on})\vec{i} + \vec{V}_t - V_p e^{j(\omega_0 t + \theta_0)} \tag{3.4}$$

Now, expressing the last relation using the *dq-frame* transformation, i.e. considering $\vec{i} = i_{dq} e^{j\phi}$ and $V_t = V_{tdq} e^{j\varphi}$, it becomes

$$L\frac{d}{dt}(i_{dq} = -j(L\frac{d\varphi}{dt})i_{dq} - (R + r_{on} i_{dq} + V_{tdq} - V_p e^{j(\omega_0 t + \theta_0 - \varphi)} \tag{3.5}$$

Splitting the previous equation in the real and imaginary parts, and introducing a new control variable defined as $\omega = \frac{d\varphi}{dt}$, leads to

$$\begin{aligned} L\frac{di_d}{dt} &= L\omega(t) i_q - (R + r_{on}) i_d + V_{td} - V_p cos(\omega_0 t + \theta_0 - \varphi) \\ L\frac{di_q}{dt} &= -L\omega(t) i_d - (R + r_{on}) i_q + V_{tq} - V_p sin(\omega_0 t + \theta_0 - \varphi) \end{aligned} \tag{3.6}$$

In the last relationships, i_d, i_q and ϕ are the state variables, while V_{td}, V_{tq} and ω are the inputs of the controller. Observing 3.6, it is easy to understand that it is a non-linear function, due to the presence of $\omega i_d, \omega i_q$, $cos(\omega_0 t + \theta_0 - \varphi)$ and $sin(\omega_0 t + \theta_0 - \varphi)$.
It can be proved that the utility of the *dq-frame* depends on the choice of $\varphi(t)$

and ω; therefore, considering $\omega = \omega_0$ and $\varphi(t) = \omega_0 t + \theta_0$, equation 3.6 can be rewritten as

$$\begin{aligned} L\frac{di_d}{dt} &= L\omega_0 i_q - (R + r_{on})i_d + V_{td} - V_p \\ L\frac{di_q}{dt} &= -L\omega_0 i_d - (R + r_{on})i_q + V_{tq} \end{aligned} \tag{3.7}$$

The system that has been obtained is a linear second-order one, excited by V_p. This means that, if V_{td} and V_{tq} are DC quantities, also i_d and i_q will be DC variables. The component that guarantees that $\varphi(t) = \omega_0 t + \theta_0$ is the PLL, whose structure is going to be analyzed in the next paragraph.

3.1.2 The phase-locked loop (PLL)

The correct design of the phase-locked loop represents one of the crucial point in the building of a grid-following device. Here, the structure is presented before from a theoretical point of view and in the second part it will be also shown the one that has been taken into account for the simulations.
Recalling 3.2, recalling the transformation in *dq-frame*, it is possible to write

$$\begin{aligned} V_d &= V_p cos(\omega_0 t + \theta_0 - \varphi) \\ V_q &= V_p cos(\omega_0 t + \theta_0 - \varphi) \end{aligned} \tag{3.8}$$

Using this relation, equation 3.6 can be rewritten in the following way

$$\begin{aligned} L\frac{di_d}{dt} &= L\omega(t) i_q - (R + r_{on})i_d + V_{td} - V_d \\ L\frac{di_q}{dt} &= -L\omega(t) i_d - (R + r_{on})i_q + V_{tq} - V_q \end{aligned} \tag{3.9}$$

From the second relation in 3.8, setting $\varphi(t) = \omega_0 t + \theta_0$ leads to have $V_q = 0$; based on this, the aim is to design a component which drives V_q at zero. For this purpose, it can be assumed a feedback law of the type

$$\omega(t) = H(p)V_q(t) \tag{3.10}$$

where $H(p)$ is a transfer function that represents the compensator, while $p = \frac{d(\cdot)}{dt}$ is a differentiation operator. Combining the second equation in 3.8 and reminding that $\frac{d\varphi}{dt} = \omega(t)$, it results

$$\frac{d\varphi}{dt} = H(p)V_p sin(\omega_0 t + \theta_0 - \varphi) \tag{3.11}$$

This last equation is the one that describes the PLL and it represents a nonlinear dynamic system; as it has been explained also previously, the goal of this component is to design φ in order to have $\varphi = \omega_0 t + \theta_0$. Due to the non-linearity of the system, it could be that the PLL does not work properly. For example, taking

as assumptions that $\varphi(0) = 0$ and $\omega(0) = 0$, leads to have a sinusoidal function of time in $V_p sin(\omega_0 t + \theta_0 - \varphi)$; if $H(p)$ has a low-pass frequency response, there are also small perturbations and the PLL generates an undesired behaviour in the system. In order to avoid this issue, it is reasonable to impose an initial condition to $\omega(t)$, defining $\omega(0) = \omega_0$, and also to set an upper and a lower limit that it can assume. Specifically, ω_{min} and ω_{max} have to be chosen close to ω_0, with the goal of guarantee small variations for $\omega(t)$. With the assumption that it has been made of choosing $\varphi = \omega_0 t + \theta_0$, the term $sin(\omega_0 t + \theta_0 - \varphi$ can be approximated with $(\omega_0 t + \theta_0 - \varphi)$. It results that equation 3.11 can be rewritten as

$$\frac{d\varphi}{dt} = H(p)V_p(\omega_0 t + \theta_0 - \varphi) \tag{3.12}$$

This relation represents a feedback loop, were $\omega_0 t + \theta_0$ is the input, while φ constitutes the output. In the block diagram of the PLL, represented in Fig. 3.4, the transfer function is represented by the product between $H(p)$ and V_p.

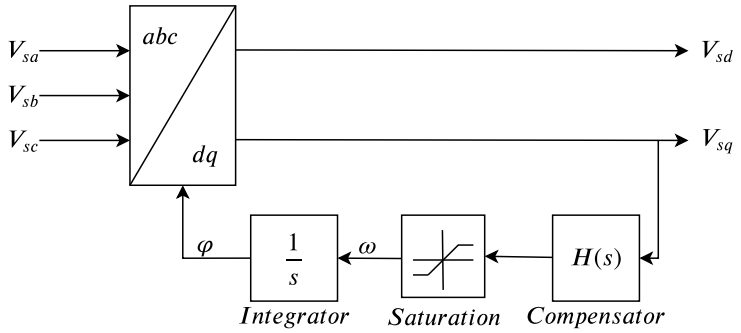

Figure 3.4: Structure of the PLL

In the simulations, it has been used the PLL block of the *Simscape* library of Simulink; the schematic diagram is reported in Fig. 3.5.

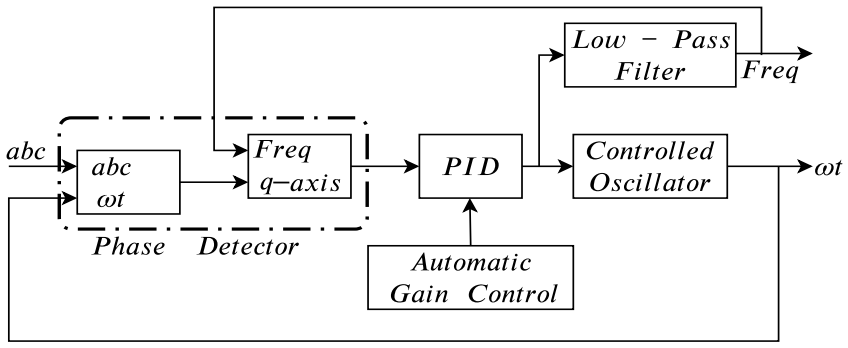

Figure 3.5: Structure of the PLL-block of the Simscape library

Comparing the two schemes, in the one implemented in Matlab the transfer

function is represented by a PID controller and the integrator is substituted by a voltage-controlled oscillator (VCO); this last block works as an integrator, that is reset each time that its output, φ, reaches 2π. Finally, with respect to Fig. 3.5, in the simulations the automatic gain control has been disabled. The control is simply the PID, which balances the difference in frequency.

3.2 Grid-forming Converters

The main drawback of the grid-following inverters is that they require the presence of a stable AC voltage, that has to be provided by other elements of the network (SM or grid-forming converters). For this reason, it is not possible to obtain a full replacement of all the synchronous generators with grid-following devices.
Grid-forming converters have a totally different control approach and represent the best solution available nowadays in order to achieve a converter-based system. At the moment, the focus is to move the use of this topology of inverters from the isolated system and micro-grid to the transmission and distribution network; in the simulations, it will be shown that it is possible to increase the level of penetration of grid-forming converters inside the grid, till the achievement of a 100% converter-based system. However, in this work, it has not been taken into consideration that the converters that are used in the reality are able to provide less power compared to the quantity available from a synchronous generator. This will imply to have a more-populated network, i.e. an high number of devices that will replace the traditional power plant. The main advantage of the grid-forming converters is that they are able to set the amplitude and the grid voltage, and so a PLL is not required to compute the frequency of the network. As it has been mentioned before, they are also able to support black-start and load-sharing, without the need of a minimum quantity of inertia, if their control-system is well built.
In Fig. 3.6, the common structure of the grid-forming converter used in simulations is represented. It works as an (ideal) AC voltage source, where on the DC-side there is a controllable current source, i_{dc}, which provides the energy to the system. It is connected in parallel with a resistance, R_{dc} and a capacitance, C_{dc}. Here, it is not represented in detail the stage of conversion from AC to DC voltage, but it can be considered the same of the one used for grid-following devices. The principle of operation is a three-phase average model which is driven through a modulating signal, m_{abc}. On the AC-side, there is a three-phase RLC filter, where the parameters are C_f, R_f and L_f and are the same for all the phases.
Specifically, looking at the model reported previously, it is possible to write the equations for the DC and AC side of the converter, indicating with i_{dc} and $v_{dc}$the current and voltage at the DC source, with C_{dc} and R_{dc} the capacitance and the resistance on the DC side and with i_p, v_p and i_s, v_s the current and voltage

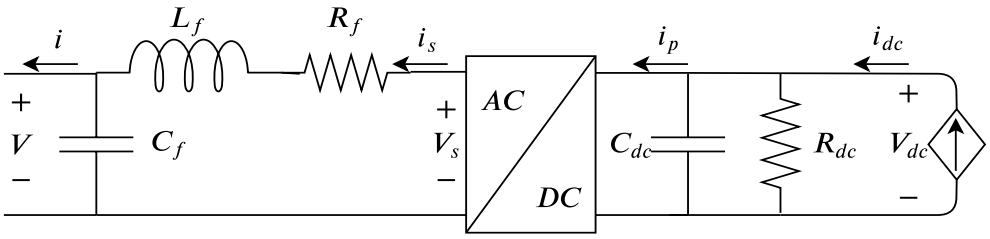

Figure 3.6: Model of a converter with RLC filter

before and after the conversion, respectively. Finally, the i and v quantities indicate the final current and voltage. It results, for the current on the capacitor on the DC side,

$$C_{dc}\dot{v}_{dc} = i_{dc} - \frac{v_{dc}}{R_{dc}} - i_p \tag{3.13}$$

while, the voltage at the inductance and the current on the capacitor on the AC side are given by

$$\begin{aligned} L_f\dot{i}_s &= v_s - R_f i_s - v \\ C_f\dot{v} &= i_s - i \end{aligned} \tag{3.14}$$

Referring to the nowadays situation, there are four main techniques of control which have been developed to regulate the grid-forming converters and which are going to be analyzed in the next paragraphs: droop, virtual synchronous machine, matching and dispacthable virtual oscillator control [22, 10]. In the next sections, these methods will be analyzed in details, but before it is useful to review the design of the control of the DC voltage that is the same for all the models.

3.2.1 DC Voltage Regulation

First of all, in order to have a more realistic model of the DC side [22], it has been used a first order system to obtain the current which enters in the energy source. In particular, defining τ_{dc} as the DC source time constant, i_{gen} as the current which is generated by the source and i^*_{gen} as the reference current for the DC side, it leads to

$$\tau_{dc}\dot{i}_{gen} = i^*_{gen} - i_{gen} \tag{3.15}$$

Moreover, the focus is also on the control of the reference current i^*_{gen}, which is realized through a combination of a proportional control of the voltage on the DC side and a feed-forward control of the nominal AC active power. The relation that governs the reference current is the following

$$i^*_{gen} = k_{dc}(v^\star_{gen} - v_{dc}) + \frac{v_{dc}}{R_{dc}} + \frac{p^*}{v^*_{gen}} + \frac{v_{dc}i_p - p}{v^*_{gen}} \tag{3.16}$$

where p^* stands for the reference of the AC power, p is the active power on the AC side injected in the system and the last term represents the feed-forward action; this control of the reference current on the DC side is needed in order to obtain a perfect tracking of the power and it is therefore applied for all the techniques. In the Fig. 3.7, the schematic of this controller is reported.

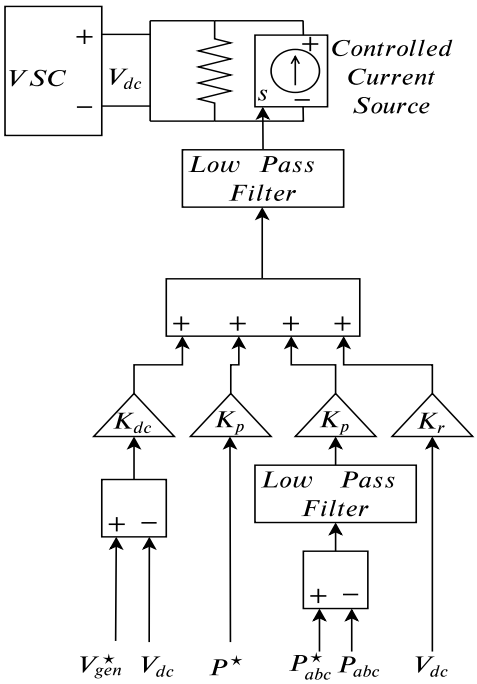

Figure 3.7: Scheme of the DC voltage regulation [22]

3.2.2 Droop Control

The first approach of control is strictly related to the speed droop property of the regulator of a synchronous generator [22, 23, 24, 25]; indeed, the power of a SM at the operating point is governed by the following law

$$p = p^* + d_p(\omega^* - \omega) \tag{3.17}$$

where p^* represents the reference power, ω^* the frequency set-point, p and ω the measured quantities and d_p is the droop gain.
In Fig. 3.8 the scheme of the droop control used in the simulation is drawn; the current and voltage measured after the filter on the AC-side, i and v, are used to compute the active and reactive power, p and q; In order to avoid the oscillations, before the computation these signals are filtered through a low-pass filter of the first order, described by

$$H(s) = \frac{\omega_f}{s + \omega_f} \tag{3.18}$$

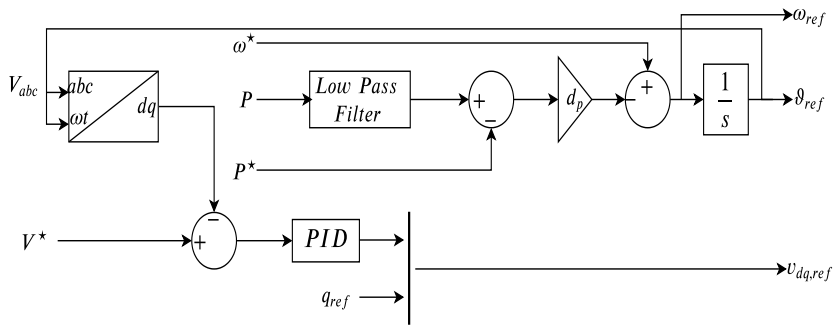

Figure 3.8: Scheme of the Droop Control Technique

where ω_f represents the cut-off frequency. Using the dq reference frame, it is obtained

$$\begin{bmatrix} p \\ q \end{bmatrix} = \begin{bmatrix} v_d & v_q \\ v_q & -v_d \end{bmatrix} \begin{bmatrix} i_d \\ i_q \end{bmatrix} \tag{3.19}$$

The droop gain, indicated as d_ω, regulates the frequency behaviour, through the balance of the active power, in the same way of 3.17; indicating with θ the angular position, it is possible to write the control law in the following way

$$\begin{aligned} \dot{\theta} &= \omega \\ \omega &= \omega^* + d_\omega(p^* - p) \end{aligned} \tag{3.20}$$

The part of the voltage control is built with the aim of mimicking the *automatic voltage regulator* (AVR) of a synchronous generator and it is obtained through a PI controller. Therefore, the reference voltage $v_{ref,d}$ and $v_{ref,q}$ for the converter results

$$\begin{aligned} v_{ref,d} &= k_p(v^* - ||v||) + k_i \int_o^t (v^* - ||v(\tau)||)d\tau \\ v_{ref,q} &= 0 \end{aligned} \tag{3.21}$$

It is useful to remind that $v_{\text{ref,q}}$ is balanced through the reactive power, whose injection is done in order to obtain the exact voltage regulation.

3.2.3 Virtual Synchronous Machine

This second approach, that is also called VSG (Virtual Synchronous generator), aims to mimic the behavior in terms of dynamic response of a SM, in order to take the advantages of the SM in terms of stability properties. Specifically, the common converters are not able to contribute to the damping of the system, which instead the SM can provide thanks to their inertia. Moreover, the virtual parameters of the VSM can be chosen arbitrarily. This means that it is possible to consider inertia, field and mutual inductance coefficients which are far from the ones of a real SM, with the advantage of no having magnetic saturation or

eddy currents. Finally, it can be observed that this approach results particularly simple from a conceptual point of view, since it is based on the emulation of the behavior of a physical machine.
Before going on with the model that has been adopted in the simulation, it is worth to remind that there are different typologies of VSM that have been proposed in the literature, but some of them do not exploit all the advantages that are offered from this technique, i.e. the possibility of working as grid-forming converter. Indeed, in some cases, a PLL is still used , with the goal of detecting the grid frequency and the voltage phase angle; as it has been explained before, when there is this component in the grid, the inverter has been classified as a grid-following one. As a drawback, adopting this design, it is not possible in most cases to obtain an only converter-based system.
In Fig. 3.9 it is drawn the scheme of the VSM with PLL, realized in accordance to what has been developed in [26]. In this configuration, the *reference current* block takes into consideration the information that the PLL provides and the voltage measured after the filter in order to compute the error signal, i_{dq}; after that, the current control part, based on the error, is responsible to provide the reference signal $V_{ref,abc}$ that governs the PWM process. The PLL, in this model, emulates the electro-mechanical behavior of a SM and also detects the phase angle of the grid, which is used in the $sbc - dq$ conversion.

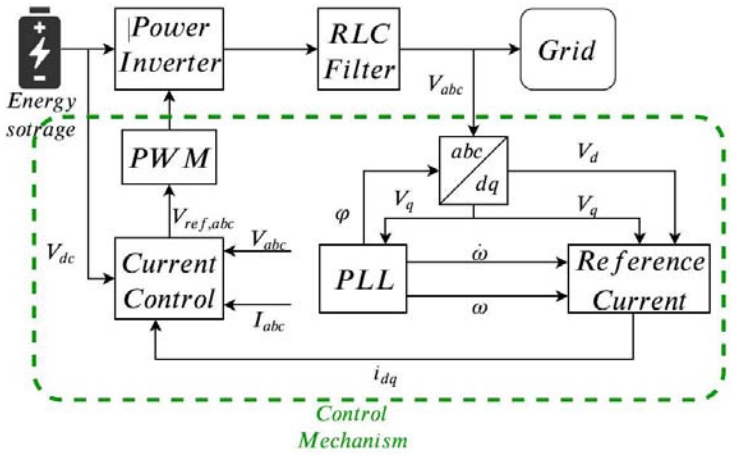

Figure 3.9: Scheme of the VSM Technique with PLL [26]

At this point, the model of VSM that has been used for the simulations is explained in detail and reported in Fig. 3.10, reminding that it has been built following what has been suggested in [22, 27, 28]. The frequency dynamics is controlled by

$$\begin{aligned} \dot{\theta} &= \omega \\ \ddot{\theta} = \dot{\omega} &= \frac{D_p}{J}(\omega^* - \omega) + \frac{1}{J\omega^*}(p^* - p) \end{aligned} \tag{3.22}$$

where the virtual damping and the inertia coefficient are indicated as D_p and J respectively, while p stands for the power that is measured after the filter. Of course, setting these parameters allow to obtain a converter that is able to emulate the damping characteristics of a real SM, but without having the mechanical inertia. These relations, which describe the frequency-droop behavior of a SM, is based on the concept of delivering to the grid a quantity of active power in relation with the frequency which is detected. Indeed, it is known that when an increment in the demand of the active power is detected, the speed of the generator decreases due to the bigger electromagnetic torque. Here, this mechanism is reproduced comparing the reference frequency, which is represented by the nominal frequency of the grid, with the angular speed and adding this difference multiplied by the gain D_p to the active torque.
The voltage control that generates the reference voltage for the converter is derived through

$$v_{ref} = 2\omega M_f i_f \left[sin(\theta) \qquad sin(\theta - \frac{2\pi}{3}) \qquad sin(\theta - \frac{4\pi}{3}) \right]' \tag{3.23}$$

where M_f and i_f represent the mutual inductance magnitude and the excitation current. The exact voltage regulation is obtained through a PI controller, similar to the one that has been implemented in the previous section for the droop control, with the goal of reproducing the AVR function of a SM. The law which regulates this part is the following

$$\begin{aligned} v_{ref,d} &= \frac{k_p}{M_f}(v^* - ||v||) + \frac{k_i}{M_f}\int_o^t (v^* - ||v(\tau)||)d\tau \\ v_{ref,q} &= 0 \end{aligned} \tag{3.24}$$

A useful thing to remind is that with this technique, in particular for a real implementation, is necessary to implement a low-pass filter (as the one that is drawn in the block diagram) to reduce the ripple in the measured voltage, since the terminal voltages could be not correctly balanced. This shrewdness will be essential especially for the simulations with the Quebec model and it is also suggested in [27].

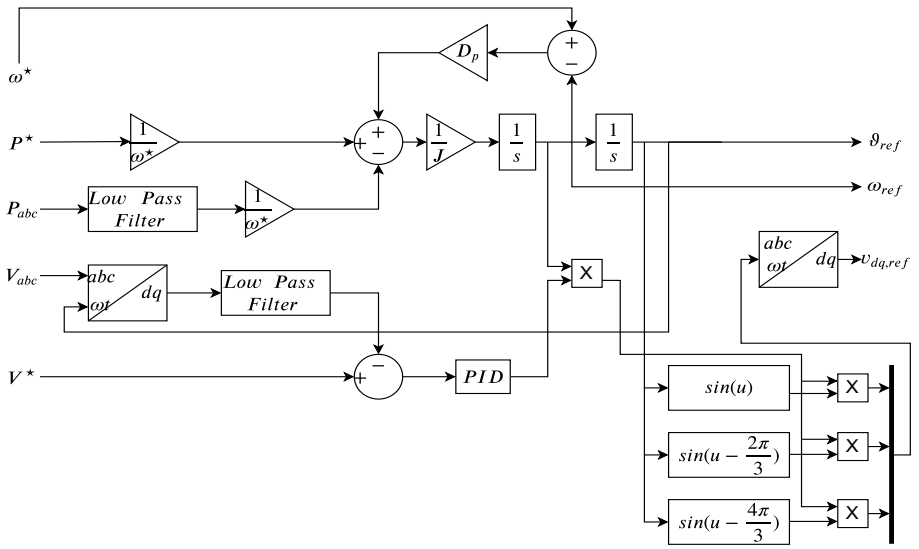

Figure 3.10: Scheme of the VSM Technique

3.2.4 Matching Control

This technique of control is partially different to the ones that have been presented before; as the name itself suggests, the matching approach is based on the attempt of drawing a correspondence between the model of a SM and the one of a power converter. Differently form the previous techniques, which were based on the measurement of AC quantities after the *RLC* filter (the injected power, for example), in this case the idea is to consider the DC voltage as a feedback signal of the power imbalance [22, 29, 30, 31]. Increasing the dynamics of the converter, an harmonic oscillator is implemented inside the model and looking at its frequency, it is possible to track the voltage on the DC bus. The output signal of the oscillator is therefore taken as input in the converter's PWM. The other properties of the previous inverters, i.e. droop and power-sharing, are still available also with this model.
To better understand how this control technique works, it is worth to analyze with more details the equations of the converter and of a synchronous generator. Referring to the model considered previously, assuming that the switching block is lossless so it guarantees energy conservation, it is possible to write in $\alpha\beta$ frame

$$i_p = \frac{1}{2} m'_{\alpha\beta} i_s, \qquad v_s = \frac{1}{2} m_{\alpha\beta} v_{dc} \tag{3.25}$$

where $m_{\alpha\beta}$ is the modulation signal. It is possible to rewrite relations 3.13 and 3.14 as it follows

$$\begin{aligned} C_{dc}\dot{v}_{dc} &= i_{dc} - \frac{v_{dc}}{R_{dc}} - \frac{1}{2}m'_{\alpha\beta}i_s \\ L_f\dot{i}_s &= \frac{1}{2}m_{\alpha\beta}v_{dc} - R_f i_s - v \\ C_f\dot{v} &= i_s - i \end{aligned} \tag{3.26}$$

In Fig. 3.11, the block diagram of this control scheme is drawn. With the goal of controlling the quantity of AC power which is provided, the DC current is taken into account; the equation for matching control results

$$\dot{\theta} = \omega = k_\theta v_{dc} \tag{3.27}$$

where $k_\theta = \frac{\omega^\star}{v^\star_{dc}}$. Considering a modulation signal in polar coordinates

$$m_{\alpha\beta} = \mu \begin{bmatrix} -sin(\theta) \\ cos(\theta) \end{bmatrix} \tag{3.28}$$

and defining the amplitude $\mu = -2k_\theta L_m i_f$, 3.25 can be rewritten as

$$i_p = -k_\theta L_m i_f \begin{bmatrix} -sin(\theta) \\ cos(\theta) \end{bmatrix} i_s, \qquad v_s = -L_m i_f \begin{bmatrix} -sin(\theta) \\ cos(\theta) \end{bmatrix} \omega \tag{3.29}$$

Referring to 3.26 it is possible to arrive at

$$\begin{aligned} \frac{C_{dc}}{k_\theta^2}\dot{\omega} &= \frac{i_{dc}}{k_\theta} - \frac{\omega}{R_{dc}k_\theta^2} - \frac{1}{2k_\theta}m'_{\alpha\beta}i_s \\ L_f\dot{i}_s &= \frac{1}{2k_\theta}m_{\alpha\beta}\omega - R_f i_s - v \\ C_f\dot{v} &= i_s - i \end{aligned} \tag{3.30}$$

In Appendix A, the model of the SM is developed in details; here it is of interest only to recall the dynamic model, to see in which way it is possible to compare it to the model of the converter that has been obtained. Combining the model of the stator and the rotor, it results

$$\begin{aligned} M\dot{\omega} &= -D\omega + P_m + L_m i_f \begin{bmatrix} -sin(\theta) \\ cos(\theta) \end{bmatrix}' i_s \\ L_f\dot{i}_s &= -L_m i_f \begin{bmatrix} -sin(\theta) \\ cos(\theta) \end{bmatrix} \omega - R_f i_s - v \\ C_f\dot{v} &= i_s - i \end{aligned} \tag{3.31}$$

where M and D stand for the rotor inertia and damping coefficients, while P_m is the mechanical power. Choosing $\frac{C_{dc}}{k_\theta^2} = M$, $\frac{1}{R_{dc}k_\theta^2} = D$ and $\frac{i_{dc}}{k_\theta} = P_m$, the two relationships result equal.

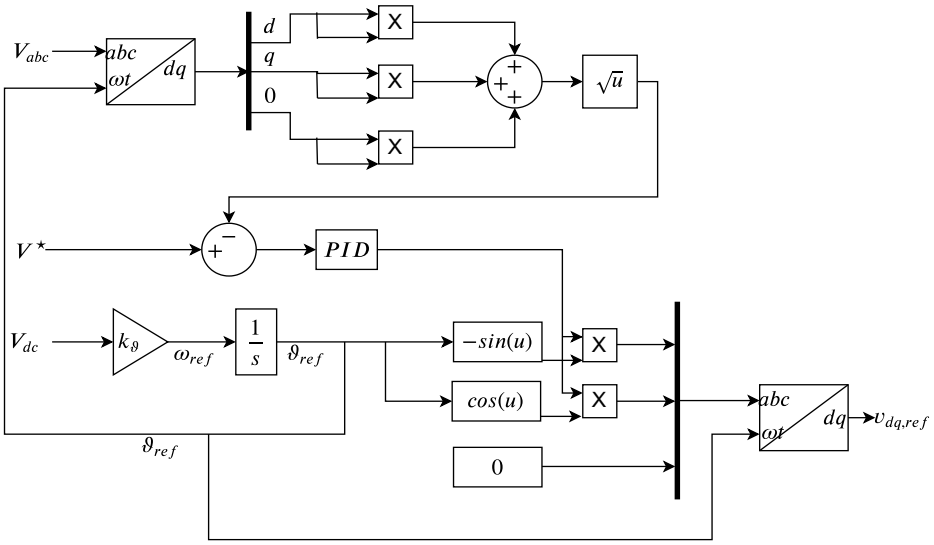

Figure 3.11: Scheme of the matching Technique

The voltage is controlled as in the other cases by the mean of a PI controller, which provides the modulation magnitude according to the following rule

$$\mu = k_p(v^\star - ||v||) + k_i \int_o^t (v^* - ||v(\tau)||)d\tau \tag{3.32}$$

Finally, the reference voltage for the controller in $\alpha\beta$ coordinates is given by

$$v_{ref} = \mu \begin{bmatrix} -sin(\theta) \\ cos(\theta) \end{bmatrix} \tag{3.33}$$

3.2.5 Dispatchable Virtual Oscillator Control

The previous approaches that have been studied try to mimic the behavior of SM and its droop characteristic, but to reach the goal inverters are used, which are characterized by a fast action but that have not inherent energy storage (i.e. they are low-inertia devices), in place of generators that have, instead, slow actuation but lot of energy stored in the rotor inertia. The *dispatchable virtual oscillator control* (dVOC) maintains the droop characteristic close to the steady state, but also enhances the dynamic performances, guaranteeing better voltage control.
This technique aims to reach synchronization in an inverter-based grid, but leaving the possibility to control the power-injection and the voltage regulation independently between the converters [22, 32, 33].

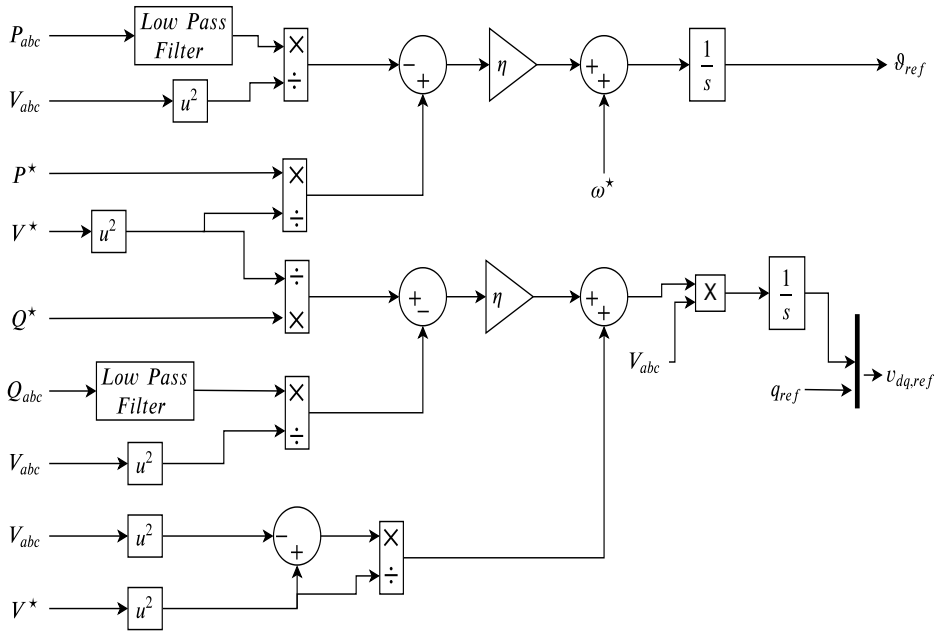

Figure 3.12: Scheme of the dVOC Technique

As it is possible to observe from the schematic above 3.12, the goal is, as for the other techniques, to provide a reference voltage to the inverter. Specifically, the dVOC control law is given by

$$\frac{d}{dt}v_{ref} = \omega^\star J v_{ref} + \eta\left(Kv_{ref} - R(k)i + \frac{\alpha}{v^{\star 2}}(v^{\star 2} - ||v_{ref}^2||)v_{ref}\right) \tag{3.34}$$

where v_{ref} represents the reference voltage written in $\alpha\beta$ frame, i is the measurement of the inverter current, the matrix $R(k)$ stands for a $2D$ rotation matrix of an angle k, i.e.

$$R(k) = \begin{bmatrix} cos(k) & -sin(k) \\ sin(k) & cos(k) \end{bmatrix}, \tag{3.35}$$

J represents the rotation matrix of $k = \frac{\pi}{2}$, i.e. $J = R(\pi/2)$. Furthermore, the matrix K is defined in the following way

$$K := \frac{1}{v^{\star 2}} R(k) \begin{bmatrix} p^\star & q^\star \\ -q^\star & p^\star \end{bmatrix} \tag{3.36}$$

The control parameters are respectively the angle k and the gains α and η, while the quantities $v^\star, p^\star, q^\star$ represent the set-point for the system. It is useful to make a note about the choice of the parameter k, which has to be set according to the line parameters; specifically, if there are resistive line the choice is $k = \frac{\pi}{2}$, while if there are inductive lines $k = 0$.

Being the relation written in the form of 3.34 not easy to understand, it is possible to rewrite it in the following way:

$$\frac{d}{dt}v_{ref} = \omega^\star J v_{ref} + \eta\left(Kv_{ref} - R(k)i + \alpha\phi v_{ref}\right) \tag{3.37}$$

where ϕ is defined as

$$\phi := \frac{v^{\star 2} - ||v_{ref}^2||}{v^{\star 2}} \tag{3.38}$$

In the form of Eq. 3.37, the term $\omega^\star J v_{ref}$ stands for the harmonic oscillation of the voltage v_{ref} around the frequency of the grid, $\omega^\star$. The term expressed by ϕv_{ref} can be interpreted as a voltage regulator; indeed, basing on the voltage error, whose expression is given by 3.38, the voltage is increased or decreased thanks to this term. Finally, the part given by $(kv_{ref} - R(k)i)$ has a double role, since it is used for phase synchronization with the rest of the grid but also to track the power reference.
It is worth to remind that the dVOC is reduced to a simple harmonic oscillator when the synchronization is reached and the reference voltage for the PWM is equal to the set point. In other terms, if

$$\begin{aligned} &(Kv_{ref} - R(k)i) = 0 \\ &||v_{ref}|| = v^\star \end{aligned} \tag{3.39}$$

that implies to have $(v^{\star 2} - ||v_{ref}||^2)v_{ref} = 0$, and choosing the case of inductive lines (i.e. $k = \pi/2$) expressed in polar coordinates, it is highlighted the droop characteristic of this technique of control. Indeed, reminding that

$$\dot{\theta} = \omega = \omega^\star + \eta\left(\frac{p^\star}{v^{\star 2}} - \frac{p}{||v_{ref}||^2}\right) \tag{3.40}$$

when the system is in the condition of being around the nominal voltage $v^\star$, i.e. $||v_{ref}|| \approx v^\star$, the relationship 3.40 is equivalent to 3.17 (that is the one that governs the simple droop control) whit droop gain $d_p = \frac{\eta}{v^{\star 2}}$.

Chapter 4

The network components

4.1 Network models

In all engineering applications, it is necessary to create a model in order to better understand how the object of the study behaves and how it is possible to control it. Also in the case of a network, as the ones that are studied in this work, a models constituted by set of equations is necessary to go on with the power system analysis. Properly, a model can be seen as a set of relations that describes the interactions between quantities in a particular frame of time. Depending on the level of accuracy that is required and on the goal of the study, different types of models can be obtained. In the specific case of network, it is possible to distinguish between two different levels of models:

- model based on the telegraph equation: it represents the general model of a transmission line, which consists on a partial differential equation that is transformed into a ordinary differential equation under the assumption of stationary sinusoidal conditions. The study of the stationary conditions at the nodes is based on these equations; however, these relations also include the transient along the lines and this implies a more expensive computational cost. Indeed, the interest is focused on the conditions of the network after the transient, but in order to reach this point also that region is taken into consideration.

- the lumped-circuit line models (π-models): it is obtained by solving the ordinary differential equations that have been obtained with the telegraph ones and focusing at the conditions at the end of the lines. Clearly, a model based on these equations, will contain the same quantity of information of the one analyzed before, but the computational cost will be much lower.

In this case, it is not difficult to understand which kind of model is the most convenient, but there are many applications in which is not easy to choose the correct one. In the specific, it is necessary to find the right trade-off between

the complexity of the chosen model, which is strictly related to the computational cost, and the capability of describing correctly the system basing on it. Moreover, higher is the complexity of the model, higher is also the number of parameters that need to be defined and the research of the appropriate value of these parameters can require lot of work. In the following, the algebraic models of the principal components of the network are described. In the rest of the work, when real networks will be analyzed, it will be not possible to describe them from a mathematical point of view, due to the huge number of parameters that is involved. However, the block of the models that are taken from the *Simulink* library are all based on differential equations.

4.1.1 Lines and cables

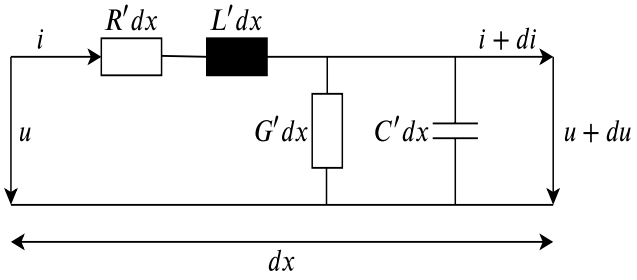

Figure 4.1: Diagram of the equivalent circuit of an element of length dx [34]

The equivalent general model for lines and cables is depicted in fig. 4.1 and it is described by two different types of parameters, the series and the shunt respectively. Considering the case of a line element of length dx, the quantities involved are:

- R' = series resistance/km per phase (Ω/Km)
- X' = series reactance/km per phase (Ω/Km)
- B' = shunt susceptance/km per phase ($siemens/Km$)
- G' = shunt conductance/km per phase ($siemens/Km$)

The parameters that have been mentioned are all specific for a given line and vary according to geometrical arrangements. It is also useful to remind that the reactance represents the imaginary part of the impedance, while the subsceptance constitutes the imaginary part of the admittance.
Starting from this model, after having studied the telegraph equations, the π-model is obtained, which is reported in fig. 4.2 [34]; in this case, the parameters necessary to describe the circuit between the generic nodes k and m are:

- $Z_{km} = R_{km} + jX_{km}$ = series impedance (Ω)

- $Y_{km}^{sh} = G_{km}^{sh} + jB_{km}^{sh}$ = shunt admittance ($siemens$)

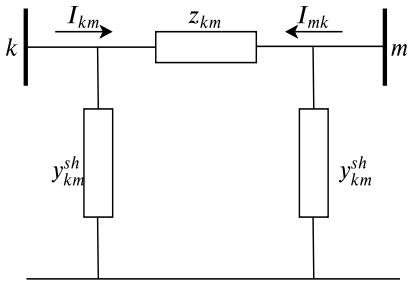

Figure 4.2: π-model of a transmission line between two nodes

Comparing to the general parameters mentioned before, these relations represent the one for the impedance and the admittance of the network. Regarding the notation, here the apex is missing being the model more general; in the remaining part of the chapter, moreover, the capital letters will stand for quantities expressed in *ohm* or *siemens*, while the lower case letters will indicate quantities expressed in *p.u.*. In order to formulate the network equations, it is requested to know the admittance matrix; for this reason, it is useful to derive the series admittance of the line, which results

$$y_{km} = z_{km}^{-1} = g_{km} + jb_{km} \tag{4.1}$$

where, respectively,

$$g_{km} = \frac{r_{km}}{r_{km}^2 + x_{km}^2} \qquad b_{km} = -\frac{x_{km}}{r_{km}^2 + x_{km}^2} \tag{4.2}$$

In the case of real lines, both the parameters x_{km} and r_{km} are positive and the consequence is that g_{km} is always positive while b_{km} is always negative. Moreover, in an actual line also y_{km}^{sh} and g_{km}^{sh} are positive, but the last one is in the majority of the cases so small that it can be considered negligible.
From the fig. 4.2, it is now of interest the expression of the complex currents I_{km} and I_{mk} that can be obtained through the analysis of the voltage at the respective nodes. Specifically,

$$\begin{aligned} Ikm &= y_{km}(V_k - V_m) + y_{km}^{sh} V_k \\ Imk &= y_{km}(V_m - V_k) + y_{km}^{sh} V_m \end{aligned} \tag{4.3}$$

In the last relationship, V_k and V_m denote complex voltage quantities. It is also possible to rewrite these relationship in matrix form, with the goal of highlighting the admittance matrix, which results symmetric with equal elements on the diagonal; the result is contained in the following relationship:

$$\begin{bmatrix} I_{km} \\ I_{mk} \end{bmatrix} = \begin{bmatrix} y_{km} + y_{km}^{sh} & -y_{km} \\ -y_{km} & y_{km} + y_{km}^{sh} \end{bmatrix} \begin{bmatrix} V_k \\ V_m \end{bmatrix} \tag{4.4}$$

4.1.2 Transformers

In the following analysis of the component, a simplified model is taken into consideration, where the magnetizing current and the no-load losses are ignored. It results an ideal transformer, with turns ratio t_{km} in series with an impedance, z_{km}, which represents resistive losses and the leakage reactance. Here, it is necessary to make a distinction, depending on if the ratio t_{km} is real or complex. Specifically, in the first case the transformer is called *in-phase*, while the other one is said *phase-shifting*[34]. In the following chapters, only the firs kind of transformer is going to be used; for this reason, it is the unique briefly described.

In-phase transformers

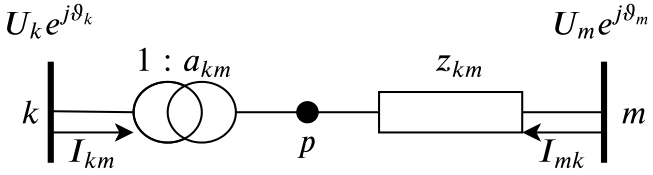

Figure 4.3: Scheme of the in-phase transformer [34]

In Fig. 4.3 an in-phase transformer is depicted. Considering also the node in the middle of the transformer, before the impedance, the ideal voltage magnitude ratio is defined as

$$a_{km} = \frac{U_p}{U_k} \tag{4.5}$$

Being in this specific case also $\vartheta_p = \vartheta_k$, the ratio just reported is also the one existing between the complex voltages at nodes k and p, i.e.

$$a_{km} = \frac{U_p e^{j\vartheta_p}}{U_k e^{j\vartheta_k}} = \frac{V_p}{V_k} \tag{4.6}$$

Being the transformer ideal, there are no losses between the nodes k and p; this means that

$$V_k I_{km} + V_p I_{mk} = 0 \tag{4.7}$$

Combining this relation with eq. 4.6, the ratio between the currents is

$$\frac{I_{km}}{I_{mk}} = -a_{km} \tag{4.8}$$

It means that the complex currents are out of phase of 180°, being the parameter a_{km} real.
In order to obtain the π-model of the transformer, the coefficients of the equations of the currents I_{km} and I_{mk} are needed. It is possible to derive from the

model 4.3

$$\begin{aligned} I_{km} &= -a_{km}y_{km}(V_m - V_p) = -a_{km}y_{km}V_m + a_{km}^2 y_{km}V_k \\ I_{mk} &= y_{km}(V_m - V_p) = y_{km}V_m - a_{km}y_{km}V_k \end{aligned} \tag{4.9}$$

which is equal, in matrix form, to

$$\begin{bmatrix} I_{km} \\ I_{mk} \end{bmatrix} = \begin{bmatrix} a_{km}^2 y_{km} & -a_{km}y_{km} \\ -a_{km}y_{km} & y_{km} \end{bmatrix} \begin{bmatrix} V_k \\ V_m \end{bmatrix} \tag{4.10}$$

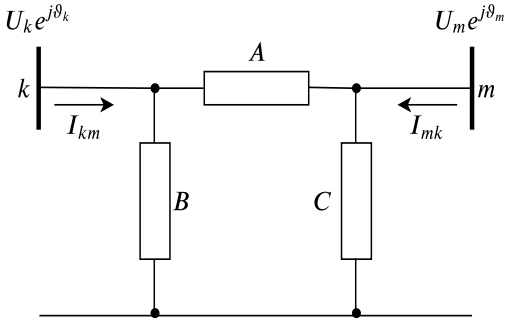

Figure 4.4: Scheme of the π-model of the in-phase transformer [34]

Referring to the π-model depicted in fig. 4.4, using the symbols A, B and C, the currents result

$$\begin{aligned} I_{km} &= (A + B)V_k - AV_m \\ I_{mk} &= -AV_k + (A + C)V_m \end{aligned} \tag{4.11}$$

which becomes in matrix form

$$\begin{bmatrix} I_{km} \\ I_{mk} \end{bmatrix} = \begin{bmatrix} A + B & -A \\ -A & A + C \end{bmatrix} \begin{bmatrix} V_k \\ V_m \end{bmatrix} \tag{4.12}$$

Combining now the coefficients of the eq. 4.10 with the ones of the last relation, it is possible to determine the parameters of the π- model. It yields that

$$\begin{aligned} A &= a_{km}y_{km} \\ B &= a_{km}(a_{km} - 1)y_{km} \\ C &= (1 - a_{km})y_{km} \end{aligned} \tag{4.13}$$

4.1.3 Loads

The loads constitute fundamental elements inside the network and in many high voltage systems, they constitute the source of power in the grid at a lower voltage level. Usually, the voltage in the distribution network, i.e. at low voltage, is kept constant and this implies that the power, both active and reactive, can be seen

as independent from the voltage at high voltage. As a consequence, the complex quantity $V_k(I_k^{load})^\star$ is maintained constant and it is not related to the voltage magnitude U_k. Referring to fig. 4.5, the current is considered to be positive when it enters in the network and it is governed by

$$I_k^{load} = I_k^{load}(U_k) \tag{4.14}$$

where $I_k(\cdot)$ represents the transfer function of the load. It is worth to remind that in lot of cases, the transfer function are given separately for the active and reactive power, resulting in

$$\begin{aligned} P_k^{load} &= P_k^{load}(U_k) \\ Q_k^{load} &= Q_k^{load}(U_k) \end{aligned} \tag{4.15}$$

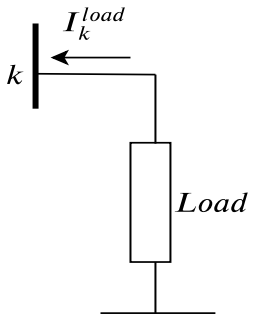

Figure 4.5: Model of a generic load connected to a node k [34]

In the models that are going to be taken into consideration, only constant impedance loads are involved, i.e an unchanging impedance like a resistor. Only in one situation (the simulation for the failure of the HVDC connection, that will be analyzed in the sixth chapter, a constant current load has been considered; this type of load varies its internal resistance to achieve a constant current regardless of the voltage which is being fed to it.

4.1.4 Generators

As it is possible to see from fig. 4.6, in load flow analysis generators are considered source of current. Their system of control is designed with the goal of keeping constant the active power and the voltage provided to the network at the generators terminals. Of course, generators supply a quantity of active power which depends on the demand of the network and that has to be in the range of what the generator can provide. Usually, generators are not forced to work at their limit conditions, because if in this situation an instantaneous supplement of power is needed, they saturate; in most of the case, they work around a nominal value, which is far from saturation.

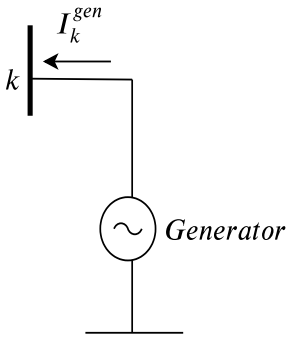

Figure 4.6: Model of a generator connected to a node k [34]

4.2 Scaling of a converter

The last component of interest for the tests that are going to be presented in the next chapters is the converter, that has yet been discussed in the previous chapter. In this part, a brief reminding of the converter's model is given, but the attention is centred in the way in which it has been designed a converter of huge dimension. As a matter of fact, in terms of dimension it is not possible to compare a converter unit with a real power plant, being the first a power electronic device with small capability while the second is usually a big size synchronous generator. Nevertheless, the goal of the following simulations will be the attempt to substitute the SMs which are located in different parts inside the network and that are the generators that nowadays supply the network with the converters technologies. In the real case it is known that converters of relatively small size are installed for different applications, especially on the root of the houses or of the factories. However, the strategy that will be taken into consideration in the next section is the scaling of a converter, i.e. taking as reference a converter of a specific size for which the parameters are known, bigger units will be considered as an aggregation of converters opportunely scaled.

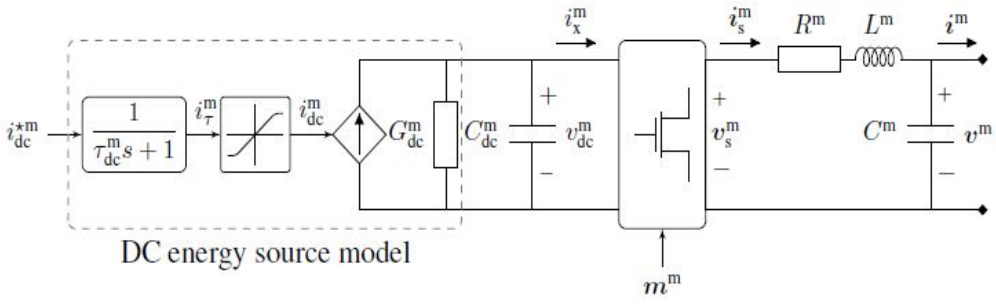

Figure 4.7: Scheme of the model of the converter with the DC-part [22]

First of all, it is useful to recall the model of a single converter, which is represented in fig. 4.7, where also the DC side is represented in detail. For all the remaining part of this chapter, it is possible to refer to [22]. The relations which describe the model depicted are the following:

$$\begin{aligned} C_{dc}\dot{v}_{dc} &= i_{dc} - G_{dc}v_{dc} - \frac{1}{2}m^T i_s \\ L\dot{i}_s &= \frac{1}{2}mv_{dc} - Ri_s - v \\ C\dot{v} &= i_s - i \end{aligned} \tag{4.16}$$

where, respectively, C_{dc} and G_{dc} stand for the capacitance and conductance on the DC-side while R, L and C are the parameters of the RLC filter of the converter. Regarding the other quantities, v_{dc} and i_{dc} are the voltage and the controlled current on the DC-side, m represents the modulation signal of the full-bridge averaged converter, i_s and v_s are the AC switching node current and voltage and i and v are the output quantities.
The aggregate model is developed from this simple one, specifically considering multiple AC converters of small size (hundred kVA) equipped with a low-voltage to medium-voltage (LV-MV) transformer. The configuration which derives is a sort of clusters of these modules which are connected to the network through a medium-voltage to high-voltage transformer (MV-HV).

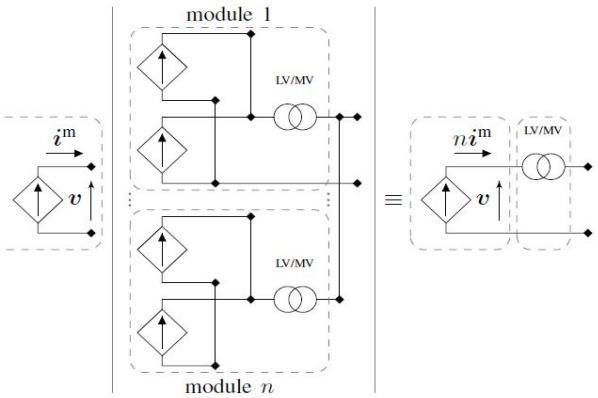

Figure 4.8: Scheme of the aggregated model of n converters [22]

In fig. 4.8, it is reported the scheme for a module of n converters. Referring to the work of [22], a scaling law is taking into account with the goal of obtaining the parameters of the modular system. Specifically, the relations that can be

found are, for the different parameters of the converter, the following ones:

$$\begin{aligned} G_{dc,scaled} &= 2nG_{dc} \\ C_{dc,scaled} &= 2nC_{dc} \\ R_{scaled} &= \frac{R}{2n} \\ L_{scaled} &= \frac{L}{2n} \\ C_{scaled} &= 2nC \end{aligned} \tag{4.17}$$

where the parameters on the right side are considered as the one of a single converter. It has been demonstrated that the choice of the parameters that result from the scaling of a converter following this idea leads to have parameters similar to the ones of the big units which exist in the reality.

Chapter 5

Simulation case study: IEEE 9-bus system

5.1 Description of the model

In this chapter, the goal is to test the techniques of control of the converters that have been described from a theoretical point of view in the previous sections, in order to validate them and to make some considerations about the results that are obtained. Specifically, the model that has been taken into consideration is the *IEEE 9-Bus System* (which is also known as the *"Western System Coordinated Council"*) and it has been widely used in studies of transient stability. There are different versions of the model which have been developed, but in this work as reference it has been considered the one used in [11].

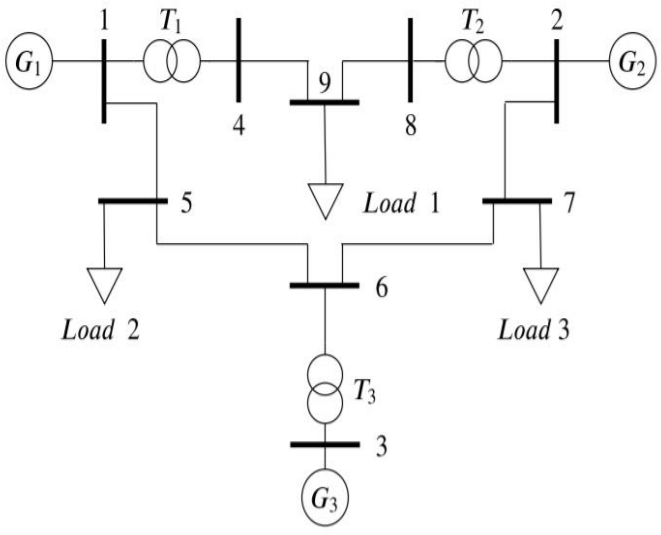

Figure 5.1: Simplified scheme of the IEEE 9-Bus System

In Fig. 5.1, it is depicted the structure of the network and the main components are highlighted. Observing the system, there are 3 generators (G) which are taken of the same size. They are located in different parts of the grid and they are connected to the network through 3 MV/HV transformers (T). Moreover, there are also 3 loads, which are located in different positions. In Fig. 5.2, it is figured the model that has been built in Simulink, where some other components have been added. In particular, the lines which link the parts of the network have been modeled using the *Three-phase RL-series branch* block of Simulink, in order to consider also the effects of the lines in the network. A switch is located after the generator n.1, which gives the possibility to simulate the behaviour of the network in case of disconnection of one power unit. Finally, a load disturbance is added to the original model, connected with an other switch; this last element is useful to study the system when a contingency happens, as it is, for example, in the case in which the load increases.

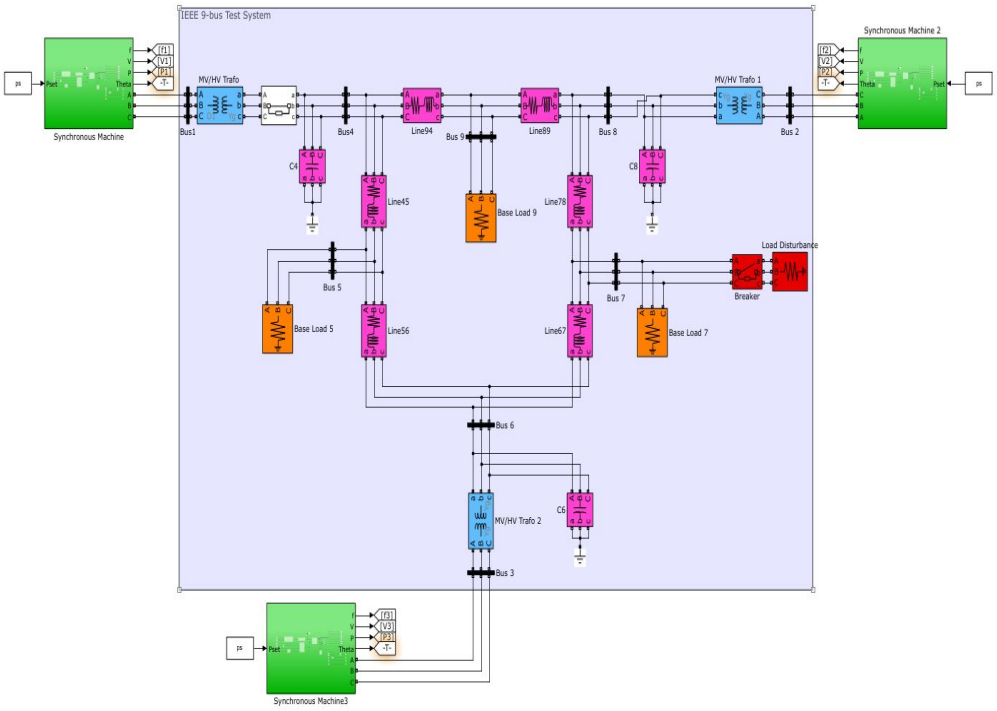

Figure 5.2: Simulink model for the IEEE 9-Bus System with all SM

In Fig. 5.2, the starting point of the study is depicted, where all the generators are represented by SM. This can be considered the model of a traditional simple network, where there are no renewable sources and all the energy is obtained through the combustion of fossil fuels. Therefore, the stability is guaranteed by the inertia of the SM, and the network is able to face the faults that could verify. Before going on with the simulations, it is worth to describe briefly the model

of the SM that is used. In Matlab/Simulink, there are different types of blocks that mimic the behaviour of the synchronous generators. The one adopted here is a three-phase SM, that can operate in both ways, i.e. as generator or motor, depending on the sign of the power that it receives as input [35]. As regards the electrical part, the machine is approximated through a sixth-order state-space model. All the quantities are viewed from the stator and the model of the circuit is described in the rotor reference frame (*dq*-frame). In Fig. 5.3, it is figured not only the SM but also the excitation system and the power regulator, in the same way in which they have been implemented in the test cases. The SM used in the simulations is equipped only with primary control on the active power; moreover, the input of the *Power regulator* and of the *Excitation system* are taken looking at the dynamics in the SM, in order to control the frequency and the power of the SM. Indeed, the goal is to reach the reference values that are chosen by the user for a specific configuration.

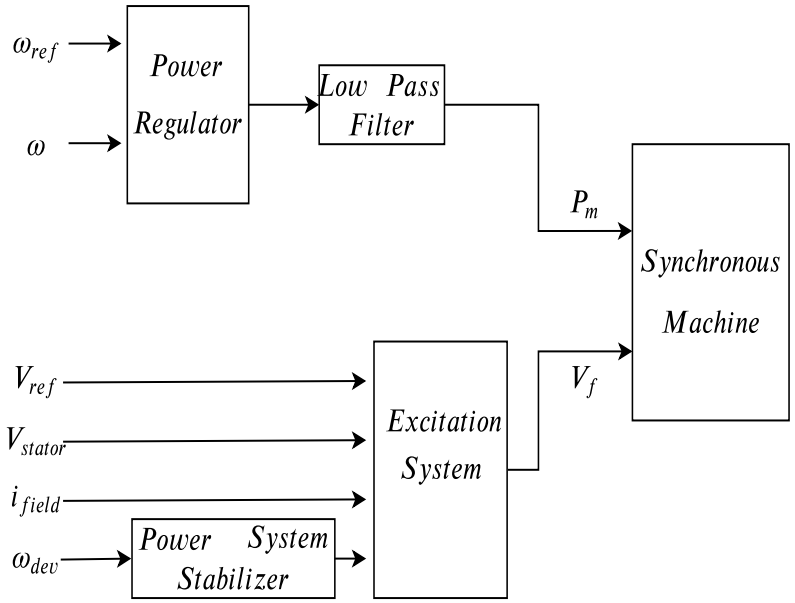

Figure 5.3: SM with excitation system and power regulator

In the tables contained in the Appendix D, the main parameters of the system are reported. In particular, at the beginning the simulations will be performed for a system where only SM are working, reproducing in this way the behaviour of a traditional system. The base values for the network and the synchronous generators are reported in Tab. D.1.It is important to remind that the MV/HV transformer is used for all the generators that are connected to the network. In the second table, Tab. D.2, there are the parameters related to a single grid-forming unit, which are scaled basing on what has been said at the end of the third chapter. Finally, in Tab. D.3, there are the values for a single grid-

following converter. It is important to remind that for the converters there is also a LV/MV transformer, which is put in the model in order to be more similar to the real case (indeed, these devices usually work with low-voltage quantity, but when the transport of energy is required, an high-voltage line is preferred).

5.2 Test case nr.1: 100% of SM

In the first simulation, the system is the original one, i.e. the one which is depicted in Fig. 5.2. There are 3 equal SM of 100MVA and they are located in different part of the system. There are also 3 loads of 0.75p.u. each, which constitute the principal resistive components of the network. Also the lines are modeled in order to obtain a more realistic system, while the transformer are all equal but not ideal.
In Fig. 5.4 the frequencies of all the SM are depicted for two different tests, i.e. a disturbance of 0.75p.u. and one of 1.25p.u., both obtained closing the red switch in the model. This configuration is equal to the case in which a sudden increment in the size of the load takes place, with the generators that have to provide more power to the network in order to keep the stability. At the beginning, the system has to face the problem of the so called *black-start capability*, that is the ability of a network of reaching a stable configuration starting from a situation where all the devices are switched-off. In the reality, especially in the case of a big grid, this situation never happens, due to the fact that the generators are always working.
As it is possible to see from the figure, the stability of the system is obtained after approximately 20s, when the frequency reaches the standard value of this network, 50Hz. At 25s, the quantity of the load in the system increases and this makes the rotor of the synchronous generator rotating slower. Due to this reason, the frequency goes down and starts oscillating, till it reaches a new equilibrium configuration around a point that is not the standard frequency. In particular, with a disturbance of 0.75p.u. the frequency is at the end around 49.87Hz, while with the bigger load it is around 49.79Hz. These represent both value acceptable in a real network where some oscillations are allowed and have no consequences on the grid. In Fig. 5.5 it is reported the behavior of the system in terms of the quantity of power that is provided by each SM. Looking at the plot, at the beginning, the 3 generators are able to follow the reference quantity of 0.75p.u., which is the signal that they receive as input. When the disturbance occurs, each SM increases the quantity of power supplied to the network, in order to face the increment of the load. Also in this case, the new equilibrium point is different according to the size of the disturbance; in the case of 0.75p.u., the final state for the power is 0.99p.u., while with bigger noise, the equilibrium is at 1.14p.u..

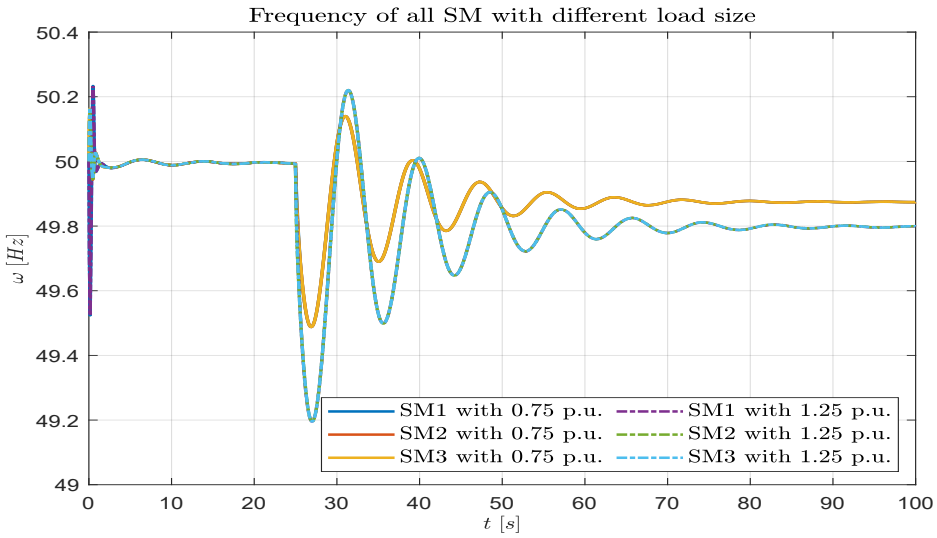

Figure 5.4: Model with all SM. A disturbance of 0.75 p.u. and 1.25p.u., respectively, is applied

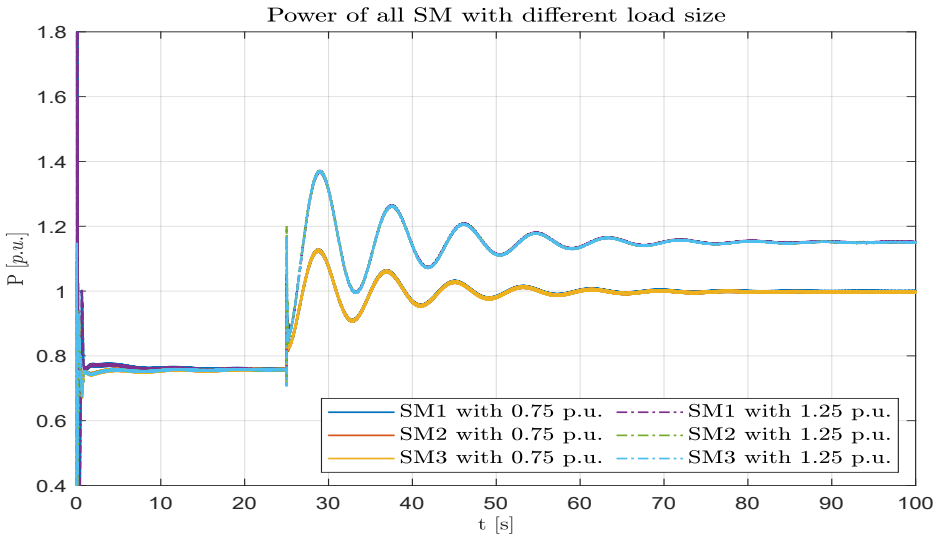

Figure 5.5: Model with all SM. A disturbance of 0.75 p.u. and 1.25p.u., respectively, is applied

A further consideration is that the generators are able to synchronize themselves after a very short transient after the simulation starts (actually, it has not

been analyzed what happens if the generators are at different initial conditions). This happens either when the system is switched on either when the disturbance is applied to the grid. For this reason, from the plot is not possible to distinguish between the lines of the different SM, which are perfectly superposed. In the following simulations, when also power-electronic devices will put inside the network, it will be observed some differences especially in the transient study.
In Fig. 5.6 and Fig. 5.7 it has been chosen to zoom on the transient situation that takes place after the disturbance is applied in the system. As a matter of fact, the focus of the study is on the behavior of the system when a contingency as the one simulated happens in the network, because it represents the most common situation in the reality. Applying a load corresponds to mimic an *electromagnetic transient (EMT)*, and offers the possibility to understand how the system reacts to an external disturbance.
From the plots, it is possible to see that increasing the size of the disturbance has two consequences, which characterize both power and frequency situation. First of all, bigger is the disturbance, lower is the minimum point for the frequency (*Nadir*) and bigger is the so called *rate of change of frequency* (*RoCoF*); referring to Fig. 5.6, the Nadir is equal to 49.19Hz for the bigger disturbance and to 49.49Hz for the smaller one. Each network is characterized from fixed value of Nadir and RoCoF which cannot be overcome, otherwise the risk is that of damaging the components. Usually, each device is equipped with special protection system that control these parameters and that in the worst case can also cause the disconnection of the devices with the goal of preserving them. The other aspect that is influenced by the size of the external load is the length of the transient situation; indeed, as the disturbance increases, the system takes more time to come to the steady-state.

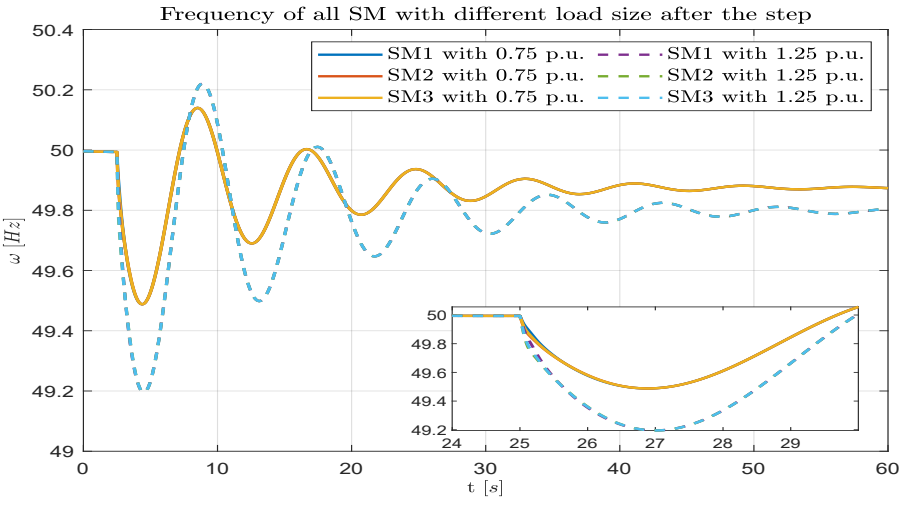

Figure 5.6: Transient of the frequency of the SM after the disturbance

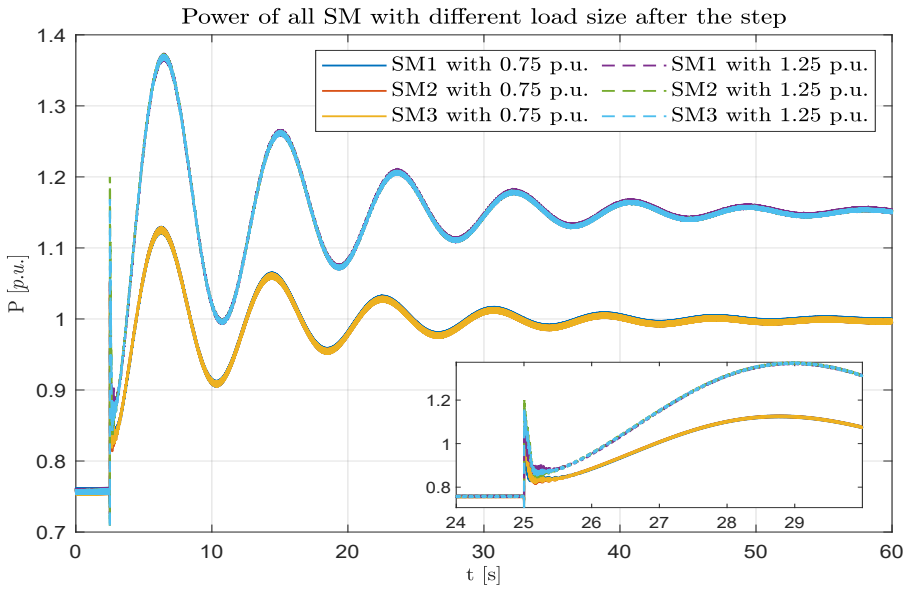

Figure 5.7: Transient of the power of the SM after the disturbance

5.3 Test case nr.2: 2SM and 1 Grid-Forming converter

At this point, the goal is to test in this network the models of the converters that have been studied previously. Being the grid selected at the moment quite simple, the aim is to substitute step by step the SMs which are in the original network with grid-forming and grid-following devices. At the beginning, the synchronous generator nr. 2 of the model is replaced with a grid-forming converter and the simulations which have been performed in the previous section are repeated, in order to understand the behaviour of the system in the case of a small quantity of power-electronic components in the network. The results obtained with this configuration are depicted in the figures below, where the two different loads are tested. The choice has been to put all the strategies studied before in the same plot, in order to have the possibility to compare the different techniques and also to analyze the similarities between them.
In Fig. 5.8a and 5.8b the frequency and the power of the different generators in the grid are depicted in the case of a disturbance of 0.75p.u.. It is useful to remark that the plot are realized only around the EMT, with the aim to study the behavior of the system when a contingency appears. It has been chosen to not give too much attention to the situation of black-start, because it represents a particular condition where there are different things to consider. It is enough to remind that all the converter techniques which are tested in this chapter are able to work starting from a black-start condition and to synchronize with the

SM of the network before the disturbances take place. Indeed, looking at 5.8a, it is not possible to see differences between the frequency of the SM and that of the converter before the contingency, because the devices are perfectly synchronized. Also after the load step, the frequency of the different generators are synchronized and the network results stable. Specifically, all the grid-forming strategies react in a similar way, except from the matching control, which have an higher level of oscillation before reaching a stable configuration. Instead, analyzing the behavior of the power in 5.8b, it is possible to see the difference between the SM and the converters. Indeed, the SM at the beginning decrease their rotational speed due to the increment of the load, while the inverters are able to provide immediately more power to balance the disturbances. This happens because the SM are mechanical generator, while the converter are electronic devices; it is know that the electrical time constant is quite faster than the mechanical one.
Comparing these graphs with the ones obtained in a condition of only SM, it is possible to note some differences. First of all, the presence of power-electronics devices, also if in a small quantity, has a strong impact in the stabilizing time of the entire network. Indeed, from Fig. 5.4 the stability after the disturbance is reached only in around 40s, while in this new test case the system is perfectly stable in less than 7 seconds. Being frequency and power strictly related, the same thing is observable looking the Fig. 5.5. Furthermore, the presence of converters in the network improve also the performance in terms of Nadir, because in this case the Nadir is at 49.75Hz, meaning 0.25Hz more than the one observed in the previous situation.
At the end, the introduction of converter technology not only helps the network reducing the oscillations and the time of the transient condition, but also improves the system behavior in terms of Nadir.
In Fig. 5.9 are figured the results that have been obtained for a load of 1.25p.u.; also in this scenario, all the grid-forming techniques are able to make the system stable and the presence of the converters improves a lot the time in which the system reaches a new steady-state configuration. Comparing with the smaller disturbance case, the value of the Nadir is lower in this case (around 49.61Hz), such as the peak of power which is supplied by the converters at the EMT. However, referring again to the configuration whit only SM, there has been a considerable improvement, especially in the Nadir value, which before was equal to 49.19Hz, and in the stabilization time. The size of the disturbance with this level of penetration does not affect the stability of the system, but simply determines lower Nadir value and an increment in the power that must be provided.

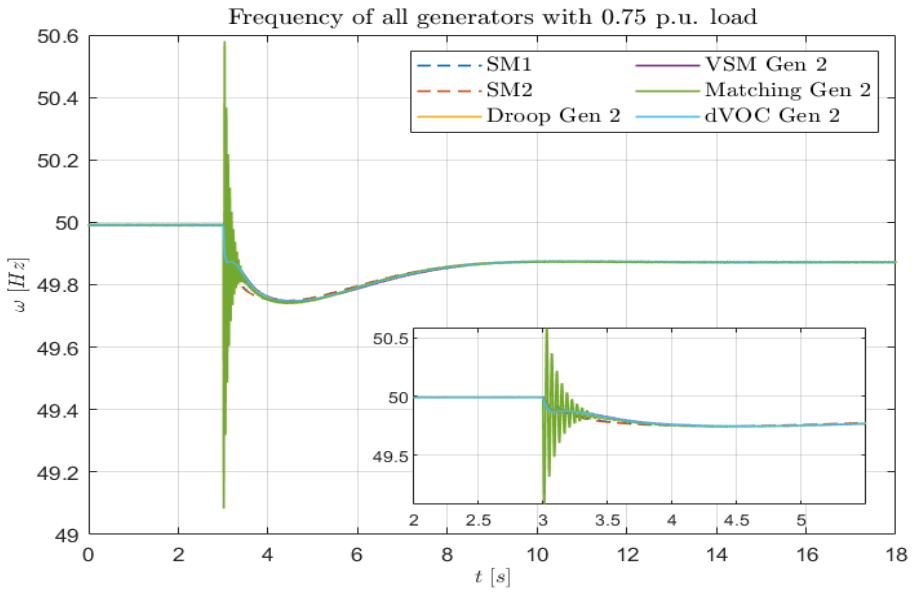

(a) Frequency of all generators

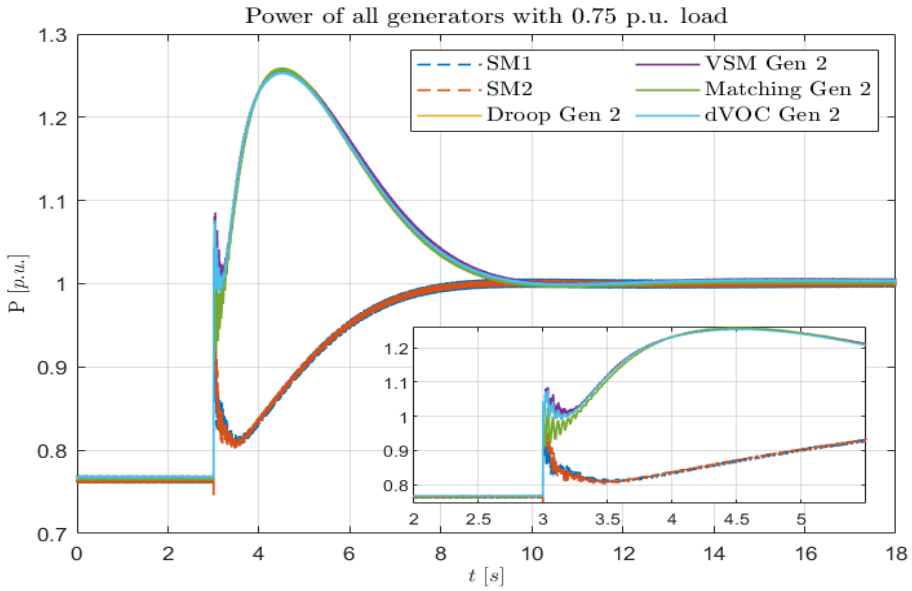

(b) Power of all generators

Figure 5.8: Model with one Grid-Forming converter and two SM with a 0.75p.u. load

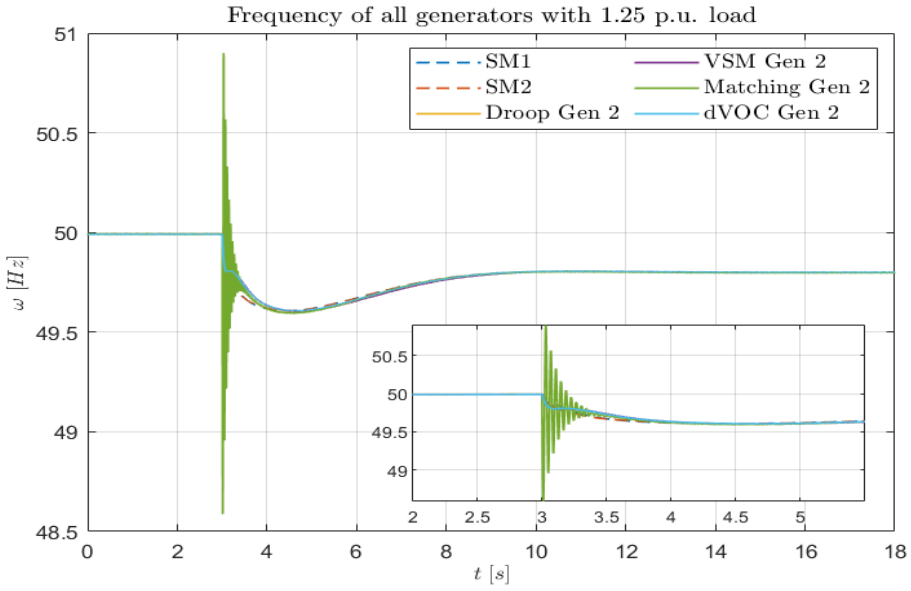

(a) Frequency of all generators

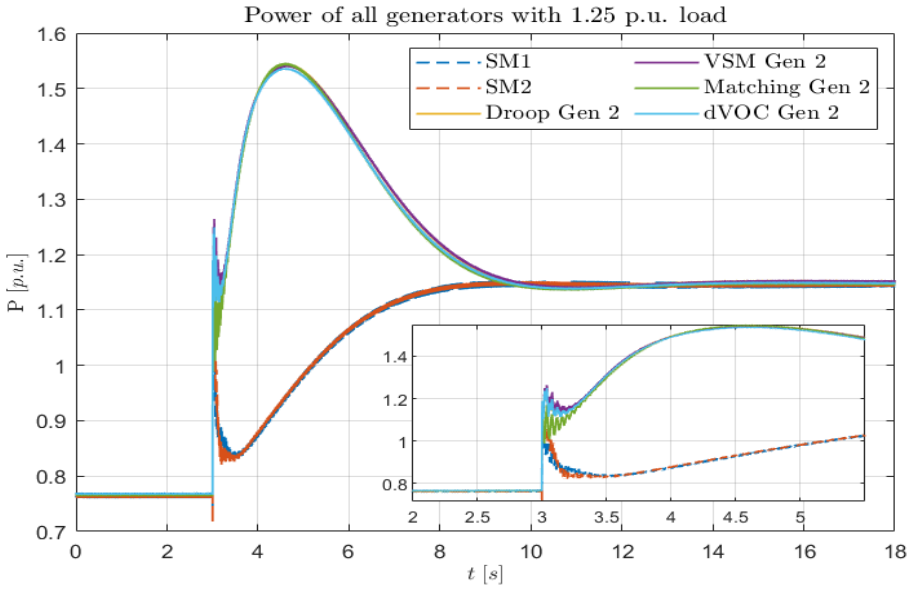

(b) Power of all generators

Figure 5.9: Model with one Grid-Forming converter and two SM with a 1.25p.u. load

5.4 Test case nr.3: 1SM and 2 Grid-Forming converters

The next scenario of study is represented by a network where there are 2 grid-forming converters and only 1 SM left, that corresponds to a low-inertia system, according to the definition given in the second chapter. From the model of the Fig. 5.2, the SM that has been substituted is the nr. 3, while the rest of the network is the same of that in the previous section. Nevertheless, if before the network was similar to a nowadays grid, with a massive presence of synchronous generators and only a small contribution of inverters, this new scenario represents the case in which the converters are the main generators of the network. It is useful to remind that this configuration can mimic a grid with a good quantity of renewable sources installed.
Similarly to what has been done previously, all the control strategies are tested in two different situations of external disturbance, respectively a load of size 0.75p.u. and one of 1.25p.u.. Also in this section, the results which regard the black-start of the system are not reported into the graphs, but it is enough to say that the system is able to switch-on with all the grid-forming techniques.
In the graphs in the following pages are reported the results of the simulation with this configuration; again, the choice has been to plot in the same figure the power (or the frequency, depending on the figure) of all generators, in order to have in the graphs the same parameters of the one reported in the section before. This allows a comparison on the behavior not only between the generators of the depicted network, but it is also possible to compare the effects of increasing the presence of grid-forming converters. Specifically, referring to Fig. 5.10a and 5.10b, the frequency and the power of all the generators in the network is depicted when a disturbance of 0.75p.u. is put in the system. It is not easy to distinguish between the lines of the frequency of the different techniques in both graphs, except for the matching techniques that have some oscillations after the load step, as it happened in the previous configuration. This is an important aspect, because it shows how the synchronization is faster between the converters than between converters and SM. Comparing 5.8a and 5.10a, it is possible to see that the synchronization time between SM and converters is similar in the two cases, while the value of Nadir is further improved, thanks to the higher level of converters in the network. The same observations can be done regarding the graphs for a bigger disturbance.
Instead, analysing Fig. 5.8b and 5.10b, the interesting aspect is that increasing the level of converters in the grid, also increases the time in which the same quantity of power is provided from SM and inverters. This fact is not easy to explain, but it is linked to the different dynamics of the devices, which is faster in the converter than in the SM. Regarding the Nadir value, in the case of a load of 0.75 p.u. the lower point for the frequency is at 49.81Hz and at 49.73 with an higher disturbance. In both case, the value results better if it is compared to

the ones with a lower level of converters in the network.

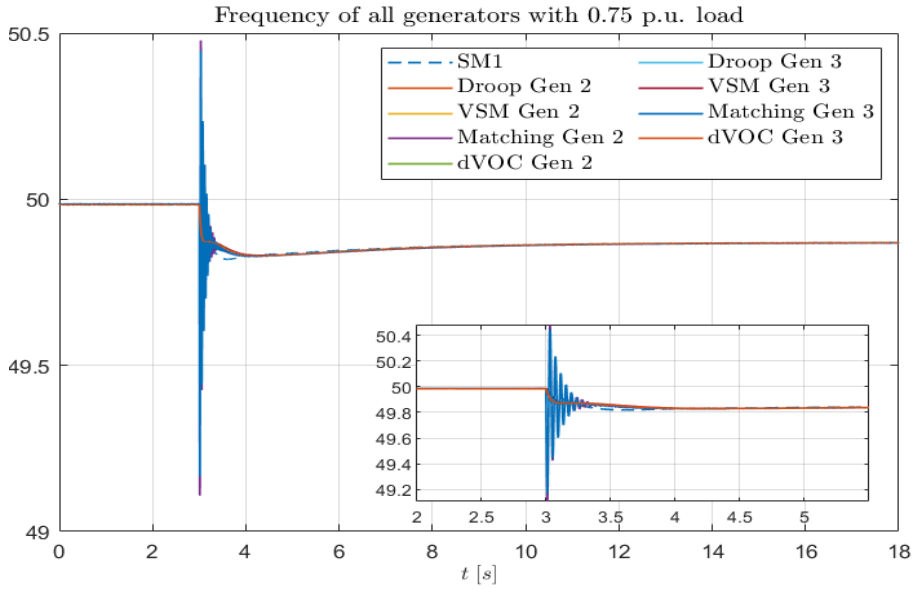

(a) Frequency of all generators

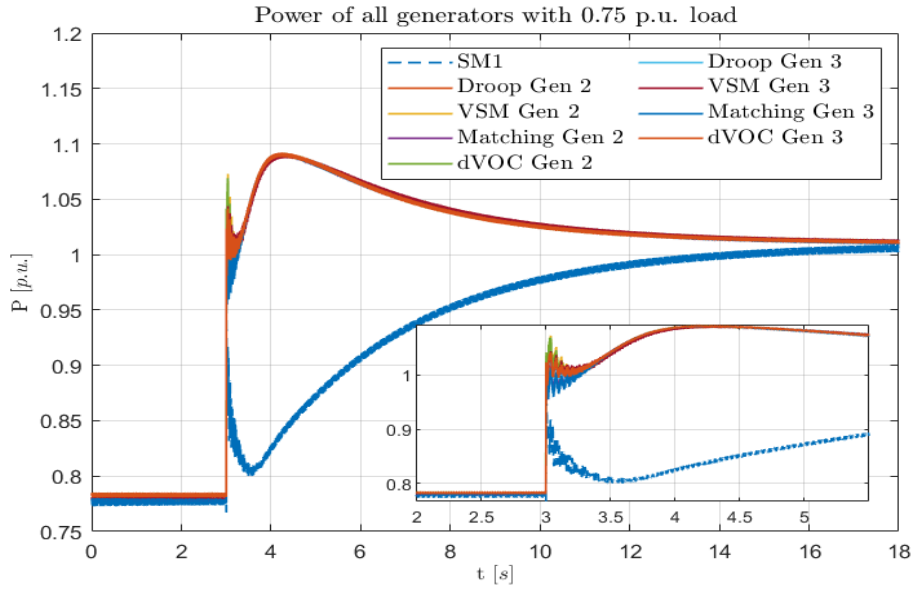

(b) Power of all generators

Figure 5.10: Model with two Grid-Forming converter and one SM with a 0.75p.u. load

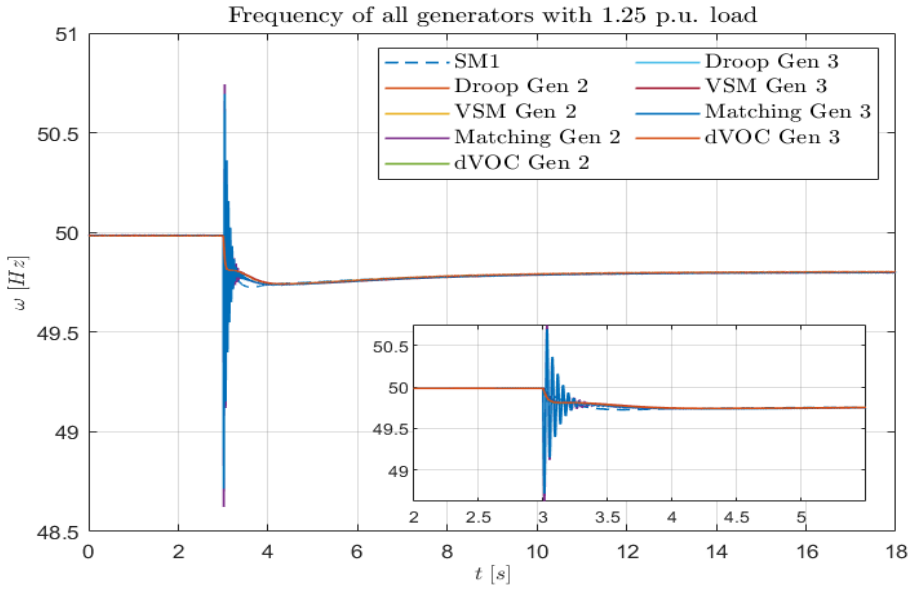

(a) Frequency of all generators

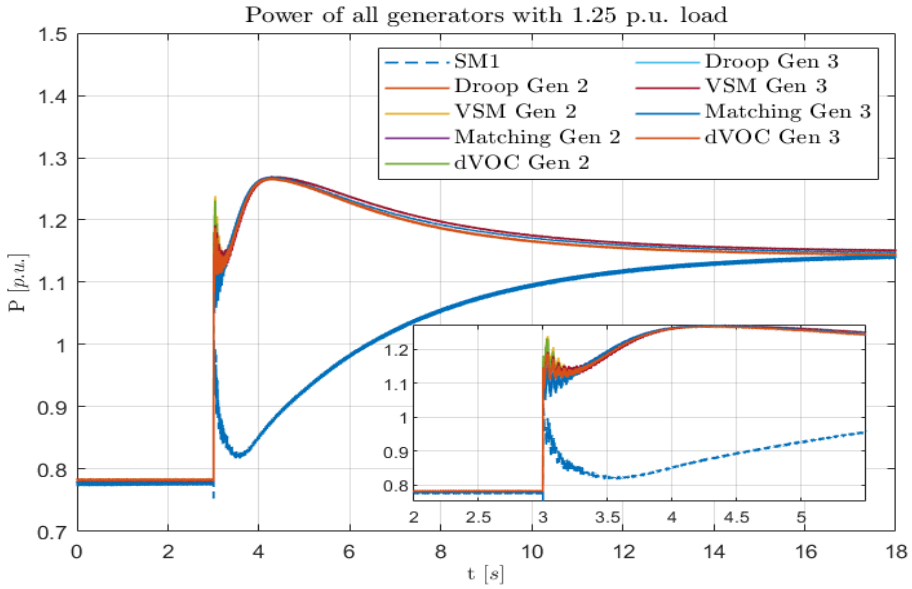

(b) Power of all generators

Figure 5.11: Model with two Grid-Forming converter and one SM with a 1.25p.u. load

5.5 Test case nr.4: all Grid-Forming converters

With this configuration, a complete transition from a system based only on SM to a fully converter-based network is realized. Also the first SM of the initial model 5.2 is substituted with a converter and the system can be called a no-inertia system, due to the fact that there are no more inertia sources in the grid. Ideally, this configuration corresponds to a future scenario, in which all the traditional power plants are replaced by renewable sources which are able to produce the total amount of energy required by the network. Of course, it is an ideal case of study, because it is considered that the number of inverters is equal to the previous number of SM in the system. As it has been yet explained before, this scenario is far from reality, because especially the solar and PV panels, but also the wind turbines are smaller devices compared to the big SM, and are distributed in different areas of the network. However, the purpose of this work is to prove that a grid with only converters opportunely controlled can work, without the need of having source of inertia. Therefore, the model that has been obtained with the substitution of the SM with inverters of the same size can be considered satisfactory.
Also in this case, it has been thought to simulate the system with two disturbances of different size and observe in which way it reacts. Being a no-inertia system, the mechanical part is quite completely removed from the network and the only devices are power-electronics based. It has been seen from the previous simulations that the converters have a great synchronization capability and this happens also in this case. For this reason, it has been chosen to not consider to plot only the results of the generator nr. 1 of the network, in order to not have too many lines superposed.
In Fig. 5.12a and 5.12b the frequency and the power of the network in this configuration are reported. It is possible to notice that the behavior is quite different from that seen in the previous simulations, especially in the graph of the power. In both the figures it has been chosen to figure the behavior in the case of the two different load size. Considering first of all the frequency, it is possible to see how fast is the synchronization in this case; after only approximately 0.3s, the network is stabilized, without considering the small oscillations due to the matching techniques. Also in the behavior of the power, the improvement with respect to the previous configuration is impressive; before, after 15s the converters and the SM have reached an equal level of power provided to the system, while in this case, thanks to the fast dynamics of the inverters, they are able to reach the new value in less than half a second.
Regarding the Nadir value, in this case it is possible to observe it only from the frequency of the converters. It results equal to 49.87 and 49.82Hz, respectively, with the small and the big disturbance. Again, if compared to the previous simulations, the network in this case react better to the variations of load, either in terms of time needed to return in a condition of stability either looking at the

lower value of frequency.

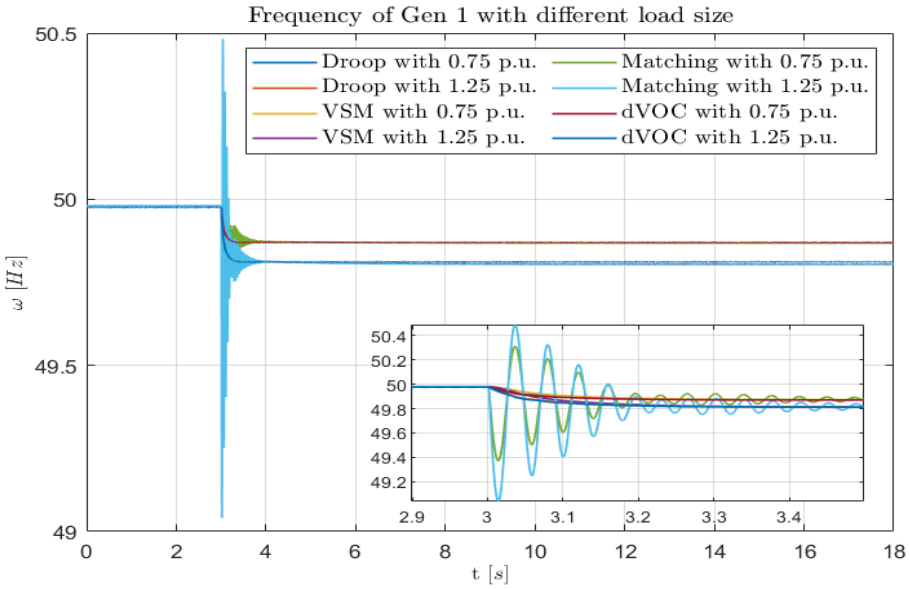

(a) Frequency of all generators

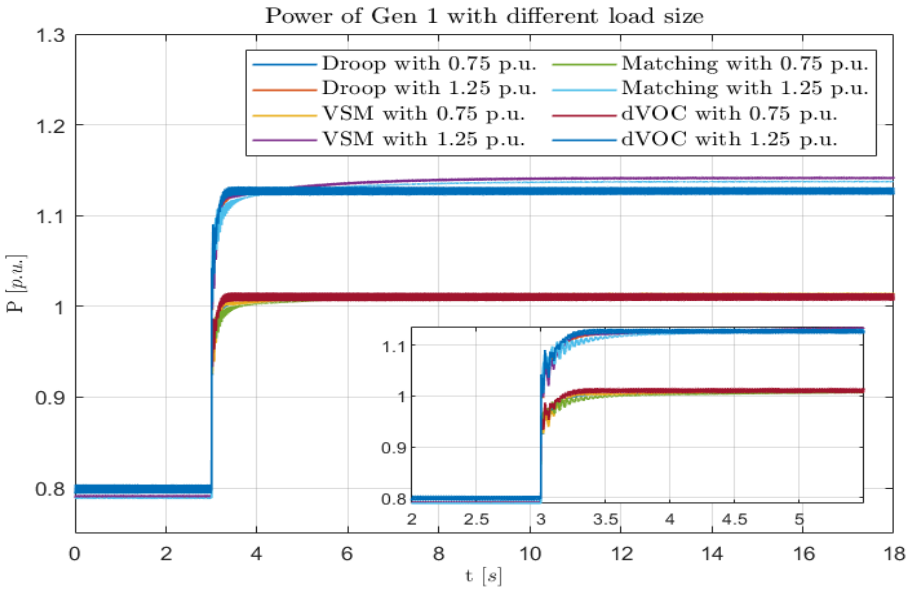

(b) Power of all generators

Figure 5.12: Model with all Grid-Forming converter and no SM with with different load size

5.6 Test case nr.5: 2SM and 1 Grid-Following converter

After having studied the performance of the grid-forming converters and having seen that it is possible to reach a fully inverter-based network, the focus is now on the behaviour of the grid-following converters in the same grid. As it has been explained in the third chapter, it is not possible to imagine a system with only this type of converters, because they need a frequency to follow (which is detected through the PLL) and that has to be imposed by an other device. From the beginning, therefore, it is known that it will be not reached the same results seen in the previous section, but the goal is the same: increase as much as possible the presence of inverters in the grid. As it has been done before, in each test case a SM is replaced by a grid-following converter and the frequency and the power of the different generators are taken into consideration. The same test cases are taken into consideration, i.e. two disturbances of different size, respectively 0.75p.u. and 1.25p.u..
In the first simulation, the SM nr. 1 in Fig. 5.2 has been replaced with a grid-following converter. The results obtained are reported in Fig. 5.13 and 5.14, where the plot of the frequency and the power for the two different disturbances are depicted. As regards the frequency of the system, in both cases the synchronization between the SM and the grid-following converter is very fast and thanks to the PLL, the inverters are able to adapt to the frequency imposed to the grid by the SM. Comparing the results of Fig. 5.13a with the ones obtained in Fig. 5.8a and 5.6, the frequency at Nadir results in this situation equal to 49.57Hz, which is a value better than the one obtained when there are only SM (49.49Hz), but not as good as that obtained with one grid-forming converter (49.75Hz). The same consideration can be made about the value of the frequency at Nadir with the bigger disturbance, which is equal to 49.31Hz (5.14a). Moreover, the introduction of a grid-following converter in the network does not give the same advantage seen in the case of grid-forming one in terms of time to reach the new condition of stability.
As regards the power of the different generators, in Fig. 5.13b and 5.14b the results are plotted; the first observation is about the fact that in this configuration the power of the grid-following device does not synchronize with that of the SMs, which instead is perfectly superposed. The explanation is that the grid-following devices are able to follow a reference value for the power, which in this case has been built as a step, when the contingency verifies. This represents one of the limit of this type of control, because it is necessary to know the new level of power that needs to be supplied to the system in order to make it the reference that needs to be followed by the inverter. At the end of the day, if the entity of the disturbance is known, the grid-following converter can react really fast, as it is possible to see in the graph. However, usually the contingencies in the grid are unknown and it is not possible to predict when they happen, so the

new reference value cannot be estimated easily.

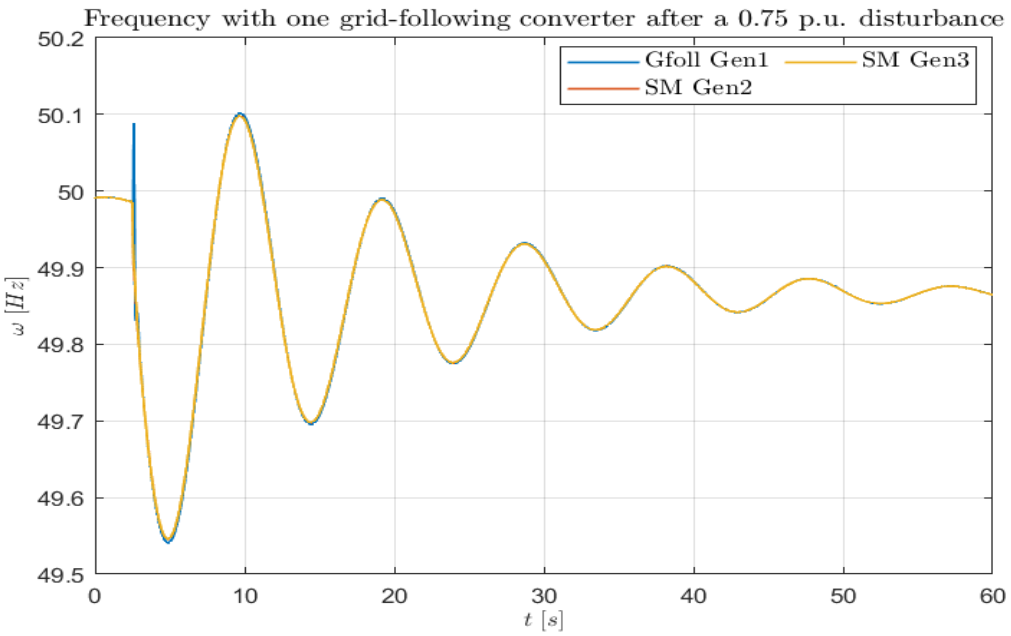

(a) Frequency of all generators

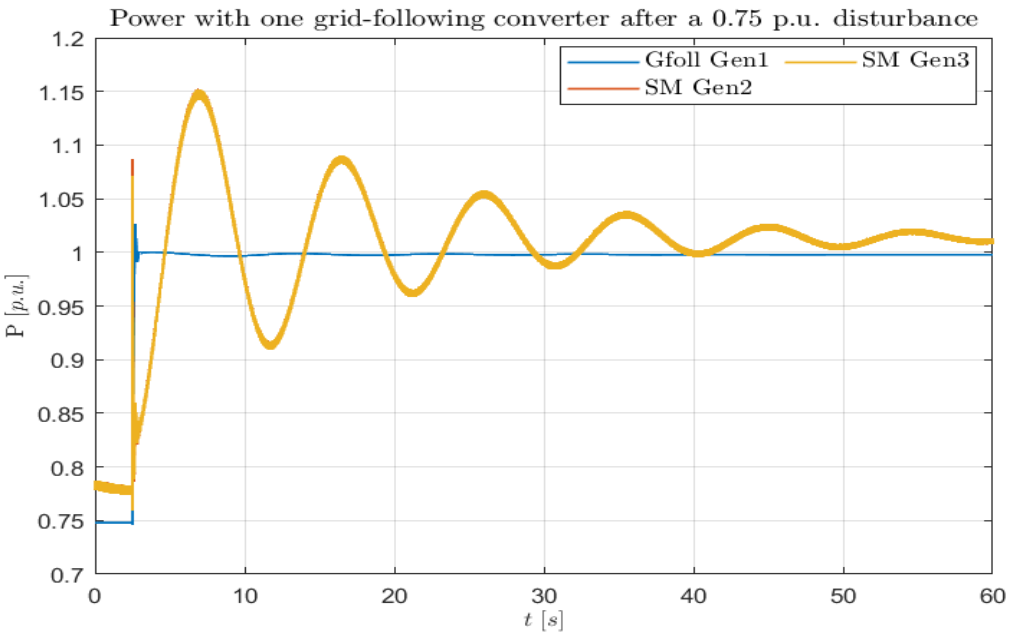

(b) Power of all generators

Figure 5.13: Model with one Grid-Following converter and two SM with a 0.75p.u. load

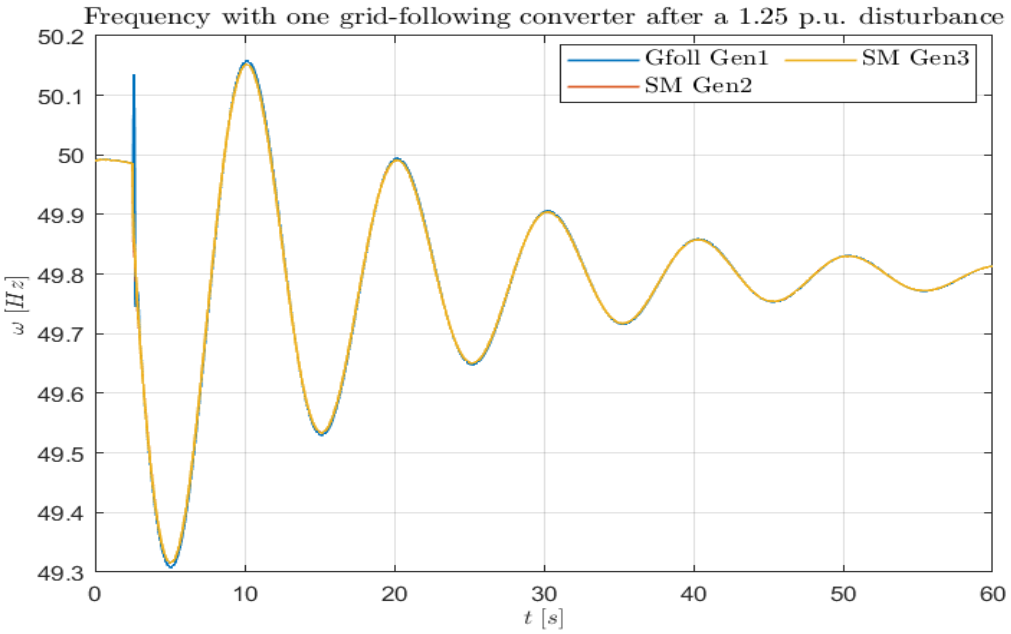

(a) Frequency of all generators

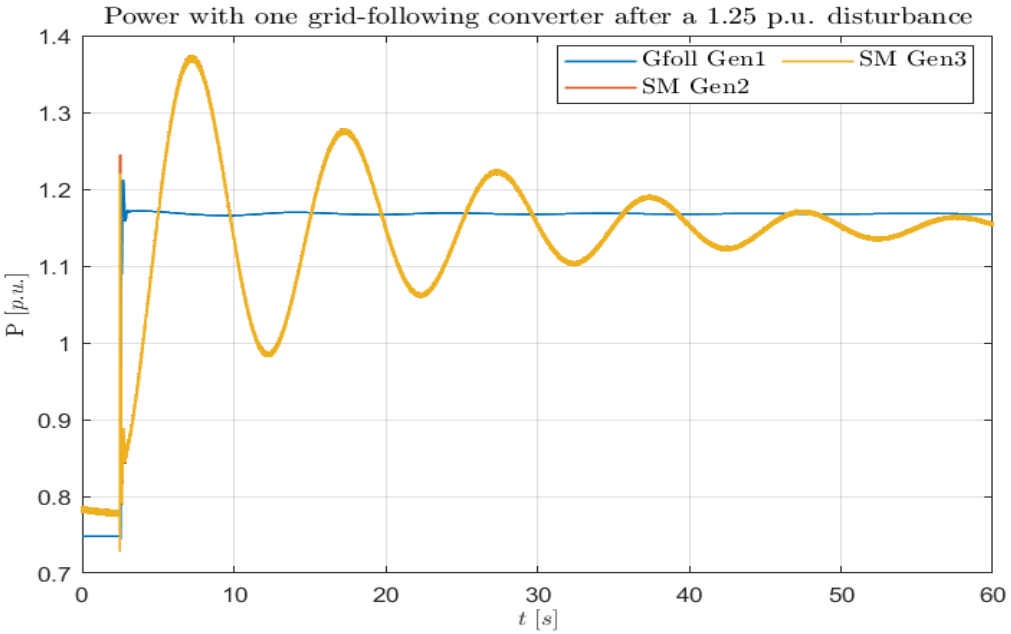

(b) Power of all generators

Figure 5.14: Model with one Grid-Following converter and two SM with a 1.25p.u. load

5.7 Test case nr. 6: 1SM and 2 Grid-following converters

The last analysis of this chapter consists on the substitution of two generators, the nr. 1 and 2 of the original model with two grid-following converters; in this way, the network can be considered an inverter-based system, because the power is provided for the 67% through converters, while the other part is supplied by a SM. For the IEEE 9-Bus system it is the limit condition studied, due to the fact that the simulation carried on with all grid-following devices did not give results, as it was expected after the theoretical considerations. Again, the system has been tested with the two disturbances adopted also previously and the results are figured in Fig. 5.15 and 5.16, respectively for the two test case. These graphs help to understand the differences between the two types of control of the converter. Indeed, in both the situation the quantity of inertia in the system is reduced but the effects are different. Adopting the grid-forming strategy of control, in particular, it has been shown that the performances of the system improve both in terms of frequency at Nadir and of time to reach a new stability condition. Instead, in the case of grid-following converters, the plots show that the value of the frequency at Nadir is higher when the converters substitute the SM, but the system take long time to stabilize, both in frequency and in power. Indeed, analyzing the data, the frequency at Nadir is equal to 49.61Hz in Fig. 5.15a and 49.58Hz in Fig. 5.16a, which are higher than with only one grid-following converter, but 60s are not enough to the network to reach the new condition of stability. It will be shown in the next chapter that it is possible to add Virtual Inertia loop and Droop control to improve the performances of the grid-following converter, but it has been chosen to implement that further action only for a more complex system.
The second problem which is useful to remark is that of the power imbalance, that is particularly visible in Fig. 5.15b; indeed, as it happens also in the previous section, the behaviour of the power is really different, with the one provided by the converters that reach quite immediately the new level while that provided by SM take more time and oscillate in the same way of the frequency. However the reference power for the inverters has been set to 1p.u. (it has considered the step of 0.75p.u. and it has been divided by 3, which is the number of generators); in the previous situation, there were two SMs and the power necessary to balance the losses in the network (due to transformers and lines for example) were supplied by two machines. Instead, with two grid-following converters, the power necessary to balance the losses is provided by a single machine, with the consequence that the difference in the new steady-state condition is higher. This situation was different with grid-forming converters that are able to adapt the power they supply according to the request of the network.
At the end of the day, the grid-following converters are not as powerful as the grid-forming ones, because they cannot allow to reach a full inverter-based grid

and also they do not guarantee a perfect balance in power.

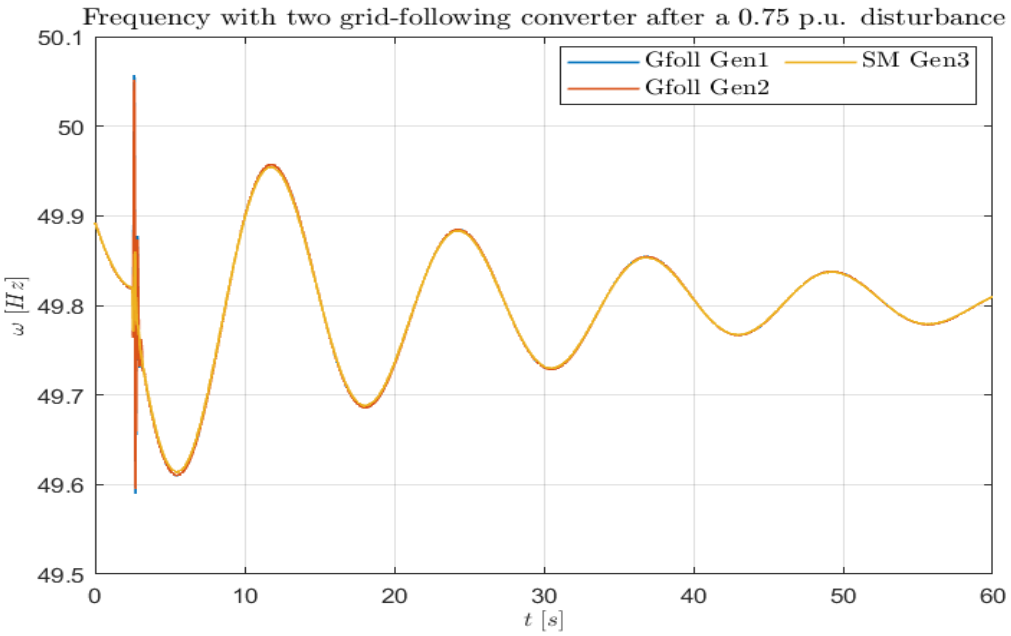

(a) Frequency of all generators

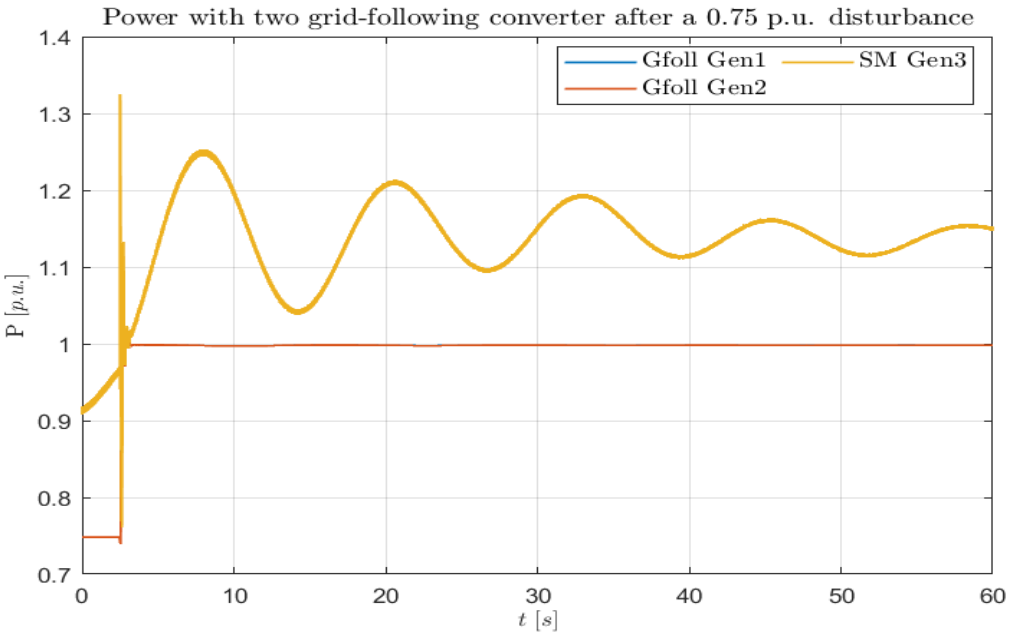

(b) Power of all generators

Figure 5.15: Model with two Grid-Following converters and one SM with a 0.75p.u. load

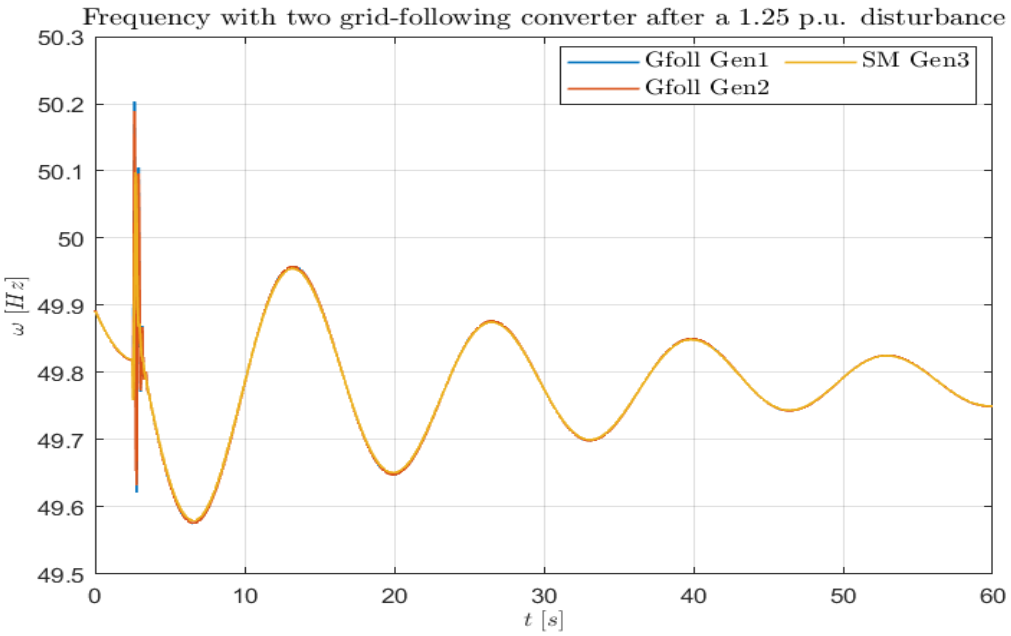

(a) Frequency of all generators

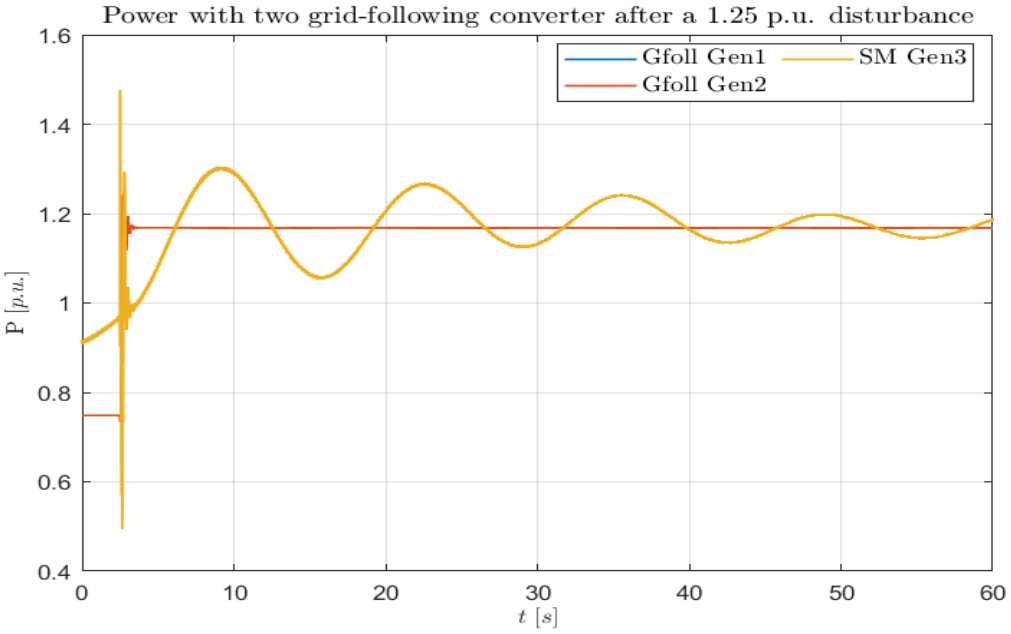

(b) Power of all generators

Figure 5.16: Model with two Grid-Following converters and one SM with a 1.25p.u. load

Chapter 6

A real system model: the Hydro-Quebec case study

6.1 The Hydro-Quebec network

In the last chapter of this work the interest is in testing the grid-forming and grid-following devices in a real network, in order to see their behavior with different contingencies. Previously, the control techniques have been put inside a simple model, with the idea of validate them in different case of disturbances. At the end, it has been seen that not only it has been possible to reach a fully converter-based network in the case of grid-forming inverters, but also the performance in terms of Nadir and stability are resulted better than in the case of only SM. At this point, it has been chosen to take into consideration a conventional system, characterized by the presence of all synchronous generators, and to increase step by step the level of penetration of inverters in the grid.
As reference model, it has been taken the *Hydro-Quebec 29-Bus Grid Model* [12] for two main reasons; first of all, the availability of the model in Matlab/Simulink, with high reliability, has avoided the building of the network from scratch. Indeed, one of the main problems in the study of the electric grid is represented by the building of the model, that needs to be complex enough to well emulate the real behavior of the system, but at the same time not too complex in order to simulate it in a reasonable time. In this sense, the one that has been taken into consideration, represents a good compromise in terms of complexity and similarity to the real system. The second advantage of the Hydro-Quebec grid is that it represents also in the reality a sort of isolated network, with only some interconnections to the U.S.A. system. This is an important observation, because the transition towards a total inverters-based grid results much easier when it is possible to do it in a limited region. Remembering what has been said in the introduction, for example, in Europe there are some countries with high-level of converters in the grid, but this is compensated by the fact that other regions of the continent are still based on SM, which provide inertia to the

network and help to keep the stability.

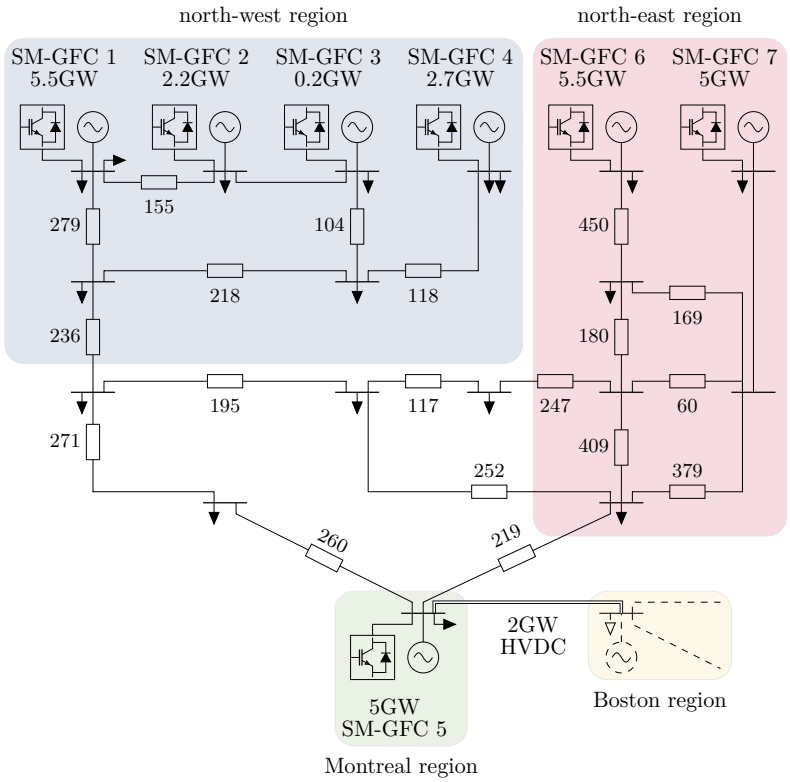

Figure 6.1: Block scheme of the Hydro-Quebec network, with the 7 generators and the length of the lines [36]

In Fig. 6.1 a simplified version of the Hydro-Quebec network is depicted; the region has a total capacity of 26.2GVA, which are supplied through seven power plants of different size and non-uniformly located. In the graph it is possible to distinguish between three regions, that are interconnected through long lines (also thousand of kilometers). As it will be clarified shortly, the most of the energy is produced in the North-West region, that is characterized by huge quantity of hydroelectric-power; the four power plants of this zone, together with the two SM of the North-East region are able to supply the quantity of energy that is needed in the South, i.e. where Montreal is located. In this part of the network, finally, there is the last SM.
The SM are not all equal, but they are of different size, from 5.6GW to 200MW; actually, they are not using fossil to work, but they exploit the hydro-power that is widely available in this region. Nevertheless, being the principle of working of hydro-turbines the same of the conventional generator, the fact that these synchronous generators yet use renewable sources is not of interest for this study. The goal is to increase the level of penetration of converters as far as possible,

keeping the system stable in terms of frequency, independently from the kind of SM that are in the original network.

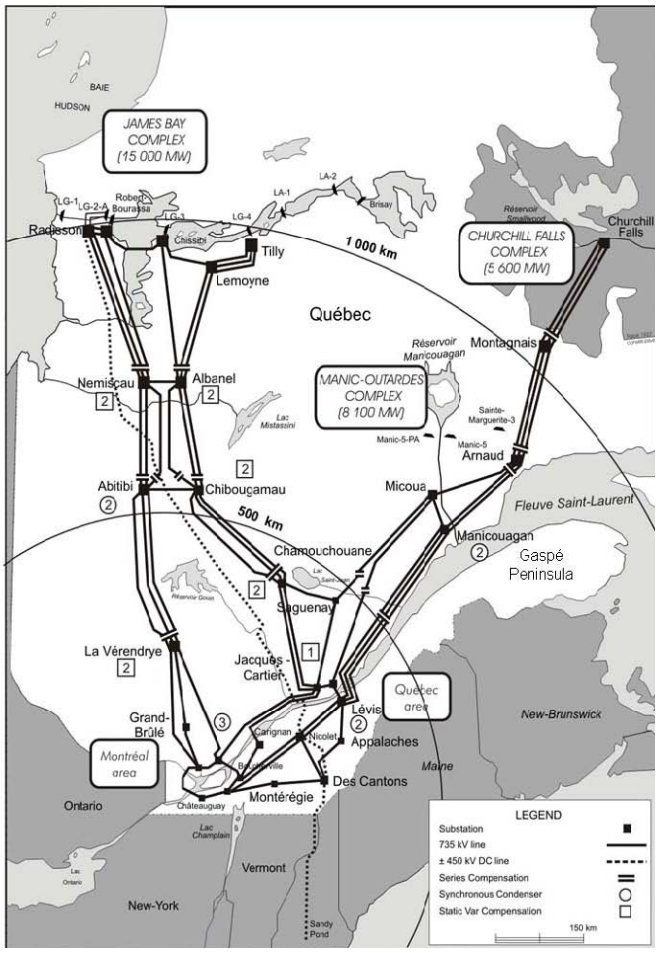

Figure 6.2: Hydro-Quebec Network with interconnection lines [37]

In Fig. 6.2 it is represented the Hydro-Quebec system with all the interconnections that link the north region, where the power is generated, to the south, when it is mostly consumed. According to what is reported in [38], the grid is long more than 34187km and counts around 530 electrical substations and it is interconnected with the Ontario, New Brunswick and Northeastern United States systems. As it is possible to see from the figure, the two main sources are constituted of the *James Bay* in the North-West, the Churchill falls and the Manic-Outardes in the North-east. Moreover, a set of six 735KV lines connects the dams of James Bay to the city of Montreal; on the other side, a set of four 735KV lines goes from the Churchill Falls and the Manic-Outardes region to the city of Quebec. There are also 735KV lines that link Quebec city and the Montreal area. Finally, in addition to the six 735KV lines from the James Bay,

an expansion has been completed in 1990 and consists on an high-voltage direct current (HVDC) of 450KV that links Quebec and New England. This line can transmit around 2000MW to Montreal and the north of the United States.
The last connection allows the transmission of the power not only in one direction, i.e. from James Bay to the south, but also in the opposite one, in case of need. This is particularly important to study the stability of the system, because it guarantees to transfer power also from very distant part in the network. This line has also been added to the original model founded in Matlab/Simulink in order to simulate some particular contingencies.
It is possible to synthesise in 3 points the main characteristic of the Hydro-Quebec network, that partially depend on the geographic characteristics of the region:

1. it is an isolated system with respect to the neighboring system;
2. the fact that the hydroelectric power plant which constitute the main sources are located far from the sites of consumption, which has lead to install high voltage 735KV lines;
3. the use of very long 735KV transmission system that is based on a limited number of lines, that basically arrives at the cities from two directions only

Mainly because of the last point, i.e. the big extension of the transmission system based only on a few lines, also with three general power failures that have taken place in the 1980s [37], has lead to an increasing interest towards the voltage and frequency stability of the system. Lot of services and plans have been developed in the last years to improve the quality of the grid and nowadays this network can be considered one of the most reliable in the world. It has been distinguished the possible contingencies in two categories:

- the ones that can be produced by the transmission system, such as the loss of some 735KV lines and that cause transient or dynamic stability problems:
- the others that are related to the balance between the generation and the load and which give as effect over-frequency or under-frequency phenomena.

The Quebec grid is part of the *Electric Reliability Organization*, that represents an association responsible for the security and reliability of the North America power system. The network is split in seven region, which are studied in two ways; first of all, each region has to ensure determined level of stability and reliability but moreover there is also a supervision on the interconnection between the different parts of the system. Each year, a *Frequency Response Annual Analysis* (FRAA) is realized and it contains the analysis of the network and the recommendation to guarantee frequency stability. According to the one of 2018

[39], the low-frequency limit of the Quebec part is set at 58.5Hz. Comparing to the values of the other region, this region accepts a lower value and this is due to the characteristics of the network described before. However, it is important to remind that the model which has been taken into consideration is a simplified version and does not contain the interconnection between this region and the ones that neighbouring to it. For this reason, in some simulations, the frequency will be also smaller than the low-limit value.

6.1.1 The Simulink Model of the Hydro-Quebec network

Before going on with the results of the simulations, it is useful to give some details about the Simulink model that has been implemented. As it has yet been said, the starting point is represented by the version developed in [12], but it has been modified in some parts. First of all, only constant impedance loads have been considered in the model; then, an HVDC link has been added to the original model, with the goal to study an event that is independent of the penetration level of converters in the system.

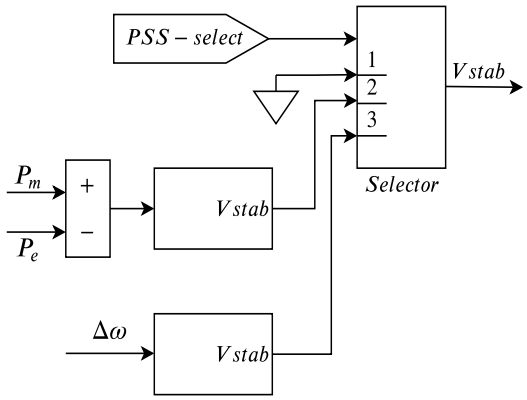

Figure 6.3: Diagram of the PSS of the SM: three modes are available

Regarding the 7SMs of the system, they are modeled through a 8th order equations, associated with hydraulic turbine, governor, automatic voltage regulator (AVR) and multiband power system stabilizer (PSS). The model of the SM is similar to the one reported in the previous chapter (Fig. 5.3), with only primary frequency control. As regards the PSS, it is possible to choose to run the simulation in three different ways in the implemented model, i.e. with PSS deactivated, with only power balancing and finally with multiband PSS. The block-scheme of this specific unit is represented in Fig. 6.3, where the parameter *PSSselection* is set with an equal value for all the generators in the network. Referring to the scheme, specifically, the first input does not provide any voltage to the output; in the second, the output is produced according to the unbalance between the electrical and the mechanical power, while whit the third mode the input is rep-

resented by the difference between the nominal frequency and the actual one. In all cases, the quantity *Vstab* represents one of the input of the excitation system of the SM. All the results that will be reported have been obtained with the third mode, because it is the method that guarantees better performance in terms of frequency stability. Nevertheless, it will be shown later that in some cases, it has also been necessary a PSS re-tuning in order to keep the network stable. Referring to [40], it is important to underline that to have stability in the SM, the excitation system needs to be opportunely controlled. Due to this reason, PID controller are used in order to regulate the terminal voltages and the power unbalance, but in some situations they do not provide enough damping characteristics, in particular when large generators are involved. This brings to low frequency oscillations, that can produce instability in the grid if not removed. The PSS represents a possible solution to this problem and in some cases it is strictly necessary. Practically, it is based on an additional signal which is supplied with the goal of increasing the damping, without influencing the voltage control. In Fig. 6.3, in the Multiband mode the unbalance frequency is used to produce the additional voltage to increase the damping of the system.
There are two more aspects, which are strictly correlated, that need to be specified before talking about the simulations. Indeed, this does not represent the first attempt in the literature of testing converters inside a grid. The research in this field is considered one of the most relevant over the last years, concerning a problem of big importance. Some studies, such as [9], have observed instability in the network when the presence of non-synchronous generators overcome determined quantities, others have tested only grid-following techniques ([41], and other still have stopped to the analysis of small networks, as the one that has been considered in the previous chapter ([22, 42]). Other reports, such as [43], have worked for real grid in the same way it has been done previously in this work for a benchmark system, i.e. substituting one by one the generators in the network with converters. Regarding this last point, in particular, it has been chosen to follow a different path, performing a transition from a SM based grid to a converters dominated one in a uniform way. As it is reported in [36], it is possible to define the percentage of converters in the grid as

$$pen_{GFC} = \frac{\sum_1^7 S_{GFC_i}}{\sum_1^7 (S_{GFC_i} + S_{SM_i})} \tag{6.1}$$

In this relationship, S_{SM_i} represents the rating of the i-th synchronous generators, while S_{GFC_i} is the quantity of power which is supplied to the grid through the i-th converter. In the original configuration, where all the generators are SM, the $pen_{GFC} = 0$ and there are no inverters connected to the grid. Similarly, when all the SM have been replaced by converters, $pen_{GFC} = 1$ and the network can be considered a full inverter-based grid. With the aim of having a more equal and gradual penetration as possible of converters in the grid, it has been developed a complex block in Simulink, that is better explained inside Appendix

B. Specifically, this structure contain the models of grid-forming converter, grid-following converter and SM (the ones of the original model). Through the mask, it is possible to decide how much of the total power has to be supplied by the converter part and how much by the synchronous generator; moreover, it is possible to select at the beginning of the simulation which is the desired technique of grid-forming converter (droop, VSM, matching or dVOC). Finally, in order to simulate a grid with only SM or converters, it is possible to disconnect the respective part from the grid. With this structure, the penetration has been realised increasing the percentage of converters of each unit of a determined quantity; the goal has been that of emulating a network where there was not the complete substitution of a big power plant with a converter, that represents a situation far from the reality, but to increase the level of converters in each region step by step. This last observation tries to mimic the nowadays transition towards renewable sources, that are going to be used little by little in the system. It is only remarkable that, at the end of the day, in the case of an inverters-based grid, the devices are of a big size (of the order of some GW), as the generators that they have replaced. This does not correspond to the real case, because they are usually installed in a non-uniform way into the network, but for what is the purpose of this work this can be considered a good approximation.
Tab. D.4 and D.5 contain the list of parameters of SM and grid-forming converters that have been used in the simulation. In particular, in Tab.D.4, the values of the original model are reported; as it is possible to see, different units have different nominal power and inertia coefficients. Moreover, they do not work at their maximum rate, but they have a specific reference value; this means that they are able to supply more power when a contingency happens. As regards the parameters of the transformer, they are not dependent on the value of nominal power, but they are the same for all the units; also if in some other studies the transformer have been scaled according to the size of the different devices [22], it has been decided to not change the original model, not being the study of the transformer the goal of the project.
Tab. D.5, instead, contains the parameters related to the grid-forming converter. At the end of chapter 4, it has been explained how the model of this unit has been built, starting from a converter of 500kW. All the parameters depend therefore on the size of the generators, and inside the mask of the block there is a variable n, which scales the converters in the right way. Furthermore, these devices have one more conversion stage, that is controlled through the LV/MV transformers. Except for the values of the voltage, the LV/MV transformers have the same parameters of the MV/HV ones, due to the choice that has been explained previously. In the table, there are also the control values that have been set for the different techniques. Some of them depend directly on the value of the nominal power that the converter has to supply to the network ($P_n^\star$).

6.1.2 Performance Metrics Definition

In order to have a better understanding on the results of the simulation, the influence on the *rate of change of frequency (RoCoF)* and on the *nadir* value has been evaluated for an increasing level of converters in the network. These two values are widely used in the study of the performance of a grid, as in [44] and in [22], and also the limits of the network are often related to these parameters. For example, in [44], where an analysis on the European network has been done basing on the frequency behaviour, it is reported that the nowadays grid can withstand changes between 500mHz/s to 1Hz/s, but the goal is to increase these limit values to 2Hz/s.

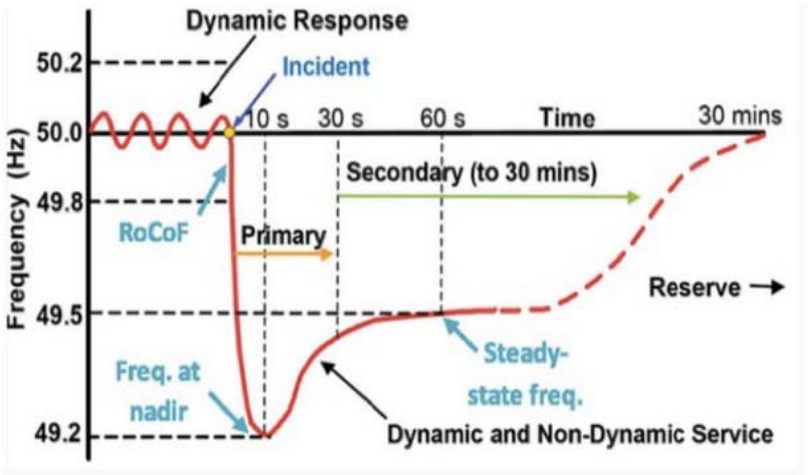

Figure 6.4: RoCoF and Nadir parameters

In Fig. 6.4 it is represented the common behavior of the frequency when a contingency appears in the system. At the beginning, the primary control acts, with the goal of keeping the stability of the frequency around a new value; after that, the secondary control, exploiting also the reserve, aims to get the frequency back to the standard value. In the graph, the two parameters of interest are highlighted.
To be rigorous, also a mathematical definition is given, according to what is reported in [22, 36]; specifically, Nadir represents the maximum deviation of the frequency from the stable value before the disturbance, i.e.

$$||\Delta\omega_i||_\infty = \max_{t \geq t_0} |\omega_i(t_0) - \omega_i(t)| \tag{6.2}$$

while the RoCoF shows how fast the frequency changes over the time after the load is applied. This last parameter is defined as

$$|\dot{\omega}_i| = \frac{|\omega_i(t_0 + T) - \omega_i(t_0)|}{T} \tag{6.3}$$

In these relationship, t_0 is the instant at which the contingency takes place, while T is the amplitude of the RoCoF window.

6.2 Test case nr.1: Loss of Generator 1

In this chapter, the simulations have been performed in a different way with respect to the model analyzed in the previous one. Due to the complexity of the hydro-Quebec grid, indeed, it has been possible to study the behaviour of the network when different contingencies take place. Therefore, also if the goal of all the tests is always to understand how the increasing level of converters influences the characteristics of the system, in the following sections different disturbances will be taken into consideration. Moreover, it is important to remind that, due to the size of the grid and the complexity of the model, the time requested to simulate the network is considerably bigger compared to the previous IEEE 9-Bus system. Indeed, at each generator corresponds a number of differential equations that Matlab needs to solve during the simulations and this number also increases when converters are put inside the network; as a matter of fact, being 7 generators in the original grid, when they are partially substituted with converters, it verifies a situation in which 14 units work together, 7 SM and 7 inverters. For this reason, in some cases, the simulations end before the steady-state is perfectly reached, but it can be considered satisfactory for the purpose of this work to analyze the transient behaviour.
The first test case considered regards the loss of the Generator 1, i.e. the disconnection from the network of the Unit 1 that is located in the North-West region; it represents the biggest generators of the area, as it is possible to see comparing the size of the first four unites in Tab. D.4. The goal of this simulations is to see how the grid reacts to one of the worst event that can happen to the network and that can take place for different reasons, i.e. failures or a safe-disconnection to preserve the integrity of the device.
All the grid-forming techniques have been tested in this case, but the focus has been more on the possibility to use all of them obtaining a stable system at the end then in the comparison between them. One of the most interesting aspect has been that, as it was for the previous chapter, with all the control techniques the system remains stable after the contingency appears, also if in some cases it is necessary to modify the PSS parameters, as it has been explained previously. Considering the system, all the SM in the Simulink model has been substituted with a block containing the model of the SM and the ones of grid-forming and grid-following converters, as it is explained in Appendix C. In this first part, the analysis is focused on the tests of the grid-forming inverters, because, as it has been highlighted also in the case of the IEEE 9-Bus system, they are the only ones that give the possibility of obtaining a fully converter-based network. In order to obtain a more constant penetration in the network, all the blocks in Simulink supply an increasing power through the converter, while the quantity

provided by the SM is equally reduced. Specifically, the presence of converter increases of 10% at each simulation, starting from a situation of only SM and arriving to an inverter-based grid. In the following pages the results that have been obtained are explained through some graphs. It has been chosen to figure only some cases for each test and, due to the complexity of the network, it was not possible to put in the same plot all the techniques.

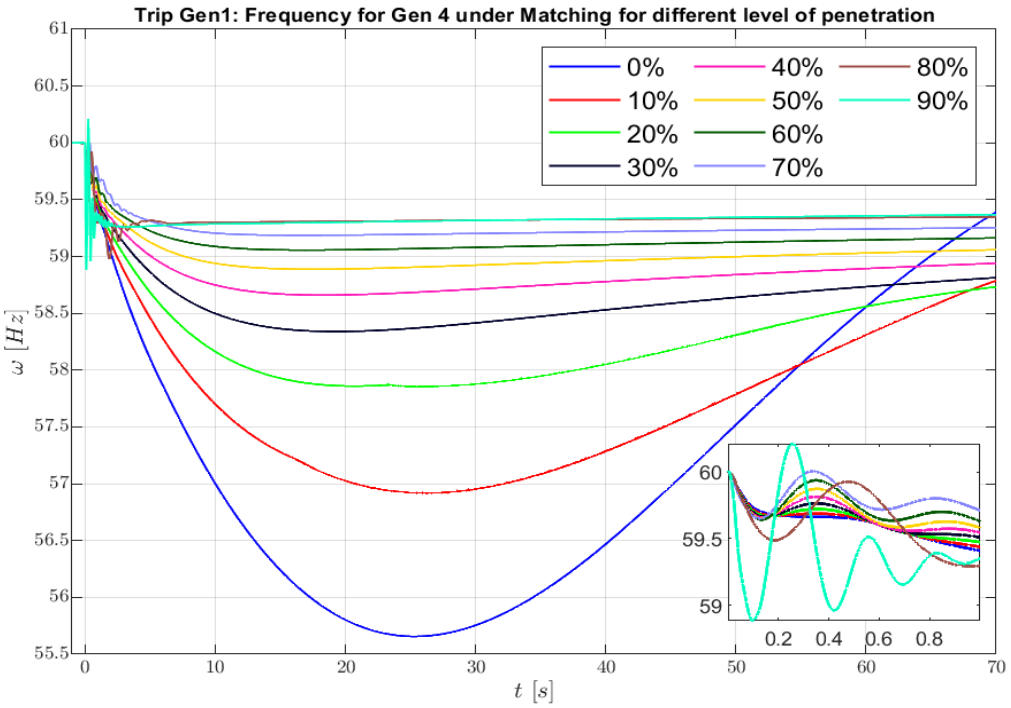

Figure 6.5: Frequency of Gen. 4 with an increasing level of grid-forming converters in the network when a failure of Gen 1 is simulated

In Fig. 6.5 it is represented how the frequency of the Gen 4 evolves with an increasing level of grid-forming converters in the grid; looking at the grid, the lowest value of the grid becomes higher as the the percentage of non-synchronous generator increases. Specifically, with only SM the frequency at Nadir is equal to 55.65Hz, that is a value lower than the minimum accepted in the specifications of the Quebec network. However, it has been yet explained that the model does not take into account all the interconnections of the grid with the other network of the North America. The low frequency value is equal to 59.19Hz when the converters constitute the 70% of the generators in the grid, showing a significant improvement. In the last two simulations, with higher value of inverters, the behaviour of the frequency is different, due to the PSS re-tuning that has been necessary in order to avoid instability in the system. Nevertheless, also if the PSS has been set through a trial and error procedure, the frequency has some

oscillations in the transient region but it is higher at Nadir compared to the previous values. An other important aspect that must be considered is that the converters also help to reach a new steady-state condition in less time, compared to what is done by the network with only SM. This aspect has also been studied in the IEEE 9-Bus and it is due to the faster characteristics of the power electronics devices.

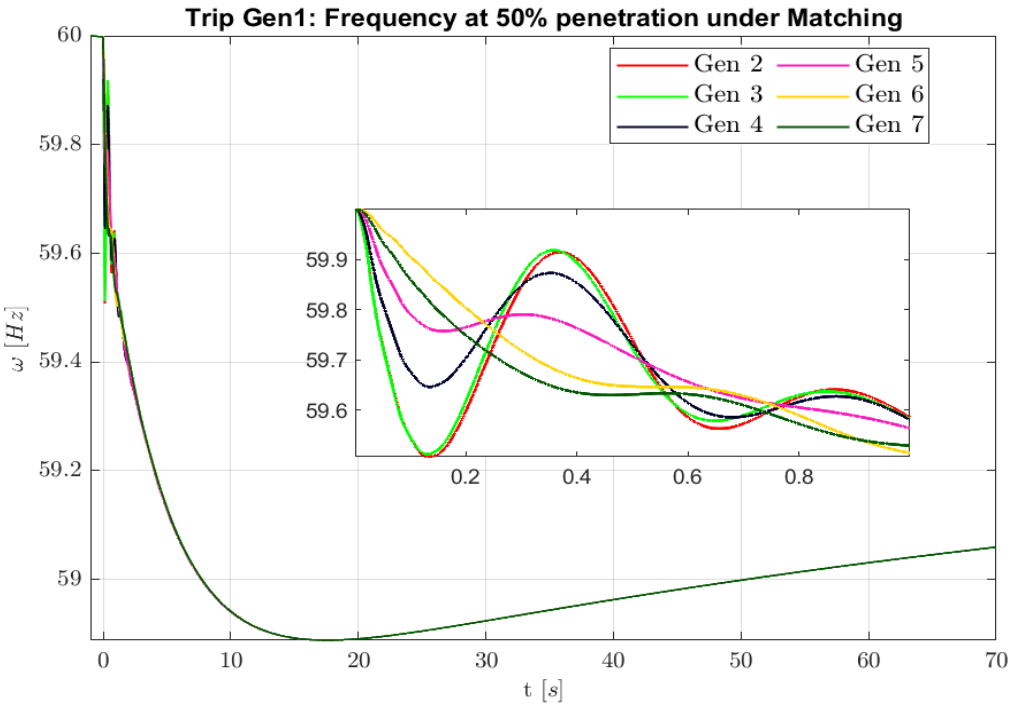

Figure 6.6: Frequency of all generators at 50% of grid-forming converters with matching control in the network when a failure of Gen 1 is simulated

Fig. 6.6 depicts the frequency of all generators of the network when the Gen. 1 is disconnected from the system and all the converters are controlled with the matching technique. As it is possible to see, the devices are able to synchronize quite fast (less than 3s, while they need some time (more than 60s) to reach the steady-state condition. Moreover, observing the zoom on the transient which is in the box in the figure and that represents the behaviour of the frequency for one second after the disturbance, a further observation can be made. Indeed, the failure happens in the North-West region where 3 generators (not considering the one that is disconnected) are located. Looking at the transient, the 3 units of the same region are exactly the ones characterized by a lower minimum value of the frequency, while the other units react in a little bit more time, due to their distance from where the contingency verifies. However, after a small transient, all the generators have the same behaviour.

The last graph about frequency is the one reported in Fig. 6.7, where it is depicted the frequency related to the Gen. 4 with 50% of converter in the grid and all the techniques of control are tested. In both the transient and the overall simulation the behaviour is quit similar, as it was also observed for the IEEE 9-Bus system. With all the typologies of control, the network results stable and the value of frequency at Nadir and for RoCoF is similar. Similar graphs are also obtained with higher level of converters in the grid or considering different generators of the network.

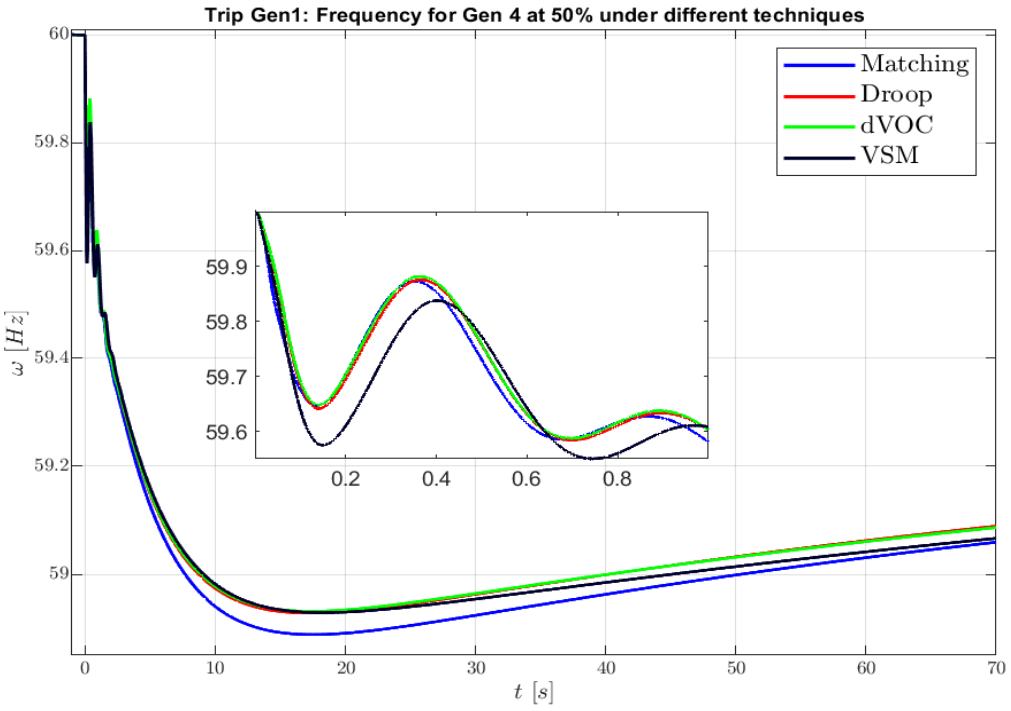

Figure 6.7: Frequency of Gen. 4 at 50% of grid-forming converters with different control techniques when a failure of Gen 1 is simulated

After having analyzed the frequency, as it has been done with the previous system the power of the different generators is taken into account. In this case, it is expressed in $p.u.$ and not in W, but is only a trick to work with simpler numerical value. In Fig. 6.8 it is figured the behaviour of the power of the Gen. 3 with an increasing level of converters in the grid, when all the inverters are controlled with the Droop techniques. Being the reference value for the different units not the same, also after the disturbance they will reach new different stability points; moreover, as it has been seen also for the frequency the simulation ends before the system is arrived at stability but this is due to the impossibility of collecting more data. However, a part from 80 and 90%, for which has been necessary a re-tuning of the PSS, it is clear that the presence of the converters

helps the system decreasing the peak of the power that is necessary to provide and also making the reaching of the stability faster.

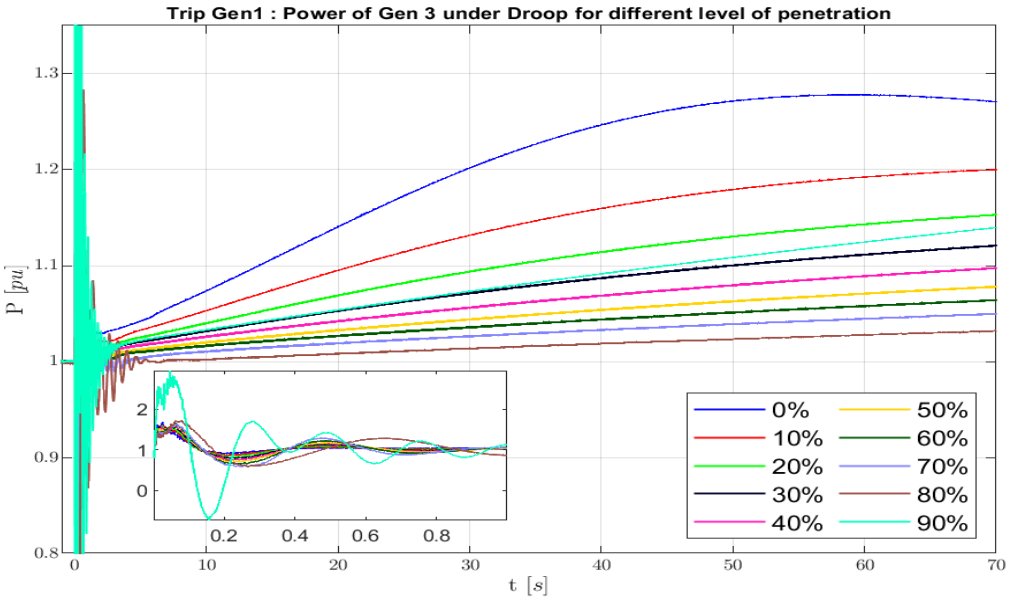

Figure 6.8: Power of Gen. 3 with an increasing level of grid-forming converters in the network when a failure of Gen 1 is simulated

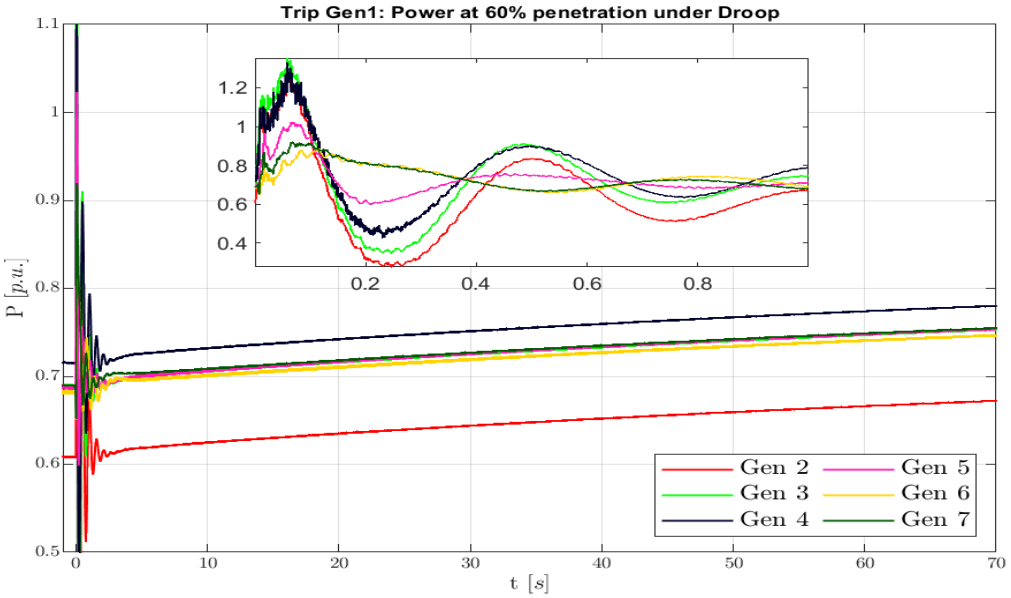

Figure 6.9: Power of all generators at 60% of grid-forming converters with droop control in the network when a failure of Gen 1 is simulated

In Fig. 6.9 the power of the different generators of the grid in the case of 60% of penetration of converters is reported. The most interesting aspect is in the zoom on the transient region, where it is possible to note that the generators in the same region where the contingency happens, react with higher peak and in a very similar way. Unit 5, that is the only one in the South region, has a less accentuated behaviour, while the units of the East region react with minimum oscillations. Of course, the large distance between the generators is a peculiarity of the Hydro-Quebec network and contributes to these differences between the units. It has also been tried to decrease the length of the connection lines and it has been observed that the behaviour of the generator in this different configuration is more similar.

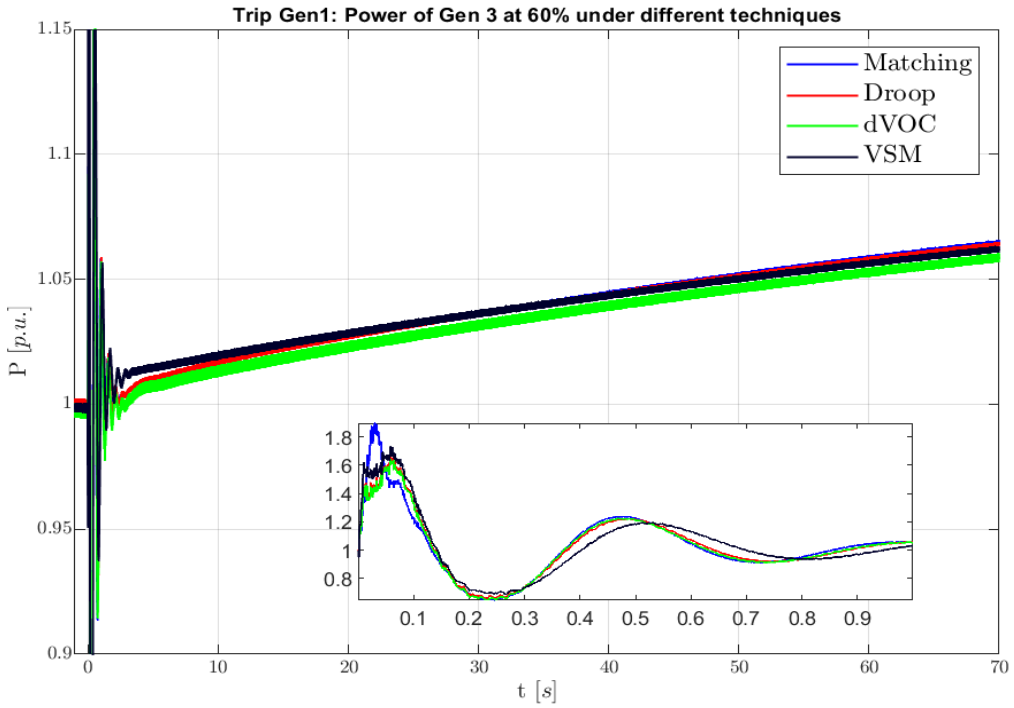

Figure 6.10: Power of Gen. 3 at 60% of grid-forming converters with different control techniques when a failure of Gen 1 is simulated

Furthermore, in Fig. 6.10 it is represented the evolution of the power of the Gen. 3 in a condition of 60% of penetration of grid-forming converters and different techniques are taken into account. As it was also for the frequency, the control techniques give similar results in terms of control and all of them guarantee the stability of the network, that is the most relevant aspect. The same plots have been obtained for different level of penetration and analyzing the power of other units of the grid.

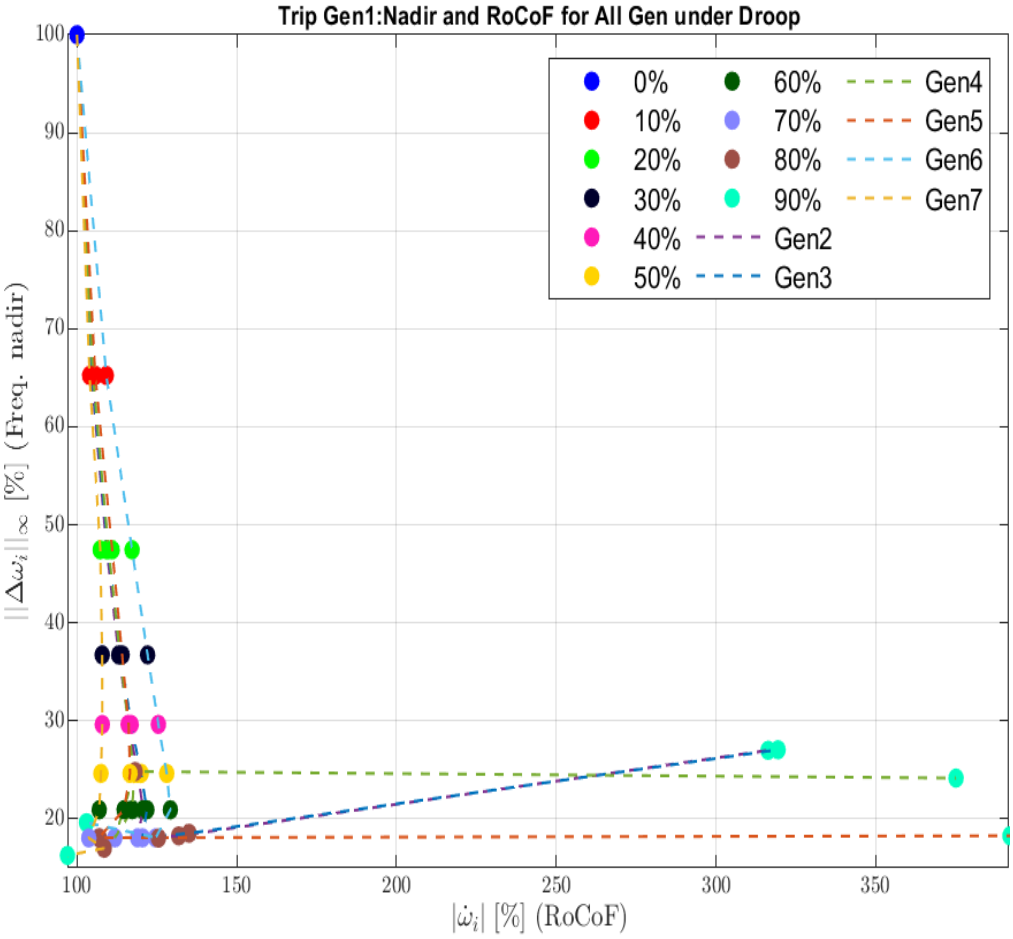

Figure 6.11: Analysis of normalized RoCoF and Nadir of all generators at different level of penetration of grid-forming converters equipped with droop control when a failure of Gen 1 is simulated

The last consideration on this case can be related to the analysis of the graph in Fig. 6.11, where the evolution of the RoCoF and Nadir values for different level of penetration of converters is depicted. The values plotted have been normalized with respect to the one of the first generator in order to make them comparable; it is possible to see that the behavior of all generators is quite similar for all level of penetration, except for 80% and 90%, which are the ones for which the PSS re-tuning has been necessary. In particular, the frequency at Nadir decreases as the percentage of grid-forming converter increases, as it is has yet seen in Fig. 6.6, while the RoCoF value has a small increment for high penetration level. Resuming, as regards this situation, the presence of inverters in the grid has the advantage of increasing the minimum value of the frequency in the transient in a significant way (more than 80% for high level of penetration); the counter-effect

is a faster change of the frequency value, that can be a limit in system in which the devices cannot accept too high value of RoCoF. This last point, particularly, is one of the reason for which there is the attempt of increasing the high value of RoCoF accepted in a specific network.

6.3 Test case nr.2: HVDC connection failure

This section takes into account the possible failure of the HVDC connection, which represents the link between the Hydro-Quebec grid and the rest of the North-America electric network. As it has been explained previously, this connection is a line which goes from the James Bay in the north to the city of Montreal and then to the north of the United States; it can transmit around 2000MW and usually the power flows from the Canada to the U.S.A.; however, it represents also an instrument of safety for the Hydro-Quebec grid, because in case of necessity the power can also be supplied in the opposite direction. This element was not in the original model, but it has been chosen to locate it near Gen. 5 and to perform some simulations in order to study a disturbance that is independent of the penetration level of grid-forming converters. In the following pages, the results are reported and discussed; as it was for the previous case, in the plot the complete steady state is not reached, due to the complexity of the system which needs lot of time of simulation.

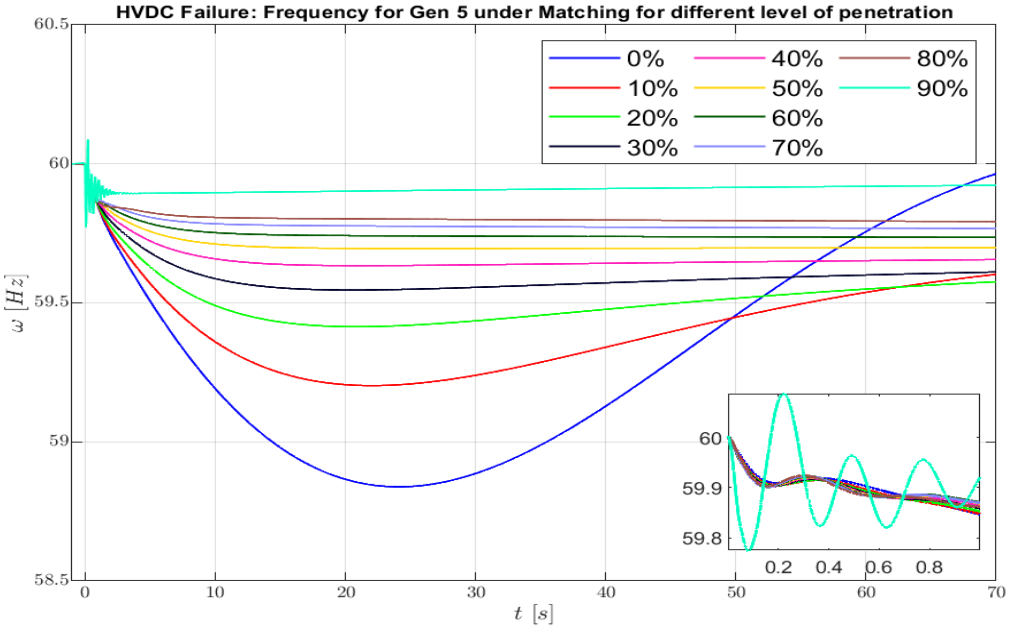

Figure 6.12: Frequency of Gen. 5, equipped with matching control, with an increasing level of grid-forming converters in the network when the failure of the HVDC connection is simulated

Fig. 6.12 depicts the evolution of the behaviour of the frequency of a specific generator when the quantity of SM in the network and consequently the inertia decreases. As it has been observed also in the situation of failure of one unit, also in this case the inverters in the grid help to improve the system in terms of frequency at Nadir and of time requested to reach the stability. Indeed, if with 100% of SM there are still oscillations after 70s of simulation, with high level of penetration the network reaches the steady-state after less than 20s. However, also with this contingency it has been necessary a PSS re-tuning (specifically for 90%), meaning that it is requested for high level of penetration of converters in the grid independently on the disturbance. Due to the smaller size of the contingency, the frequency deviation results lower compared to the previous case. Indeed, the frequency at Nadir is equal to 58.83Hz with all SM, while with the failure of Gen. 1 it was 55.65Hz. Only introducing a little quantity of inverters in the grid brings a good improvement, because the value of the frequency at Nadir is 59.20Hz yet with 90% of SM. The results improves as the converters in the grid increase, and for 20% of SM the value is equal to 59.79Hz.

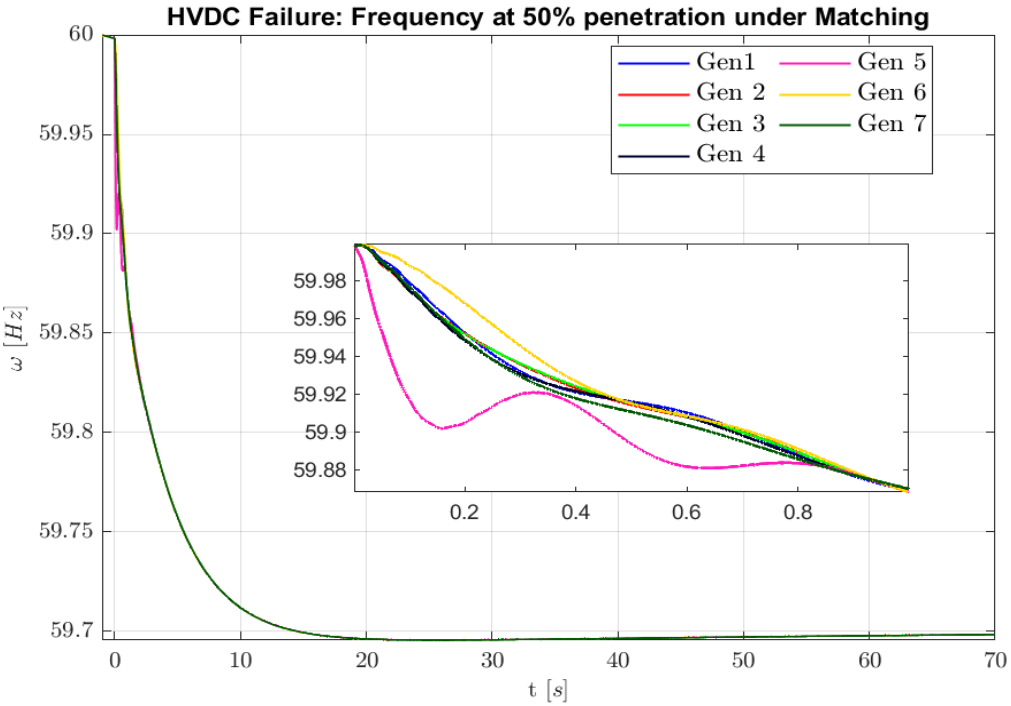

Figure 6.13: Frequency of all generators, equipped with matching control, for 50% penetration of grid-forming converters in the network when the failure of the HVDC connection is simulated

In Fig. 6.13, the frequency of all the generators after the failure is depicted. There are two important aspect that can be analyzed; first of all, the capability

of the generators of synchronizing in a fast way after the contingency happens, that has as consequence the same frequency at Nadir for all the units in the network. The second thing, instead, regards the transient region; in this simulation, being the HVDC connection near the Gen. 5, in the zoom part it is clear that the closest unit is the one that is more influenced by the disturbance, as it was predictable and as it has yet been seen in the previous test case. The other devices in the network, instead, react slower but all in a quite similar way. It is also important to remind that these ones are the frequency of the SM, while the ones of the converters have not been figured. However, the units are after a short transient all synchronized and they reach the same value at Nadir.

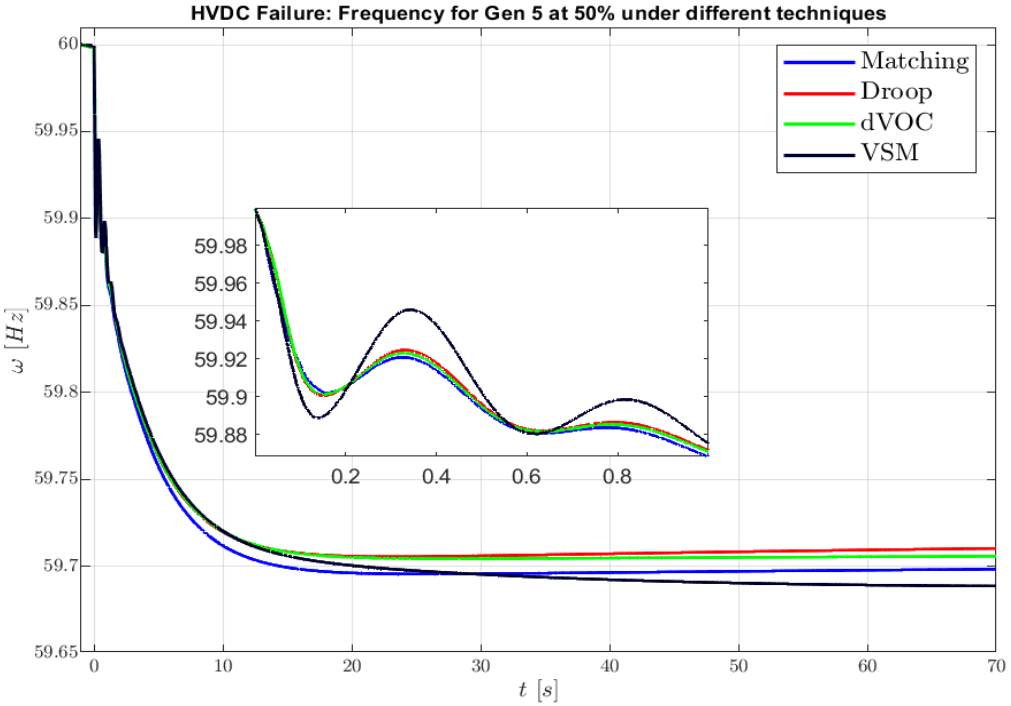

Figure 6.14: Frequency of Gen. 5, equipped with different control techniques, for 50% penetration of grid-forming converters in the network when the failure of the HVDC connection is simulated

Fig. 6.14 depicts the evolution of the frequency of unit 5 with different techniques of control, with a 50% of penetration of converters in the network. The behaviour is quite similar for all of them and with each one the goal of stabilizing the system is reached. Focusing on the transient, and also comparing with the one in Fig. 6.7, the only technique for which there is a difference is the VSM; indeed, it is the only one that requests one filter also on the measured voltage to remove the ripple, as it has also mentioned in [27]. In both the test cases, the simulations run without this component were totally unstable, while the ones

made adding the filter have given good results.
Similarly to what has been done before and for completeness, also the results related to the power are reported and some further considerations are made. In Fig. 6.15, the behaviour of the power of the unit 5 is represented for all the levels of penetration of converters in the network. Apart from the last simulation run with 90% of inverters in the grid that have the strange behaviour linked to the re-tuning of the PSS, in all the other case the more important aspect is the reduction in the power deviation as the level of grid-forming converter in the grid increases. This is an immediate consequence of the smaller value of the frequency at Nadir, that has been observed previously.

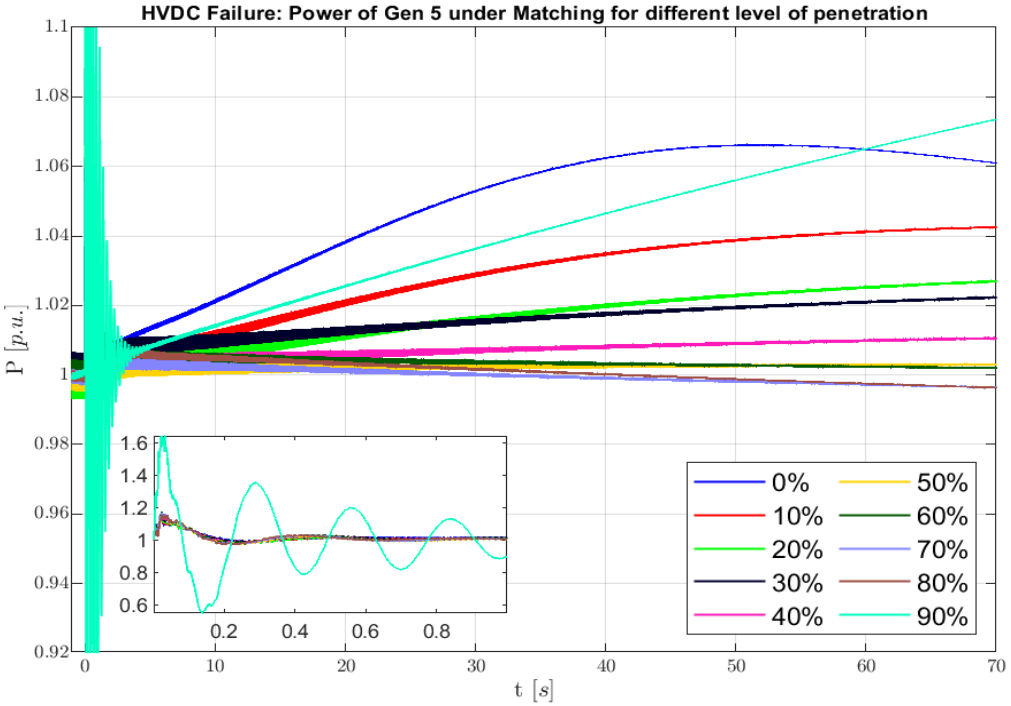

Figure 6.15: Power of Gen. 5, equipped with matching control, for different level of penetration of grid-forming converters in the network when the failure of the HVDC connection is simulated

Fig. 6.16 shows the power of all the generators which are all controlled with matching and where there is a penetration equal to 50%; as it is possible to see, the transient is really short (less than 2s) and all the generators contribute in the same way to supply more power due to the contingency. This principle, that is commonly called *load-sharing*, is of particular interest, because it guarantees that, with good synchronization between the units, none of them has to supply all the power necessary but they all contribute in the same quantity, without exceeding their limits. This mechanism is obvious with SM, where the mechan-

ical part guarantees this sharing, but is an important aspect also in the case of converter. The only difference is, again, in the transient, where the closest generator have the fastest reaction to the disturbance.

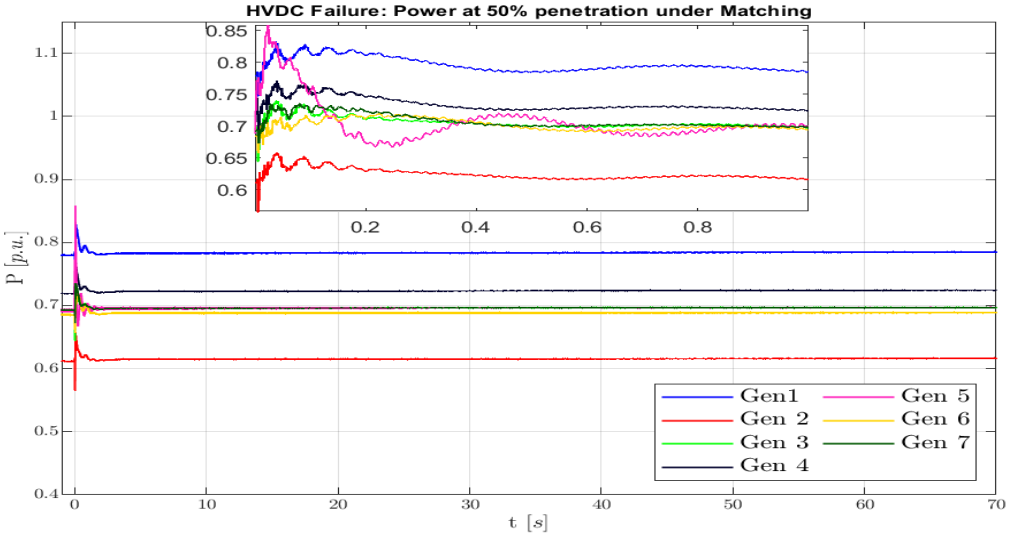

Figure 6.16: Power of different generators, all equipped with matching control, for a penetration of 50% grid-forming converters in the network when the failure of the HVDC connection is simulated

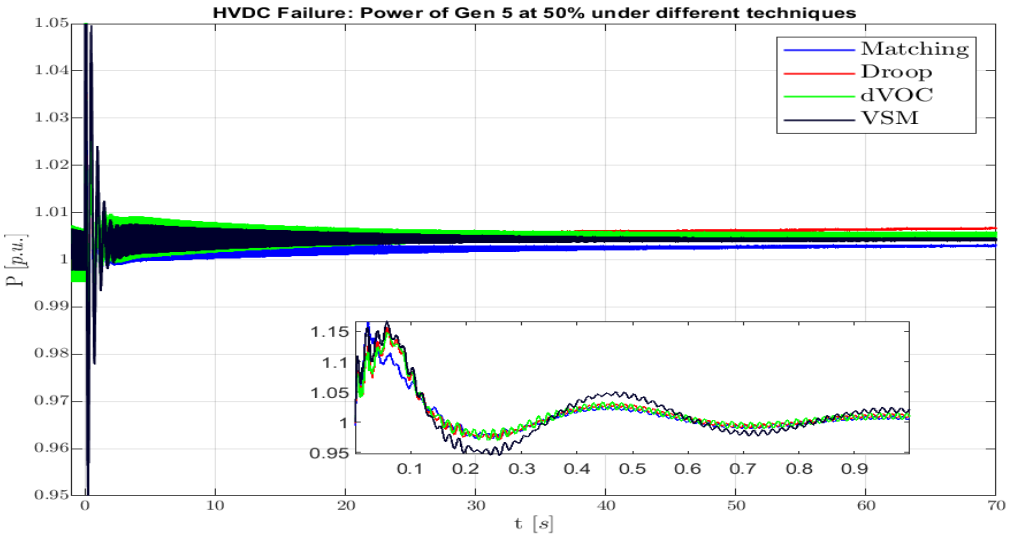

Figure 6.17: Power of Gen. 5, equipped with different control techniques, for a penetration of 50% grid-forming converters in the network when the failure of the HVDC connection is simulated

Furthermore, with the idea of showing that all the four techniques of control taken into account are able to stabilize the system, in Fig. 6.17 it is represented the power of Gen. 5 when the simulations are run under all the control methods. Specifically, all of them are able to keep the system stable, but also in this case, as it has been observed for the frequency, the introduction of a filter to reduce the ripple of the measured voltage makes the transient obtained using VSM a little bit different from the one obtained with the other techniques of control. Furthermore, it is good to remark that the noise superposed to the signal can be attenuated tuning better the filter parameters, but it was not an object of interest of this work.

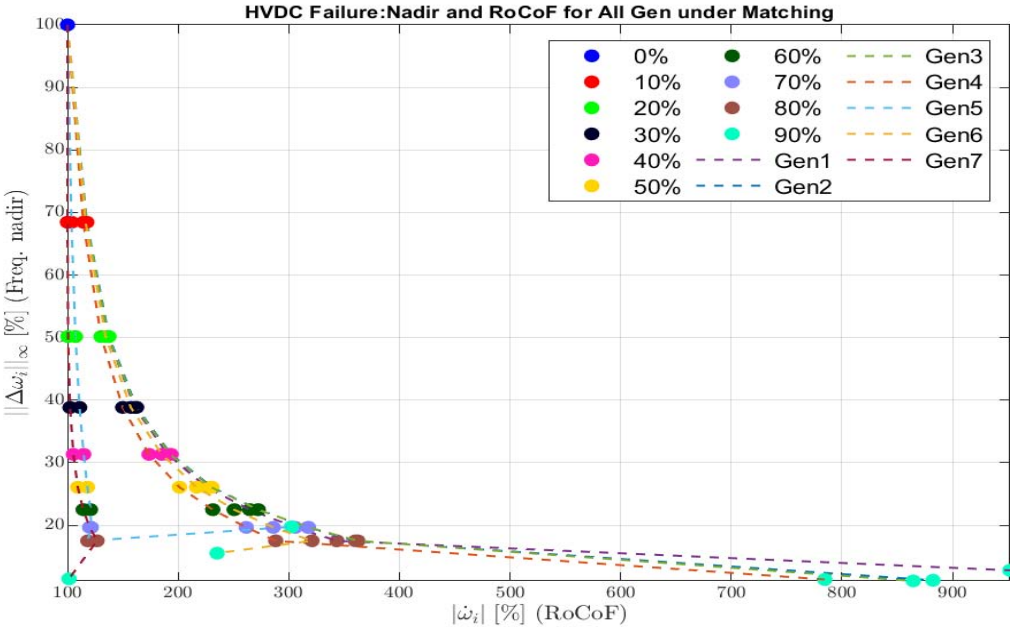

Figure 6.18: Analysis of normalized RoCoF and Nadir of all generators at different level of penetration of grid-forming converters equipped with matching control when the failure of the HVDC connection is simulated

Finally, the evolution of RoCoF and Nadir values of all generators in the network is reported in Fig. 6.18, when all of them are controlled with matching technique. What has been observed for the failure of the Gen. 1 at high percentage of penetration is still valid, and also in this case the value of the frequency at Nadir is higher as the percentage of converters in the grid increases. However, in this situation, the Gen. 5 and 7, which are the closest to the contingency, have a slightly different behaviour compared to the other ones, which is accentuated when the penetration is more consistent. Indeed, the RoCoF value increases less for this generators than for the other in the network, probably due to the oscillations that are visible for this units in the frequency.

6.3.1 Grid-following converter

As last analysis, also in this system the grid-following converters have been tested, with the goal of studying the behaviour of the network with this type of inverters when contingencies occur. According to what has been seen in the case of the IEEE 9-Bus system and also basing on what has been discussed in the chapter 3, it is not possible to obtain a grid with only grid-following converters; the goal, in this scenario, is to increase as much as possible the presence of converters in the grid. It has been considered only the HVDC connection failure as test case, but the results have been obtained in two different ways; in one situation, the virtual inertia and the droop control inside the model of converters have been kept disabled, while in the other one they have been turned on. Before seeing the results that have been obtained, it is useful to review the part related to the control of the active power in the grid-following converter. When there are no virtual inertia and primary droop control, the reference power is directly compared with the quantity measured in the system; a PI controller is used to balance the difference between these two signals, as it is depicted in Fig. 6.19a. Instead, in the other situation, a further action of control is implemented, which

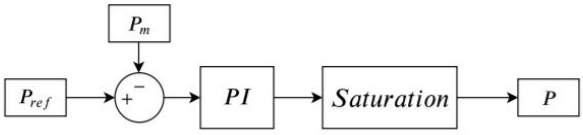

(a) Scheme without Droop Control and Virtual Inertia Loop

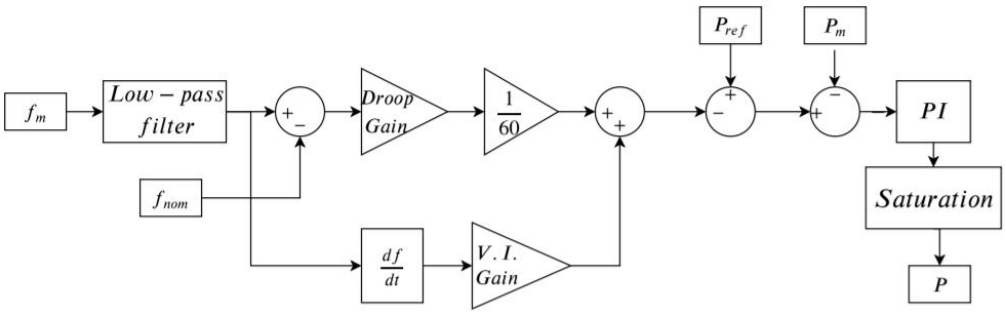

(b) Scheme with Droop Control and Virtual Inertia loop

Figure 6.19: Control of the active power in grid-following inverter with and without droop and virtual inertia loop

aims to regulate the power imbalance using also the frequency signal captured through the PLL. In Fig. 6.19b, the block scheme is reported; the droop part acts as a primary control action, while the virtual inertia takes into account the derivative of the frequency with a negative gain. The sum of this two parts is subtracted to the reference signal, while the remaining part of the scheme is

equal to the previous situation. In Tab. D.6, the parameters related to the grid-following converters are reported; according to the model that has been used, in this case also the LV/MV transformer is scaled, starting from the base value reported in the table. On the other side, the MV/HV transformer is the one that was already in the Simulink model available at [12].
In Fig. 6.20, the results related to the behaviour of the frequency of the generator 5 in the case of HVDC failure are reported for both the situations; in particular, in Fig. 6.20a there is the graph obtained when the droop control and the virtual inertia loop are enabled, while in Fig. 6.20b this part of the control is disabled. As it is possible to observe, the system is able to work till 80% of penetration of grid-following inverters. Overcoming this level of penetration, it has been seen in other simulations (the figures are not reported) that the system becomes unstable. For this reason, according to the model of grid-following converter that has been used, it is not possible to obtain a fully converter-based network; indedd, grid-following inverters need a frequency to which adapt to. As it has yet been explained, they are able to detect the frequency of the grid through the PLL and then to follow it. Problems arise when, due to the increasing presence of this type of converter, the frequency of the entire network is not defined and the grid-following converters are not able to impose it to the other generators of the grid.
Looking at the two figures, it is possible to note that there are some differences when the further part of control is enabled. Specifically, with droop control and virtual inertia, the results obtained are more similar to the ones studied in the same condition when grid-forming converters have been applied (6.12); the value of the frequency at Nadir increases at each iteration and the system reaches the steady-state as faster as the percentage of converters in the grid increases. However, when the presence of converters becomes more significant, some oscillations appear and their amplitude becomes bigger for higher levels; in this case, the frequency reaches in a short period of time a stability point, but it continues oscillating around this value. The reason of this behaviour is the delay introduced by the PLL to detect the frequency of the network, which is not able to estimate correctly the frequency of the system; the error in the measurement is propagated to the PI controller and causes the oscillations.
Referring instead to Fig. 6.20b, the oscillations for higher percentage of penetration are disappeared, because as it has been shown also in the block scheme, the measured frequency does not contribute to the control part. Nevertheless, the absence of droop and virtual inertia, have two drawbacks on the system, that lead to not consider this type of control efficient. First of all, the system is not at steady-state after 70s and the time arises when the percentage of converters in the grid increases. This represents the unique situation in which this behaviour has been seen; the other negative aspect is linked to the value of the frequency at Nadir, which becomes lower at each iteration. In the reality, this type of grid-following converters could not substitute the SM in the Quebec grid.

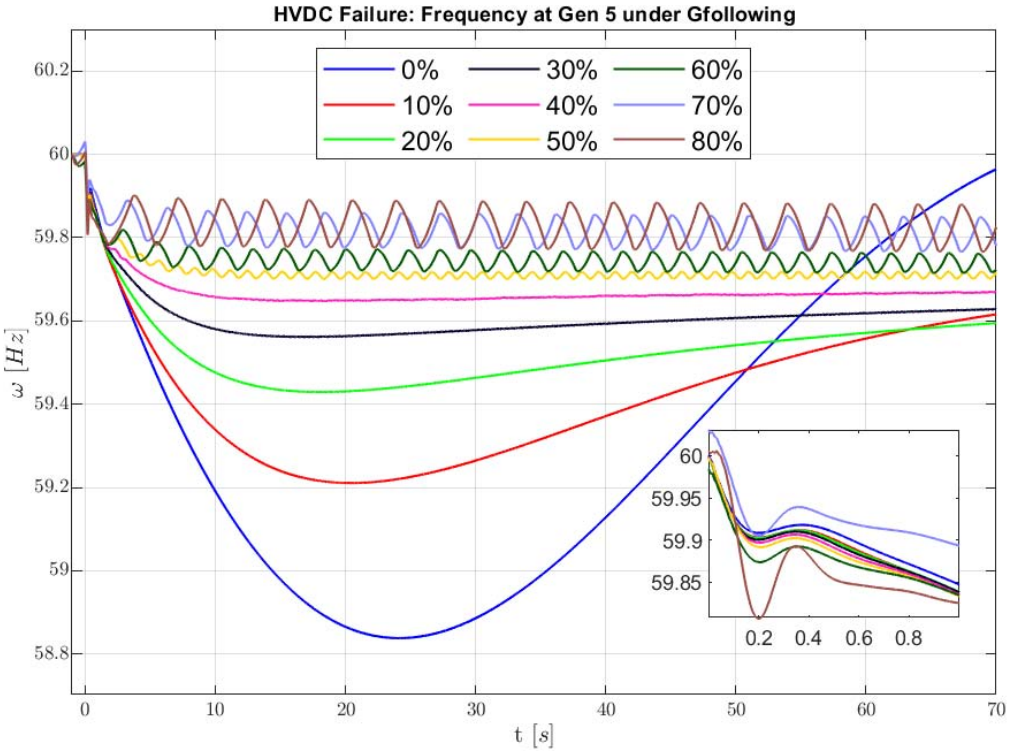

(a) System equipped with Virtual Inertia and Droop control

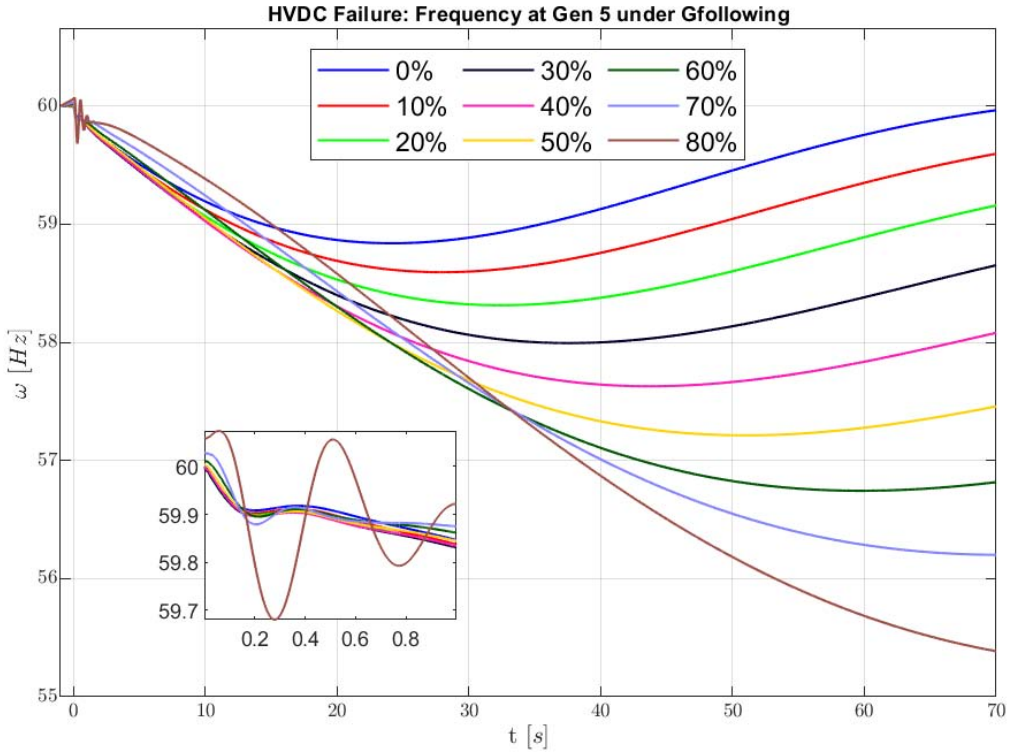

(b) System without Droop Control and Virtual Inertia

Figure 6.20: Frequency of Gen. 5, equipped with grid-following control, for different level of penetration of converters when the failure of the HVDC connection is simulated

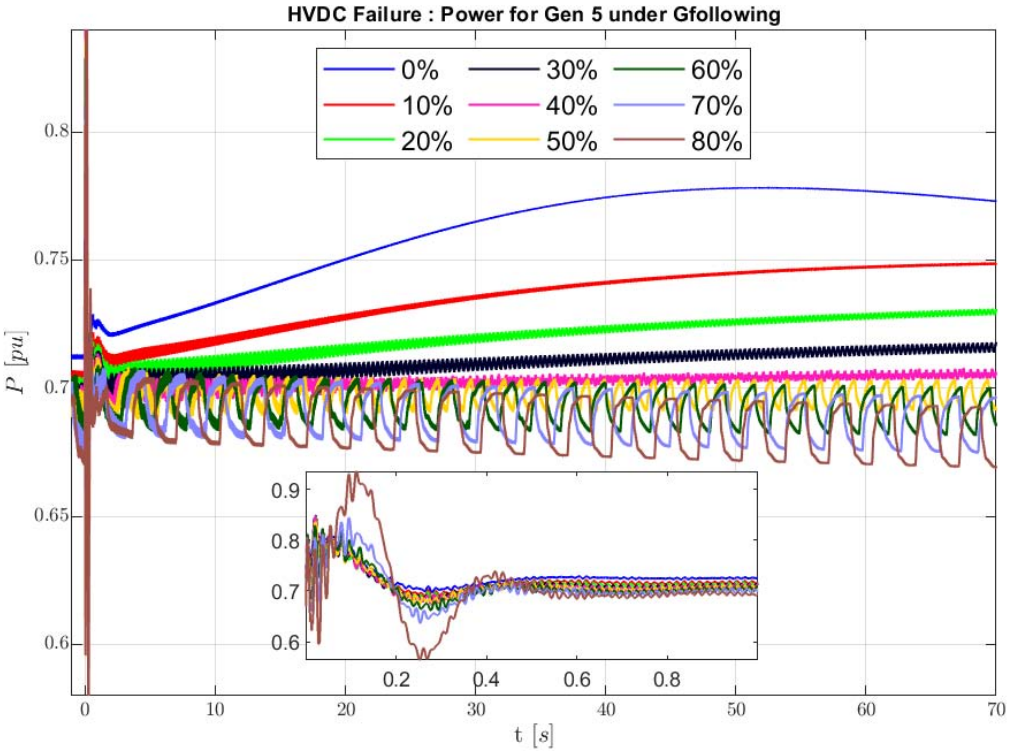

(a) System equipped with Virtual Inertia and Droop control

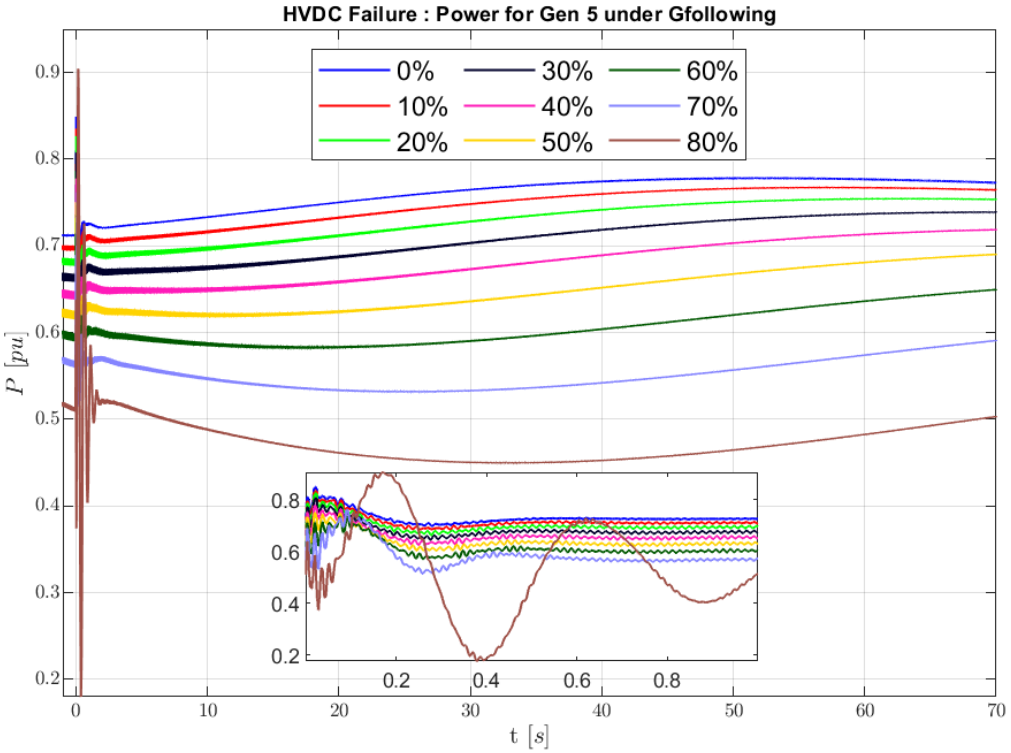

(b) System without Droop Control and Virtual Inertia

Figure 6.21: power of Gen. 5, equipped with grid-following control, for different level of penetration of converters when the failure of the HVDC connection is simulated

Some considerations can be made also about the power of the different generators, that are reported in Fig. 6.21; in both cases, the general behaviour is similar to the one of the frequency, as it has been seen in all the simulations. After the contingency, the higher request of power is supplied by the different generators. Of course, the gen 5, which is the closest to the HVDC connection is the one that reacts faster, but after a small transient due to the length of the connections, all the generators are able to synchronize in frequency and to provide the same quantity of power (i.e. they are characterized by the same step in the quantity of the power that they need to provide to the system). However, the same differences which have been described previously in the analysis of the frequency are detected also in the power behaviour. Especially, when droop and virtual inertia are enabled, some oscillations appear, especially for high level of penetration of converters. Increasing the percentage of inverters decreases the time in which the stability is reached and also reduces the step in the power, as it is possible to see in Fig. 6.21a. On the other side, in Fig. 6.21b, there are no oscillations but the system requires more time to reach a new condition of stability, as it was observed also for the frequency.

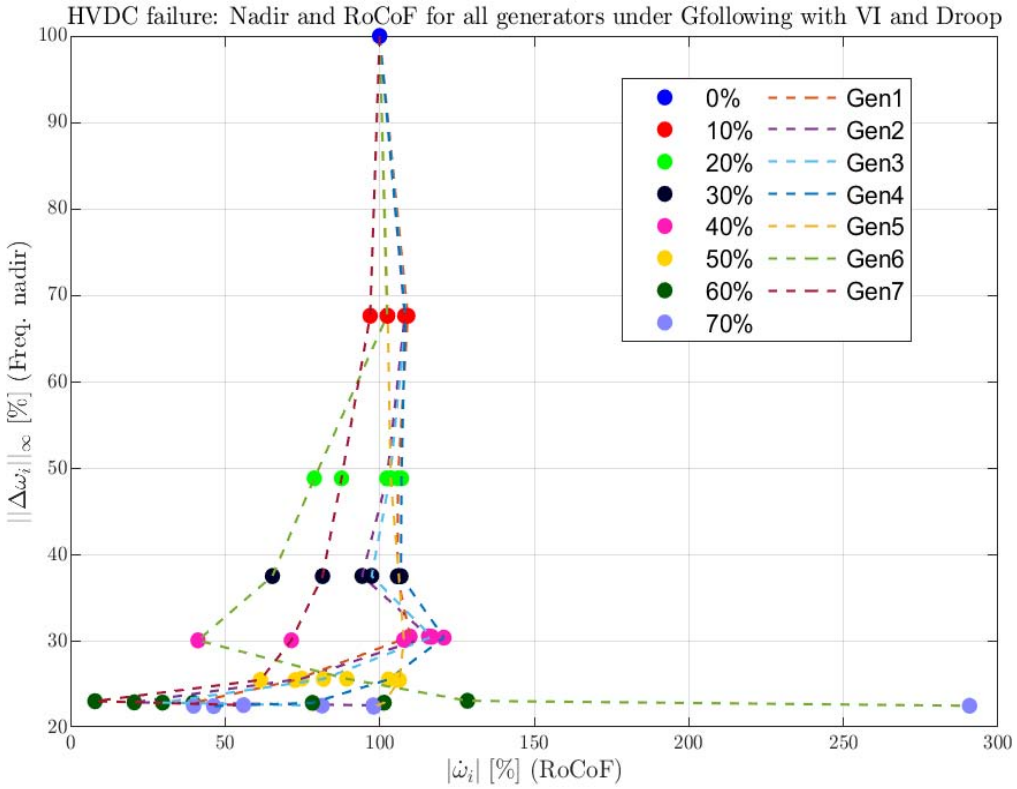

Figure 6.22: Analysis of normalized RoCoF and Nadir of all generators at different level of penetration of grid-following converters equipped with Virtual Inertia and Droop control when the failure of the HVDC connection is simulated

The analysis on the performances of the grid-following converters in the hydro-Quebec network also involves the frequency at the Nadir and the RoCoF values, as it has been done previously. In Fig. 6.22 the values are reported for all generators for the level of inverters penetration which are permitted with this strateg of controly; the interest is not only to understand the general behaviour of the frequency as the percentage of converters in the network increases, but also to make a brief comparison with what has been observed in the case of grid-forming converters. First of all, when the Virtual Inertia loop and the Droop control are enabled, the value of the frequency at Nadir decreases at each iteration (6.22), as it has been seen also when grid-forming converters were used. As regards the RoCoF values, some differences can be observed between the two kinds of control, i.e. grid-forming and grid-following. Indeed, in Fig. 6.18 the performances are worst in terms of RoCoF as there were more converters in the grid. Instead, in the case of grid-following, at least for low percentage of inverters, there is also an improvement in the RoCoF values.

6.4 Final considerations on the Hydro-Quebec network

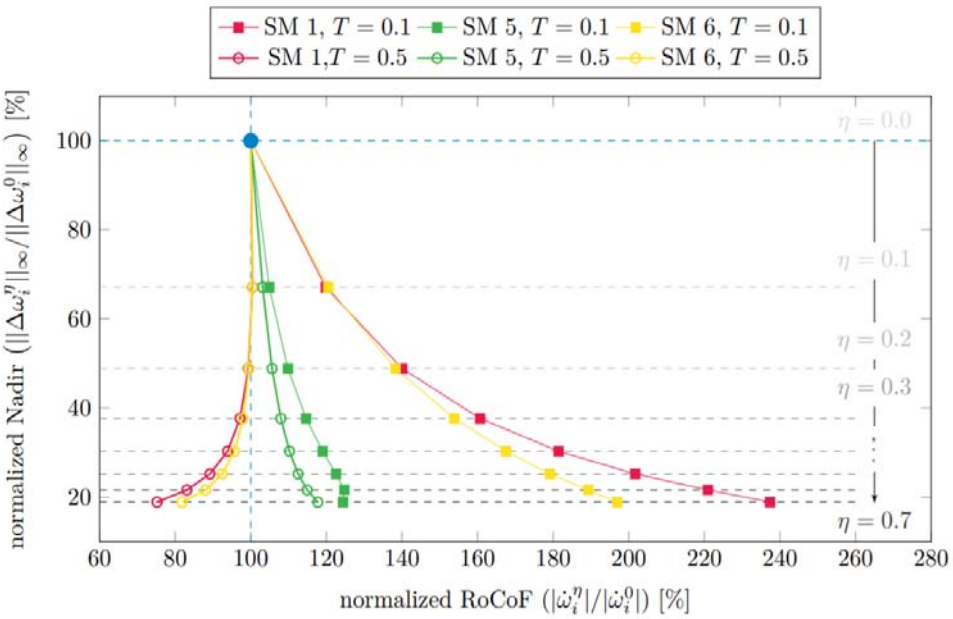

Figure 6.23: Normalized frequency Nadir vs RoCoF, computed over two distinct time window, for different penetration levels for three SMs when the failure of the HVDC connection occurs [36]

Different simulations and tests have been performed on this model, with the

goal of better understanding the behaviour of the network when the presence of SMs is reduced. The main results have been summarized in [36], but in the paper only grid-forming strategies have been taken into consideration. In Fig. 6.23 it is depicted the evolution of the behaviour of the frequency for three different generators, respectively unit 1, 5 and 6 (one for each area of interest) when a trip on the HVDC line takes place. Comparing this graph with the ones analyzed previously, two different time windows for the computation of RoCoF have been considered; indeed, recalling Eq. 6.3, the parameter T can influence the value of the RoCoF. In the graph, the time windows considered are, respectively, equal to 0.1 and 0.5s. Some considerations can be drawn from the analysis of Fig. 6.23. First of all, in both cases, the value of frequency at Nadir results lower as the percentage of converters increases; as regards the RoCoF, it is necessary to distinguish between the generators. Indeed, for SM 1 and 6 (which are located far from the HVDC connection), with smaller window the RoCoF increases, while enlarging T, smaller values also for this parameter are observed. Instead, the RoCoF of the SM 5 is less sensitive to the variation of the time window; in this case, in particular, the behavior of the RoCoF is pretty similar in the two different conditions. Similar results have been observed also in the case of the failure of the SM 1 and, generally, the behaviour of the generators far from the event is different and more sensitive to the variations of the time window.
At the end of the day, also if further investigation over the size of the window is necessary to better understand the phenomena, the results show that, as the inertia decreases in a uniform way in the network, at the beginning the response provided by the converters is slower compared to the instantaneous inertia one; however, considering a larger interval of time, the inverters are able to stop the frequency decay and also to guarantee better performances compared to the SMs.

Chapter 7

Conclusions and future research

7.1 Conclusions

The work has taken into consideration a problem of extreme actuality, i.e. the transition towards a more sustainable way of generating electricity and has given some interesting results, summarizing in [36]. Specifically, the pollution produced by the combustion of the fossil fuels, the consequent problem of the global warming and the fact that these sources are limited have raised the demand for new form of energies. All these reasons have brought to a strong interest for the so called *green energies*, such as hydro-power and geothermic energy at the beginning, while in the last decade the field of wind and solar energy has seen a rapid increment.
In the first chapter the nowadays situation has been analyzed, showing the differences existing between countries in the world; indeed, some of them, exploiting advantageous situations (for example, the availability of hydro-power or geothermic energy). have yet reached the goal of a 100% renewable grid (Iceland), others are trying to increment the quantity of electricity produced by wind and solar energy (German, China and Australia in particular). Policies that encourage the transition towards renewable sources are promoted also by the European Union, which has imposed that by 2020 at least the 20% of the energy of each country must come from green sources.
Nevertheless, this transition has brought also significant changes in the network, which often represent the main obstacle in order to guarantee an higher penetration of renewables in the grid. Indeed, while the frequency of the SMs depends on the angular speed of the rotor and they are connected to the grid through a simple transformer, wind turbines and solar panels require power electronics converters in order to be connected to the network. These devices are different from synchronous generators for two main reasons; first of all, being power-electronics based, they are characterized by faster dynamics with respect to SMs (therefore they need faster control action) and then, due to the absence of rotor, they are characterized by low (mechanical)-inertia. This last point, in

particular, constitutes a limit in the increment in the use of renewable sources, because the inertia of the rotor guarantees stability to the system. The problems related to a low-inertia network have been explored in the second chapter and three different types of stability have been highlighted: rotor angle, voltage and frequency stability. In the following part of the thesis, the interest has been mostly on the frequency stability, which represents a fundamental characteristic of each network. Indeed, all the devices connected in a grid are characterized by protection system that cause their disconnection when the frequency of the network overcomes some limit values. This has been the reason, for example, of the blackoout that has verified in Australia in 2016.
By the way, due to the impossibility of modifying all the networks and of recreating them in order to adapt to the converters, different strategies of control have been proposed with the goal of expanding the use of inverters in the grid, without loosing the stability that was guaranteed by SMs. In the third chapter, grid-following and grid-forming converters have been taken into consideration; being the definition of these two strategies not the same in literature, in this work these two kind of devices are distinguished according to the presence (or not) of the PLL.With grid-following converter there is only the possibility to adapt to the frequency of the network (that is detected by a PLL), that has to be imposed by other devices (SMs or grid-forming inverters, for example). On the other side, grid-forming converters (which do not need the PLL to work) try to emulate the properties of the synchronous generators and are also able to impose the frequency to the grid. For these reasons, only with this kind of inverter, it has been possible to obtain a stable full converter-based system, i.e. a network without SMs.
After having presented four techniques of grid-forming control, that differ from each other in terms of what they emulate of a synchronous generator, and having discussed about how to scale a converter (which is typically a small size device installed on the root of industry/private property) in order to substitute big power plants at the end of the fourth chapters, two different models have been taken into account with the goal of reaching the higher level possible of penetration of inverters in the grid. Specifically, in the fifth chapter the converters analyzed previously have been tested, in order to validate them and to see how they behave in a simple grid as the IEEE 9-Bus system, that is characterized only by three generators.
Different test cases have been explored, using both grid-forming and grid-following converters; the analysis has focused on the results obtained for the power and the frequency of the different generators, when a contingency takes place. It has been seen that, as it was expected, only with grid-forming converters it is possible to reach a 100% inverter-based grid, while with grid-following the system becomes unstable when also the third generator of the network is substituted. Not only, but the performance improve in terms of frequency at Nadir and time to reach a new stability level as the percentage of grid-forming converter in the

net increases.
In the last chapter, the model of the Hydro-Quebec network has been taken into account and two types of failure have been simulated: the trip of one generator (in the specific Gen. 1, which is one of the biggest of the grid) and the failure of the HVDC connection (which constitutes a connection line between Quebec and New England). Again, it has been possible to reach a grid totally based only on grid-forming converters in both cases and to keep stability also in condition of no-inertia. Nevertheless, when the percentage of converters is high (around $80 - 90\%$), a re-tuning of the PSS of the system has been necessary, in order to keep the frequency stable. In this network, the behaviour of two parameters has been of particular interest, i.e. Nadir and RoCoF, in order to analyze the performances of the system with an increasing penetration of the inverters.
Looking at this work, the transition towards low-inertia system appears unavoidable to face the increasing demand of electricity and the simultaneously request of reducing the pollution. In some cases, virtual inertia has been added to the system, in order to keep the same properties which characterize the SM in a network converter based. However, also these types of system has been considered part of the low-inertia ones, in the sense that the mechanical inertia has been removed. In other cases, the role played by mechanical inertia has been substitute with appropriate control strategies. By the way, the results obtained in simulations show that not only converters are able to guarantee frequency stability, which is a fundamental characteristic for every grid, but they also improve the performances in terms of RoCoF and Nadir. In particular, thanks to the power electronics components, they answer faster than the SMs to the contingencies that happen in the grid. This explains the behaviour of the frequency and the power seen in the graphs: when a load is applied to the the network, at the beginning the converters provide the power necessary to balance this event. In particular, the better results have been obtained using grid-forming devices, while grid-following strategy allows only a partial penetration.
At the end of the day, the main results given by this work are:

- the necessity of substituting the SMs leads to low mechanical inertia systems, which are characterized by stability problems that need to be solved through appropriate control strategies.

- it has been proved, both in a benchmark and in a real model, that it is possible to obtain a full-inverter based grid, using grid-forming converters.

- not only these converters allow to use the renewable sources into the network, but they are also able to improve the performances in terms of frequency at Nadir and frequency RoCoF.

- when there is an high percentage of converters in the grid, some corrections are necessary, such as a PSS re-tuning.

- grid-following converters need some devices that impose the frequency to the system to work properly. However, using Virtual Inertia loop and Droop Control, their performance are similar to the one obtained with grid-forming converters.

7.1.1 Future Research

As the necessity of using more renewable sources increases, the interest towards these types of technology raises continuously. In this work, only some techniques of control have been tested and it has been considered a SIMULINK model of a real system; obviously, lot of components (transformers, lines, ecc.) have been considered ideal, but in the reality the complexity increases and further considerations need to be introduced. There are different things that could be better explored, such as:

1. grid-following and grid-forming converters can be implemented and tested in real-time simulators (for example, using *OPAL RT*), with the goal of obtaining results which are even closer to the reality.

2. the problem of the re-tuning of the PSS needs to be treated with more detail; indeed, in this thesis, the parameters have been re-set with the trial and error method, in order to keep the stability of the system, but it is necessary to analyze if they can be considered real values for the PSS.

3. other techniques of control can be investigated and implemented, with the goal of maintaining system stability and improving the performance.

4. Nadir RoCoF need to be deeper analyzed, to better understand their variance when different time windows are considered.

Appendices

Appendix A

Synchronous Machine Model

In this part the model of a synchronous machine (SM) is briefly described from both physical and mathematical sides. It does not represent exactly the one that is used in the Simulink block of Matlab, but these notes can help the reader to better understand the considerations made during the work. All the details refer to the notes of [45]. First of all, it is important to remind that the generator are called *"synchronous"* due to the fact that their rotor rotates synchronously with the frequency of the grid. In the following part, the four main components of the model are going to be considered: the rotor, the stator, the excitation system and other loop controllers. Before going into the details, it is worth to mention the assumptions that have been taken into consideration:

- It is assumed to be always in the condition of a balanced three-phase system;
- The rotor is considered to be round with a single pole pair;
- The excitation current i_f that goes inside the system is kept constant.

Defining with θ and ω the rotating angle and frequency, respectively, with $M^\star$ the total moment of inertia and with $D^\star$ the damping constant, with τ_m the mechanical torque and with τ_e the electrical torque consumed by the load, the typical swing equation of a SM is obtained

$$\begin{aligned} \dot{\theta} &= \omega \\ M^\star \dot{\omega} &= -D^\star \omega + \tau_m - \tau_e \end{aligned} \tag{A.1}$$

Multiplying A.1 with ω_0, that is the nominal frequency of the system, the swing equation can be rewritten in terms of power as

$$M\dot{\omega} = -D\omega + P_m - P_e \tag{A.2}$$

where M is the inertia constant and D is the damping coefficient. The electrical power P_e used by the load can be rewritten, using the $\alpha - \beta$ notation as

$$P_e = i_{\alpha\beta}^T \omega L_m i_f \begin{bmatrix} -sen(\theta) \\ cos(\theta) \end{bmatrix} \tag{A.3}$$

In this last relationship, $i_{\alpha\beta}$ is the current in the stator, while the i_f is the excitation current and L_m the mutual inductance. Substituting A.3 in A.1 the dynamic model of the rotor is obtained

$$\begin{aligned} \dot{\theta} &= \omega \\ M\dot{\omega} &= -D\omega + P_m - i_{\alpha\beta}^T \omega L_m i_f \begin{bmatrix} -sen(\theta) \\ cos(\theta) \end{bmatrix} \end{aligned} \tag{A.4}$$

The other main component of a SM is the stator, where there are usually three

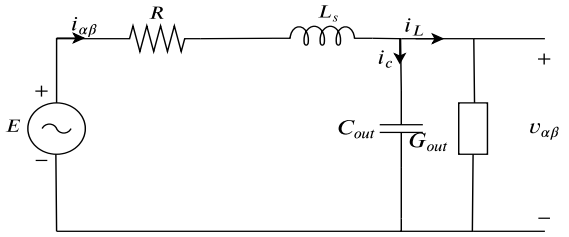

Figure A.1: Diagram of the single phase equivalent circuit of stator winding [45]

windings with a phase-shift of 120° in order to provide three phases current as output.The scheme of a single phase circuit is represented in Fig. A.1; through the mutual inductance L_m produces a voltage E, which generates the current $i_{\alpha\beta}$ that flows through the resistance R and the self-inductance L_s of the stator. At the output there are a shunt capacitor C_{out} and a conductance G_{out}.
Considering first of all the dynamics of the output capacitor, it results

$$\begin{aligned} i_c &= i_{\alpha\beta} - i_L \\ C_{out}\dot{v}_{\alpha\beta} &= -i_L + i_{\alpha\beta} \end{aligned} \tag{A.5}$$

while the dynamics of the self inductance is given by

$$L_s\dot{i}_{\alpha\beta} = -Ri_{\alpha\beta} - v_{\alpha\beta} - E \tag{A.6}$$

It has been explained that E is the voltage generated through the mutual inductance, i.e. $E = \omega L_m i_f \begin{bmatrix} -sen(\theta) \\ cos(\theta) \end{bmatrix}$, the dynamic model of the stator can be synthesized in these two equations

$$\begin{aligned} C_{out}\dot{v}_{\alpha\beta} &= -i_L + i_{\alpha\beta} \\ L_s\dot{i}_{\alpha\beta} &= -Ri_{\alpha\beta} - v_{\alpha\beta} - \omega L_m i_f \begin{bmatrix} -sen(\theta) \\ cos(\theta) \end{bmatrix} \end{aligned} \tag{A.7}$$

Combining Eq. A.4 and A.7, the full dynamic model of the SM is obtained

$$\begin{aligned}
&\dot{\theta} = \omega \\
&M\dot{\omega} = -D\omega + P_m - i_{\alpha\beta}^T \omega L_m i_f \begin{bmatrix} -sen(\theta) \\ cos(\theta) \end{bmatrix} \\
&C_{out}\dot{v}_{\alpha\beta} = -i_L + i_{\alpha\beta} \\
&L_s\dot{i}_{\alpha\beta} = -Ri_{\alpha\beta} - v_{\alpha\beta} - \omega L_m i_f \begin{bmatrix} -sen(\theta) \\ cos(\theta) \end{bmatrix}
\end{aligned} \tag{A.8}$$

The excitation system is the part of the SM responsible to generate the con-

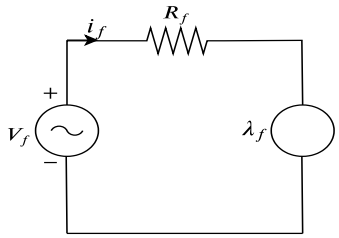

Figure A.2: Equivalent circuit of the excitation system [45]

trollable magnetic field between the rotor and the stator; the goal is reached through windings that are located around the rotor. In Fig. A.2 it is reported the equivalent circuit of this part, where V_f is the input to the system while i_f represents the current that flows in the model. Finally, there are an excitation resistance R_f and a flux linkage with the stator, λ_f.
It is of interest now to approximate the model of the excitation system through a first order dynamic system. First of all, the inductance matrix $L(\vartheta)$ is defined as

$$L(\vartheta) = \begin{bmatrix} L_s & 0 & L_m cos(\vartheta) \\ 0 & L_s & L_m sen(\vartheta) \\ L_m cos(\vartheta) & L_m sen(\vartheta) & L_f \end{bmatrix} \tag{A.9}$$

where L_s, L_f and L_m stand, respectively, for the self-inductance of the stator, the self-inductance of the excitation system and the mutual inductance between the stator and the rotor. The flux linkage λ is described through the three components

$$\begin{bmatrix} \lambda_\alpha \\ \lambda_\beta \\ \lambda_f \end{bmatrix} = \begin{bmatrix} L_s & 0 & L_m cos(\vartheta) \\ 0 & L_s & L_m sen(\vartheta) \\ L_m cos(\vartheta) & L_m sen(\vartheta) & L_f \end{bmatrix} \begin{bmatrix} i_\alpha \\ i_\beta \\ i_f \end{bmatrix} \tag{A.10}$$

It occurs to specify also the voltage equation to reach the first order model

$$\dot{\lambda}_f = R_f i_f + V_f \tag{A.11}$$

Deriving $\dot{\lambda}_f$ from A.10, it is obtained

$$L_f\dot{i}_f = L_m\omega sen(\vartheta)i_\alpha - L_m cos(\vartheta)\dot{i}_\alpha - L_m\omega cos(\vartheta)i_\beta - L_m sen(\vartheta)\dot{i}_\beta + R_f i_f + V_f \tag{A.12}$$

Imposing the external excitation voltage to be equal to

$$V_f = -L_m\omega sen(\vartheta)i_\alpha + L_m cos(\vartheta)\dot{i}_\alpha + L_m\omega cos(\vartheta)i_\beta + L_m sen(\vartheta)\dot{i}_\beta - R_f i_f + \alpha(i_f - i_f^\star) \tag{A.13}$$

The excitation current results expressed through a first order system

$$L_f\dot{i}_f = \alpha(i_f - i_f^\star) \tag{A.14}$$

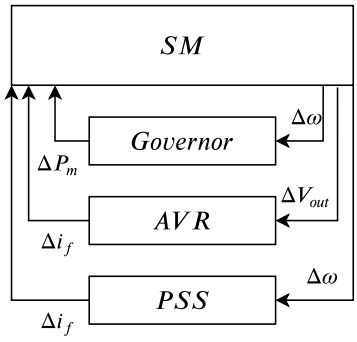

Figure A.3: Outer Loop controllers of a SM [45]

In Fig. A.3 it is depicted a scheme of the strategy of control that is built in a SM model Basically, it is possible to mention three main components:

- Governor controller: it adapts the mechanical input of the machine controlling some valves that regulate the flux of the steam inside the turbine. Through this device, the droop of the SM is set to a desirable value.
- Automated Voltage Regulator (AVR): its goal is keeping constant the output voltage constant. The variable that is controlled is the excitation current i_f that directly influences the voltage E. However, this regulation can produce some oscillations, which make necessary an other component of control.
- Power System Stabilizer (PSS): it measures the oscillations in terms of frequency deviation $\Delta\omega$ and also influences the excitation current i_f; however, to not have a stable voltage offset, its effect must disappear after a certain time, i.e. when the system is stabilized.

All these actions of control can be described by the following matrix, where the different K stand for the gains that must be adapted to the system considered

$$\begin{bmatrix} \Delta P_m \\ \Delta i_f \end{bmatrix} = \begin{bmatrix} K_g & 0 \\ K_{PSS} & K_{AVR} \end{bmatrix} \begin{bmatrix} \Delta\omega \\ \Delta V_{out} \end{bmatrix} \tag{A.15}$$

Appendix B

Clarke and Park transformation

Several times in the simulations that have been performed and also in the model which have been presented, in place of the three-phase referenced system a new one has been adopted. The goal of this part is to provide an explanation on how these transformations are obtained. First of all, the main reason which leads to consider this type of system is the fact that a reduce number of variables to control is obtained. Due to the fact that in the system analyzed lot of quantities have been taken into consideration, the advantages in terms of complexity for the controller is not negligible.
Specifically, two types of transformation have been considered: from *abc* to $\alpha\beta$ quantities and from $\alpha\beta$ to *dq* frame; these are, respectively, Clarke and Park transformation and Matlab/Simulink offers some blocks that directly perform these operations, that have been adopted frequently in the models.

B.1 From *abc* to $\alpha\beta$ frame: Clarke's transformation

This transformation converts balanced three-phase quantities in two-phase quadrature quantities. It is useful in the generation of reference quantities which represent the input of the controller. As shown in Fig. B.1, quantities are converted from the three phase referenced frame to the two-axis orthogonal reference frame. From a mathematical point of view, considering for example a balanced system (i.e. the currents satisfy $i_a(t) + i_b(t) + i_c(t) = 0$, this transformation is described by the following relation:

$$i_{\alpha\beta}(t) = \begin{bmatrix} \frac{2}{3} & -\frac{1}{3} & -\frac{1}{3} \\ 0 & \frac{1}{\sqrt{3}} & -\frac{1}{\sqrt{3}} \end{bmatrix} \begin{bmatrix} i_a(t) \\ i_b(t) \\ i_c(t) \end{bmatrix} \tag{B.1}$$

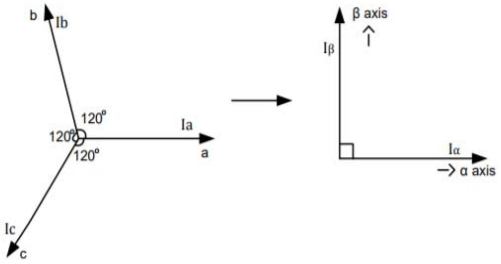

Figure B.1: Clarke's transformation

B.2 From $\alpha\beta$ to *dq* frame: Park's transformation

This transformation is used to pass from a system in which the quantities are expressed in balanced two-phase orthogonal stationary frame into an orthogonal rotating reference frame. Compared to the previous section, in this case i_d is at an angle ϑ (which is the rotation angle) with respect to the α axis and i_q is perpendicular to i_d, as it is shown in Fig. B.2 Formally, it results

$$i_{dq} = \begin{bmatrix} cos(\vartheta) & sin(\vartheta) \\ -sin(\vartheta) & cos(\vartheta) \end{bmatrix} \begin{bmatrix} i_\alpha \\ i_\beta \end{bmatrix} \tag{B.2}$$

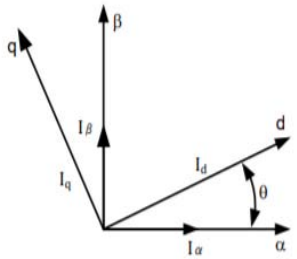

Figure B.2: Park's transformation

Appendix C

Implementation of the "hybrid block"

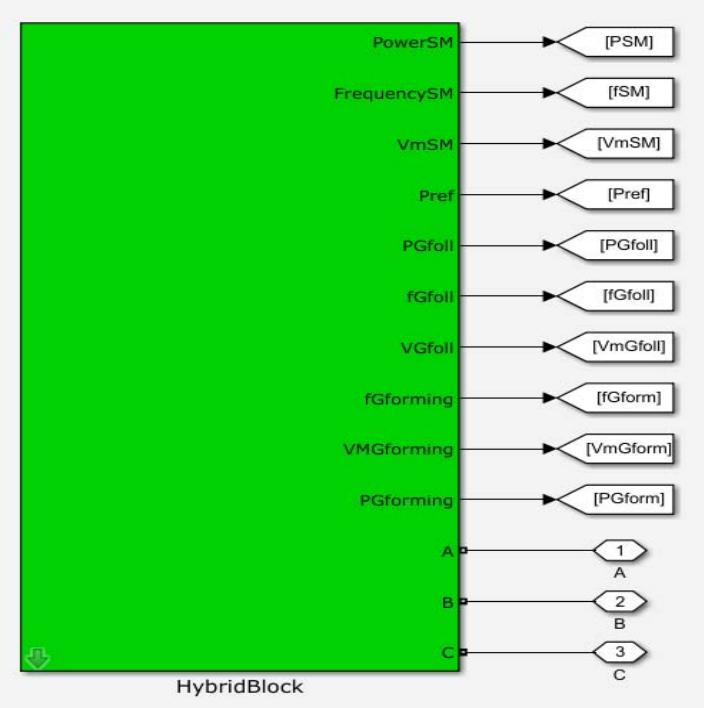

Figure C.1: Hybrid Block with associated output

In the sixth chapter, simulations have been performed in a large network, with an high number of generators and for different levels of penetration of converters. This has lead to the implementation of what has been called *"hybrid block"* in Matlab/Simulink, i.e. a structure which has inside the grid-forming converter, the grid following and the model of the SM. In particular, in this part

the interest is explaining how this block has been obtained, how the connection between different generators has been implemented and briefly explaining its principle of working. In Fig. C.1, the component is represented as it has been put inside the model; at the bottom, there are the three connectors that are used in order to link the block to the rest of the network. The other output are used in order to keep the desired quantities from the converters or the SM. In particular, frequency, voltage and power of each unit is extracted in order to be available for further analysis. The block parameters are set through a mask, which is divided in three parts, one for each element of the block. In particular, it is possible to assign the nominal power of the block, its base frequency and the percentage of power that has to be supplied through converters or SM, according to the level of converter penetration desired. An aspect to be considered is that, selecting a percentage of converter or SM equal to null quantity, causes the disconnection of that part of the block and allow the simulation with only converters or synchronous generators. In Fig. C.2 it is reported a part of the

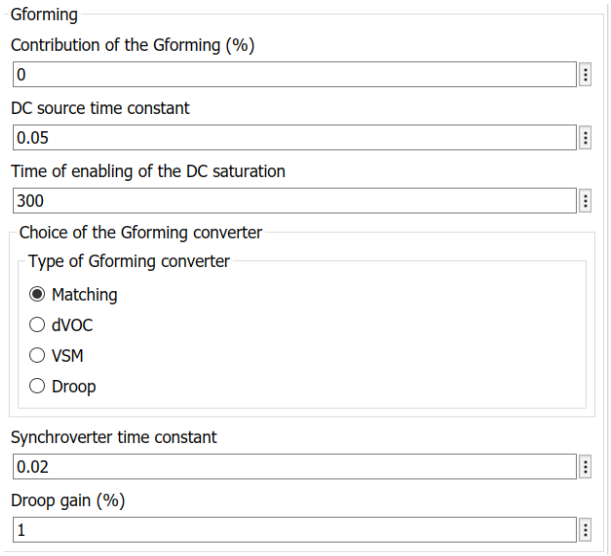

Figure C.2: Part of the mask of the hybrid block: grid forming parameters

mask of the hybrid block, i.e. the one in which the parameters of the grid-forming converters are set. In particular, it is possible to choose the percentage of grid-forming that it is desired in the network, when to enable the DC saturation and the droop gain. Moreover, this block also gives the possibility to select the kind of control of the converters between the four that have been analyzed previously. This peculiarity is due to the fact that in the part of the grid forming converter, which is at the bottom of Fig. C.3, there is a selector which guarantees to adopt the strategy that is selected in the mask. Looking more in details at the same figure, it is shown how the block is built internally; the three units are connected in parallel and inside each block there is the respective component.

In particular, referring to the Hydro-Quebec system previously discussed, in each hybrid block there is the corresponding SM (which the nominal power that it supplies to the grid) and the grid-forming and grid-following converters that have been implemented, opportunely scaled.

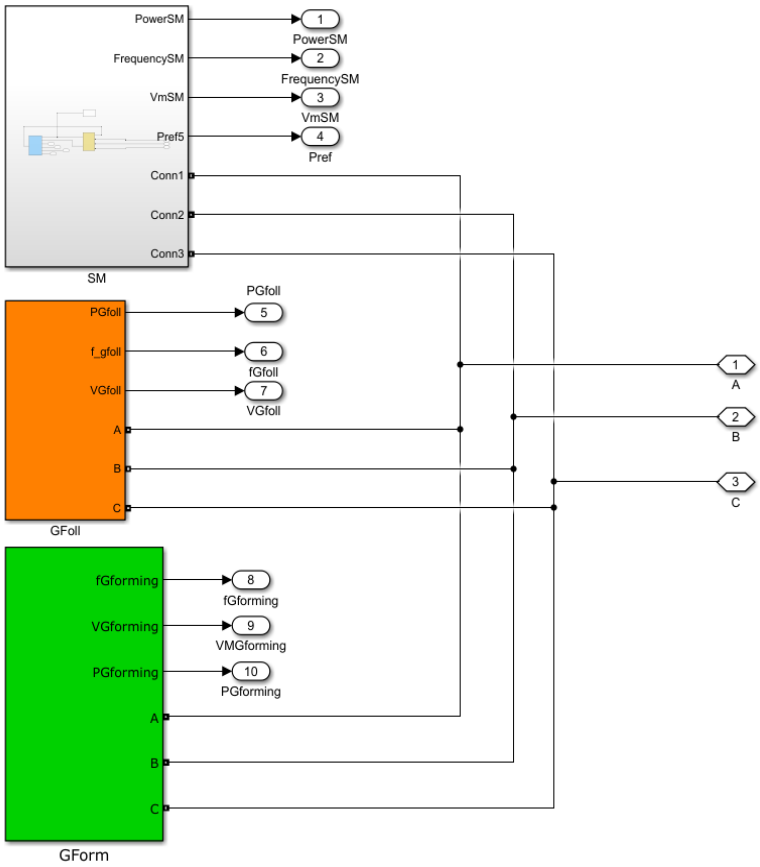

Figure C.3: Internal structure of the hybrid block with grid-forming, grid following and SM

This block has been widely used in order to obtain the results in the Hydro-Quebec system, because it allows to have a fast selection not only of the kind of generators that is desired in the grid, but also it is possible to set the desired contribution of each part. Due to this reason, tuning the parameters in the right way, it is possible to use this block also in other grids and perform similar tests.

Appendix D

Parameters used in the simulations

In this appendix, the parameters of SMs, grid-forming and grid-following converters are reported. It is useful to remind that in order to obtain converters of really large size as the ones adopted in the simulations, the scaling law explained at the end of the third chapter has been adopted.

D.1 Parameters for IEEE 9-Bus system

IEEE 9-Bus network base values		
Frequency [Hz]	**Generation Capacity [MW]**	**Voltage [kV]**
50	300	230
SM common parameters		
Nominal Power	[MW]	100
Reference Power	[p.u.]	0.75
Inertia Coefficient	[s]	3.7
Medium Voltage	[kV]	13.8
Droop Gain	[%]	1
MV/HV transformer parameters		
Medium Voltage	[kV]	13.8
High Voltage	[kV]	230
R_l (Medium-side)	[p.u.]	0.0027
R_m (High-side)	[p.u.]	0.008
L_l (Medium-side)	[p.u.]	0.0027
L_m (High-side)	[p.u.]	0.08
R_{mag} (Magnetization)	[p.u.]	500
L_{mag} (Magnetization)	[p.u.]	500

Table D.1: Network base values and SM parameters for IEEE 9-Bus system

Grid-forming converter parameters (for a single unit)	
Nominal Power [KW]	500
Voltage on DC side [kV]	2.45
DC Resistance [ohm]	0.05
DC Capacitance [F]	0.008
DC Time constant [s]	0.05
AC Filter Resistance [ohm]	0.001
AC Filter Inductance [μH]	200
AC Filter Capacitance [μF]	300
LV/MV transformer parameters	
Low Voltage [kV]	1
Medium Voltage [kV]	13.8
Low-side Resistance [p.u.]	0.0027
Medium-side Resistance [p.u.]	0.0027
Low-side inductance [p.u.]	0.08
L_m (Medium-side) [p.u.]	0.08
Magnetization Resistance [p.u.]	500
Magnetization Inductance [p.u.]	500
Droop	
Droop Gain [%]	1
AC Proportional Gain [K_p]	0.001
AC Integral Gain [k_i]	0.5
Matching	
DC-gain[η	0.154
AC Proportional Gain [K_p]	0.001
AC Integral Gain [k_i]	0.5
VSM	
Synchroverter Time Constant [s]	0.02
Damping Gain [D_p]	$20 \times P_n^\star$
Inertia constant [J]	$0.04 \times P_n^\star$
AC Proportional Gain [K_p]	0.001
AC Integral Gain [k_i]	2.1×10^{-3}
dVOC	
Control Gain [α]	6.66×10^4
Droop Gain [η]	$1.26 \times 10^7 / P_n^\star$
AC Proportional Gain [K_p]	0.001
AC Integral Gain [k_i]	0.5

Table D.2: Grid-forming converter parameters for IEEE 9-Bus system

Grid-following converter parameters (for a single unit)	
Nominal Power [KW]	100
Voltage on DC side [V]	637
DC Proportional Gain [$k_{p,DC}$]	0.3
DC Integral Gain [$k_{i,DC}$]	20
Power Proportional Gain [$k_{p,P}$]	0.1
Power Integral Gain [$k_{i,P}$]	20
AC Filter Resistance [ohm]	0.0019
AC Filter Inductance [mH]	0.25
AC Filter Capacitance [F]	0.024
LV/MV transformer parameters (for a single unit)	
Low Voltage [V]	260
Medium Voltage [kV]	13.8
Low-side Resistance [p.u.]	0.001
Medium-side Resistance [p.u.]	0.001
Low-side inductance [p.u.]	3
Medium-side inductance [p.u.]	3
Magnetization Resistance [p.u.]	500
Magnetization Inductance [p.u.]	500

Table D.3: Grid-following converter parameters for IEEE 9-Bus system

D.2 Parameters for Hydro-Quebec system

Hydro-Quebec network base values

Frequency [Hz]	Generation Capacity [MW]	Voltage [kV]
60	26200	735

Units nominal power and reference value

Generator	Nominal Power [MW]	Reference value [p.u.]
Unit 1	5500	0.98651
Unit 2	2200	0.8181
Unit 3	200	0.9
Unit 4	2700	0.9259
Unit 5	5000	0.9
Unit 6	5600	0.8928
Unit 7	5000	0.9

SM common parameters

Medium Voltage	[kV]	13.8
Droop Gain	[%]	5

SM parameters for different Units

Generator	Inertia Coefficient[s]	Time Constant [s]
Unit 1	4.1	2.67
Unit 2	3.2	2.67
Unit 3	3.2	2.67
Unit 4	3.7	2.67
Unit 5	3.7	2.67
Unit 6	4	2.67
Unit 7	3.7	2.67

MV/HV transformer parameters

Medium Voltage	[kV]	13.8
High Voltage	[kV]	735
R_l (Low-side)	[p.u.]	0.002
R_m (Medium-side)	[p.u.]	0.002
L_l (Low-side)	[p.u.]	0
L_m (Medium-side)	[p.u.]	0.12
R_{mag} (Magnetization)	[p.u.]	500
L_{mag} (Magnetization)	[p.u.]	500

Table D.4: Network base values and SM parameters for Hydro-Quebec

Grid-forming converter parameters (for a single unit)	
Nominal Power [KW]	500
Voltage on DC side [kV]	2.45
DC Resistance [ohm]	0.05
DC Capacitance [F]	0.008
DC Time constant [s]	0.025
AC Filter Resistance [ohm]	0.001
AC Filter Inductance [μH]	200
AC Filter Capacitance [μF]	300
LV/MV transformer parameters	
Low Voltage [kV]	1
Medium Voltage [kV]	13.8
Low-side Resistance [p.u.]	0.002
Medium-side Resistance [p.u.]	0.002
Low-side inductance [p.u.]	0
L_m (Medium-side) [p.u.]	0.12
Magnetization Resistance [p.u.]	500
Magnetization Inductance [p.u.]	500
Droop	
Droop Gain [%]	5
AC Proportional Gain [K_p]	0.001
AC Integral Gain [k_i]	0.5
Matching	
DC-gain[η	0.154
AC Proportional Gain [K_p]	0.001
AC Integral Gain [k_i]	0.5
VSM	
Synchroverter Time Constant [s]	0.002
Damping Gain [D_p]	$20 \times P_n^\star$
Inertia constant [J]	$0.04 \times P_n^\star$
AC Proportional Gain [K_p]	0.001
AC Integral Gain [k_i]	2.1×10^{-3}
dVOC	
Control Gain [α]	6.66×10^4
Droop Gain [η]	$1.26 \times 10^7 / P_n^\star$
AC Proportional Gain [K_p]	0.001
AC Integral Gain [k_i]	0.5

Table D.5: Grid-forming converter parameters for Hydro-Quebec

Grid-following converter parameters (for a single unit)	
Nominal Power [KW]	100
Voltage on DC side [V]	637
DC Proportional Gain [$k_{p,DC}$]	0.3
DC Integral Gain [$k_{i,DC}$]	20
Power Proportional Gain [$k_{p,P}$]	0.1
Power Integral Gain [$k_{i,P}$]	20
AC Filter Resistance [ohm]	0.0019
AC Filter Inductance [mH]	0.25
AC Filter Capacitance [F]	0.024
PLL Filter Cut-off frequency	10
PLL Proportional Gain [$k_{p,PLL}$]	180
PLL Integral Gain [$k_{i,PLL}$]	3200
PLL Derivative Gain [$k_{d,PLL}$]	1
LV/MV transformer parameters (for a single unit)	
Low Voltage [V]	260
Medium Voltage [kV]	13.8
Low-side Resistance [p.u.]	0.001
Medium-side Resistance [p.u.]	0.001
Low-side inductance [p.u.]	3
Medium-side inductance [p.u.]	3
Magnetization Resistance [p.u.]	500
Magnetization Inductance [p.u.]	500
MV/HV transformer parameters	
Medium Voltage [kV]	13.8
High Voltage [kV]	735
R_l (Low-side) [p.u.]	0.002
R_m (Medium-side) [p.u.]	0.002
L_l (Low-side) [p.u.]	0
L_m (Medium-side) [p.u.]	0.12
R_{mag} (Magnetization) [p.u.]	500
L_{mag} (Magnetization) [p.u.]	500

Table D.6: Grid-following converter parameters for Hydro-Quebec

Bibliography

[1] "AIT Austrian Institute of Technology GmbH." Online available https://www.ait.ac.at.

[2] B. Kroposki, B. Johnson, Y. Zhang, V. Gevorgian, P. Denholm, B. M. Hodge, and B. Hannegan, "Achieving a 100% Renewable Grid: Operating Electric Power Systems with Extremely High Levels of Variable Renewable Energy," vol. 15, no. 2, pp. 61–73, 2017.

[3] F. Milano, F. Dörfler, G. Hug, D. J. Hill, and G. VerbiÄ, "Foundations and Challenges of Low-Inertia Systems," in *Power Systems Computation Conference (PSCC)*, 2018.

[4] "Global Wind Solar Installations in Gigawatts (GW)." Online available http://www.fi-powerweb.com/Renewable-Energy.html.

[5] G. Denis, T. Prevost, M. Debry, F. Xavier, X. Guillaud, and A. Menze, "The Migrate project: the challenges of operating a transmission grid with only inverter-based generation. A grid-forming control improvement with transient current-limiting control," *IET Renewable Power Generation*, vol. 12, no. 5, pp. 523–529, 2018.

[6] "High Penetration of Power Electronic Interfaced Power Sources (HPoPEIPS) ENTSO-E Guidance document for national implementation for network codes on grid connection," tech. rep., ENTSO-E, 2017.

[7] "Horizon 2020 Work programme 2018-2020: secure, clean and efficient energy." Online Available https://ec.europa.eu/research/participants/data/ref/h2020/wp/2018-2020/main/h2020-wp1820-energyen.pdf, 2018.

[8] "Delivering a Secure, Sustainable Electricity System (DS3)," tech. rep., EIRGRID-SONI, 2014.

[9] "Annual Renewable Energy Constraint and Curtailment Report (2017)," tech. rep., EIRGRID-SONI, June 2018.

[10] A. Tayyebi, F. Dörfler, F. Kupzog, Z. Miletic, and W. Hribernik, "Grid-Forming Converters – Inevitability, Control Strategies and Challenges in Future Grid Applications," in *CIRED Workshop*, 2018.

[11] A.Tayyebi, D. Groß, and A. Anta, "GridFormingConverters: Implementation of grid-forming control techniques in IEEE 9-bus system." Git repository, 2019. https://github.com/ATayebi/GridFormingConverters.

[12] G. Sybille, "Hydro-Quebec 29-Bus Grid Model – Matlab/Simulink SimPowerSystem Implementation," model documentation, MathWorks, Inc. https://www.mathworks.com/.

[13] H. Ritchie and M. Roser, "Fossil fuels," *Our World in Data*, 2019. https://ourworldindata.org/fossil-fuels.

[14] P. Tielens, P. Henneaux, and S. Cole, "Penetration of Reenwables and Reduction of Synchronous Inertia in the European Power System-Analysis and Solutions," tech. rep., 2018.

[15] "Wind Energy in Europe in 2018: Trends and Statistics," tech. rep., Wind Europe, February 2019.

[16] "Powering Europe: Wind Energy and the Electricity Grid," tech. rep., EWEA, November 2010.

[17] "Global Market Outlook for Solar Power (2019-2023)," tech. rep., Solar Power Europe-Inter Solar Europe-Global Solar Council, 2018.

[18] P. Kundur, *Power system stability and control*. McGraw-Hill, 1994.

[19] "Black System South Australia 28 September 2016," tech. rep., AEMO, March 2017. Online Available https://www.aemo.com.au/-/media/Files/Electricity/NEM/Market_Notices_and_Events/Power_System_Incident_Reports/2017/Integrated-Final-Report-SA-Black-System-28-September-2016.pdf.

[20] P. Kundur, J. Paserba, V. Ajjarapu, G. Anderssona, C. Canizares, N. Hatziargyriou, D. Hill, A. Stankovic, C. Taylor, T. Cutsem, and V. Vittal, "Definition and Classification of Power System Stability," vol. 19, no. 2.

[21] A. Yazdani and R. Iravani, *Voltage-Sourced Converters in Power Systems: Modeling, Control, and Applications*. WILEY,IEEE.

[22] A. Tayyebi, D. Groß, A. Anta, , F. Kupzog, and A. Anta, "Interactions of Grid-Forming Converters and Synchronous Machines – a Comparative Study," 2019.

[23] B. Johnson, M. Rodriguez, M. Sinha, and S. Dhople, "Comparison of virtual oscillator and droop control," in *IEEE Workshop on Control and Modeling for Power Electronics (COMPEL)*, 2017.

[24] M. Chandorkar, D. Divan, and R. Adapa, "Control of parallel connected inverters in standalone AC supply systems," vol. 29, no. 1, pp. 136–143, 1993.

[25] S. D'Arco and S. J.A., "Virtual Synchronous Machines–Classification of Implementations and Analysis of Equivalence to Droop Controllers for Microgrids," 2013.

[26] H. Bevrani, T. Ise, and Y. Miura, "Virtual synchronous generators: A survey and new perspectives," *International Journal of Electrical Power & Energy Systems*, vol. 54, pp. 244–254, 2014.

[27] Q. C. Zhong and G. Weiss, "Synchronverters: Inverters That Mimic Synchronous Generators," vol. 58, no. 4, pp. 1259–1267, 2011.

[28] C. Y., R. Hesse, D. Turschner, and H. Beck, "Dynamic Properties of the Virtual Synchronous Machine (VISMA)," vol. 1, pp. 755–759, May 2011.

[29] Arghir, Catalin, Jouini, Taouba, and F. Dörfler, "Grid-forming control for power converters based on matching of synchronous machines," *Automatica*, vol. 95, pp. 273–282, 2018.

[30] Arghir, Catalin, Dörfler, and Florian, "Direct angle control and energy-shaping techniques for grid-connected converters," *submitted to IEEE Trans. Power Electron.*, 2019. https://doi.org/10.3929/ethz-b-000331022.

[31] P. Vorobev, P. Huang, M. A. Hosani, J. L. Kirtley, and K. Turitsyn, "High-fidelity model order reduction for microgrids stability assessment," vol. 33, no. 1, pp. 874–887, 2018.

[32] M. Colombino, D. Groß, J. Brouillon, and F. Dörfler, "Global phase and magnitude synchronization of coupled oscillators with application to the control of grid-forming power inverters," 2019.

[33] D. Groß, M. Colombino, J.-S. Brouillon, and F. Dörfler, "The effect of transmission-line dynamics on grid-forming dispatchable virtual oscillator control," 2019. to appear.

[34] G. Andersson, "Modelling and Analysis of Electric Power Systems: Power Flow Analysis, Fault Analysis, Power Systems Dynamics and Stability," pp. 5–20, September 2008.

[35] "Matlab/Simulink SimPowerSystem synchronous machine model," model documentation, MathWorks, Inc. mathworks.com.

[36] A. Crivellaro, A. Tayyebi, C. Gavriluta, D. Groß, A. Anta, F. Kupzog, and F. Dörfler, "Beyond low-inertia systems: Massive integration of grid-forming power converters in transmission grids," Nov. 2019.

[37] G. Trudel, S. Bernard, and G. Scott, "Hydro-Quebec's defence plan against extreme contingencies," vol. 14, pp. 958–966, August 1999.

[38] "Hydro-Quebec: System Control Centre (SCC)." Online available http://www.hydroquebec.com/learning/transport/conduite-reseau.html.

[39] "2018 Frequency Response Annual Analysis," tech. rep., NERC, November 2018.

[40] "Simulation and Application of Power System Stabilizer on Power System Transient Stability," vol. 8.

[41] U. Markovic, O. Stanojev, E. Vrettos, P. Aristidou, and G. Hug, "Understanding stability of low-inertia systems," *engrXiv preprint*, 2019. http://engrxiv.org/jwzrq.

[42] B. K. Poolla, D. Groß, and F. Dörfler, "Placement and implementation of grid-forming and grid-following virtual inertia and fast frequency response," 2019.

[43] "New Options in System Operations," tech. rep., MIGRATE, January 2019.

[44] RG-CE System Protection & Dynamics Sub Group, "Frequency measurement requirements and usage," tech. rep., ENTSO-E, 2018.

[45] tech. rep.

[46] G. Denis, T. Prevost, P. Panciatici, X. Kestelyn, F. Colas, and X. Guillaud, "Review on potential strategies for transmission grid operations based on power electronics interfaced voltage sources," in *2015 IEEE Power Energy Society General Meeting*, pp. 1–5, 2015.

[47] S. Curi, D. Groß, and F. Dörfler, "Control of low-inertia power grids: A model reduction approach," in *IEEE Conference on Decision and Control (CDC)*, pp. 5708–5713, 2017.

[48] B. K. Poolla, S. Bolognani, and F. Dörfler, "Optimal placement of virtual inertia in power grids," vol. 62, no. 12, pp. 6209–6220, 2017.

List of Tables

List of Figures